

http://researchcommons.waikato.ac.nz/

Research Commons at the University of Waikato

Copyright Statement:

The digital copy of this thesis is protected by the Copyright Act 1994 (New Zealand).

The thesis may be consulted by you, provided you comply with the provisions of the Act and the following conditions of use:

- Any use you make of these documents or images must be for research or private study purposes only, and you may not make them available to any other person.
- Authors control the copyright of their thesis. You will recognise the author's right to be identified as the author of the thesis, and due acknowledgement will be made to the author where appropriate.
- You will obtain the author's permission before publishing any material from the thesis.

Derivation and Application of Master Equation Methods for Semiconductor Lasers

A thesis submitted to the University of Waikato for the
Degree of Doctor of Philosophy in Physics
by

Andrea Eschmann

The University of Waikato
Hamilton New Zealand

April 1996



Introduction

With the advent of the laser, an interest in the statistical properties of light was born. New theories, which required an understanding of how the lasing medium interacts quantum mechanically with incident light were developed to classify and quantify light.

For many laser systems, gaining an understanding of the physical processes occuring in the medium, and translating these into a mathematical formalism has been achieved with relative speed and ease, and the resulting theories form part of the core of the field we know as quantum optics.

In the case of semiconductor lasers however, progress has not been so swift, nor the description so complete. The many and complex processes occuring in a semiconductor laser are not well understood and this has led to many-body and solid-state phenomenological descriptions of the semiconductor laser rather than a quantum optical one. Although some attempts have been made at obtaining a fully quantum mechanical description, phenomenological descriptions have been resorted to to describe poorly understood or complex processes such as pumping and scattering.

The work in this thesis was inspired by the lack of such a theory, and by the belief that it should be possible to give a description of the semiconductor laser in terms familiar to quantum opticians. With the continued and current interest in non-classical properties of light, such a theory could be very useful in predicting such properties of

semiconductor lasers. Since semiconductor lasers have great potential for use in high speed electro-optic, or even optical communications, low-noise operation of these devices is a desired and indeed essential goal.

Our first attempt at formulating such a theory was a simple single-mode description, using as a basis for comparison of results the more phenomenological work of Yamamoto and coworkers [Yamamoto 1986, Machida 1987, Yamamoto 1987]. Our work was based on a master equation description of the system however, and thus the methodology differed significantly from that of these authors.

The theory gave good agreement with their results, and so we turned our attention to a more complicated multi-mode description. The impetus for this work was provided by the results of experiments of Marin *et al.* [Marin 1995], in which the degree of non-classical character of the light emitted from the laser depended on which experimental scheme was used. Two of the experiments (the free-running and diffraction grating experiments) that Marin *et al.* had performed could be explained by the initial multi-mode theory, however a description of the third (injection locking) required a slight reformulation of the theory. In this latter case phase fluctuations were also examined. For both multi-mode descriptions, excellent agreement with the results of the experiments and the predictions of a more phenomenological theory were obtained.

This thesis is organised as follows: In Chapter 1, an introduction to the research areas of semiconductor lasers relevant to this thesis is given. In Section 1.1, the history of the semiconductor laser is discussed with particular emphasis on the development of theories describing the characteristics of semiconductor lasers. The development of single-mode theories is discussed, as are pump noise suppression, injection locking, and multi-mode theories. In Section 1.2 a brief description of the technical aspects of semiconductor lasers is given.

In Chapter 2 we introduce our master equation theory and use it in a description of a single mode semiconductor laser. In Section 2.1 we introduce the work briefly, and move on in Section 2.2 to derive a reduced master equation for the system. In Section 2.3 the master equation is solved, so that the spectrum of intensity fluctuations can be calculated. We show that qualitatively similar results are obtained to those found via a rate equation approach.

In Chapter 3 we extend the theory to a multi-mode situation. This introduces some degree of complexity into the system. In Section 3.1 an introduction to the system is given, and in Section 3.2 the modifications required to the single mode Hamiltonian are discussed. In Section 3.3 the reduced master equation is written down for the multi-mode system, and in Section 3.4 further modifications to this master equation are considered due to differences in the spatial distributions of the side modes compared to the central mode. An alternative pumping model to that given in Chapter 2 is described in Section 3.5. The master equation is transformed into a Fokker-Planck equation in Section 3.6, and in Section 3.7, the linearised equations are written down. The spectral calculation is detailed in Section 3.8, as are the parameters used in calculating the results, which are also given in this section. A discussion of the eigenvectors and eigenvalues of the drift matrix in Section 3.9 clarifies what energy-exchanging processes take place in the semiconductor. In Section 3.10, a discussion of the spatial distributions of the modes is given, and in Section 3.11 the use of electrical circuits to describe the pumping is discussed.

In Chapter 4 injection locking is considered. This involves a further expansion of the number of variables in the system, and completes a comparison with the experimental results of Marin *et al.* In Section 4.1 the concept of injection locking is introduced, and modifications to the equations of Chapter 3 are given in Section 4.2. The resulting stochastic differential equations are linearised in Section 4.3, and in

Section 4.4 a detailed discussion of the steady-state solutions is given. The results are given in Section 4.5.

Chapter 5 is a short chapter in which we discuss the conclusions of the thesis. The limitations of our approach and further work which could be carried out are also discussed.

The work in this thesis has been published in the following papers:

Chapter 2 Master Equation Theory of Semiconductor Lasers, C.W. Gardiner and A. Eschmann, Phys. Rev. A **51**, 4982 (1995).

Chapter 3 Master Equation Theory of Multi-Mode Semiconductor Lasers, A. Eschmann and C.W. Gardiner, *to appear*, Phys. Rev. A (1996).

Chapter 4 Master Equation Theory of Multi-Mode Semiconductor Lasers II: Injection Locking, A. Eschmann and C.W. Gardiner, *submitted*, Phys. Rev. A (1996).

Acknowledgements

I am very fortunate to have worked with such a distinguished physicist as Crispin Gardiner. I would like to thank him for his patience and guidance over the last three years as I have worked towards this thesis. I am very grateful for the opportunities he has given me, such as travelling overseas to work with other physicists. I would also like to thank him for his generosity in the form of the many cups of coffee, lunches and dinners over the last three years.

In addition, there are several other people whom I would like to thank for their input into this work. These are Jean-Philippe Poizat, Helmut Ritsch, and Klaus Gheri. I would also like to thank Monika Marte, Howard Carmichael, and Scott Parkins for their help and input into work carried out in other areas not related to the semiconductor laser work which appears in this thesis.

I would like to thank the staff and students at the University of Waikato for their friendship and help. In particular I would like to thank my mum for help with various administrative hassles, Dale Carnegie and Andrew Taberner for explaining the vagaries of p-n junctions and equivalent circuits, and James Shepherd, John Woffinden, and Bill Munro for help with Unix.

In addition, I wish to extend my gratitude to staff and students at the University of Innsbruck for their help with acquainting myself with a new country and system. In particular, I thank Marion Grünbacher, Stefan Marksteiner, Rheinhold Walser, Monika Marte and

Helmut Ritsch for their kindness. Thanks are also due to Simon Gardiner for his companionship, particularly in the initial weeks in Austria.

I would particularly like to thank all the friends who cheered me up while I was away with all the letters and e-mail, which really did make the tough time away from home more bearable.

I am also very grateful to Liz Doolin and Andrew Robertson in Wellington for generously providing a place to stay for three months.

Thanks are also due to the University of Waikato Scholarships Committee, the NZVCC, the Waikato branch of the Federation of University Women, and the Austrian government, for providing funding through scholarships and a stipend to make this doctorate possible.

Finally, I wish to thank every member of my family for their unflagging support and encouragement, and also John, who has constantly run around for me, sorting things out while I have been away from home, has encouraged me to keep going and has always maintained faith in my ability to complete this doctorate. Especially, I would like to thank him for putting up with my lengthy absences from home, which were not easy for either of us to cope with.

Contents

Introduction iii

Acknowledgements vii

Glossary of Symbols xix

1 Introduction 1

1.1 History 1

1.1.1 Single Mode Theories 2

1.1.2 Pump Noise Suppression 4

1.1.3 Injection Locking 16

1.1.4 Multi-Mode Theories 21

1.2 Technical Aspects of Semiconductor Lasers 24

1.2.1 Introduction 24

1.2.2 General Features 24

1.2.3 Modes and Mode Structure 25

1.2.4 Laser Structures 28

2 Master Equation Theory for a Single Mode Semiconductor Laser 33

2.1 Introduction 33

2.2 Derivation of a Reduced Master Equation 35

2.2.1 Description of the System 35

2.2.2 Adiabatic Elimination 37

2.2.3 Inclusion of non-lasing modes and other losses . . 46
2.2.4 Inclusion of Pumping 47
2.3 Solution of the Master Equation 50
2.3.1 Deterministic Equations for Mean Values 51
2.3.2 Stochastic equations for numbers of electrons, holes and photons 52

3 Master Equation Theory of Multi-Mode Semiconductor Lasers 63
3.1 Introduction 63
3.2 Hamiltonian 65
3.3 Master Equation 66
3.4 Coupling of the Field to the Semiconductor 67
3.5 Pumping 69
3.6 Transformation to a Fokker Planck Equation 71
3.7 Linearised Stochastic Differential Equations 73
3.8 Calculation of the Spectrum 74
3.9 Eigenvectors and Eigenvalues 81
3.10 Mode Spatial Distributions 85
3.11 The use of Electrical Circuits to Describe Pumping . . . 86

4 Injection Locking of Multi-Mode Semiconductor Lasers 89
4.1 Introduction 89
4.2 Inclusion of Injection Locking 90
4.3 Linearised Equations 94
4.4 Steady-State Solutions 98
4.5 Results 101

5 Conclusion 105

A Simplification of Steady-State Solutions 109

B Calculation of Spectrum in Terms of Photon Number Correlation Function **111**

C Pumping **117**

D Transformation to a Fokker-Planck Equation **121**

E Stochastic Differential Equations **129**

F Steady-state solutions **135**

G Linearised SDEs **139**

List of Figures

2.1 (a) A schematic of the pumping part of the semiconductor system. (b) An example of an equivalent circuit for the pumping part of the semiconductor system. 48

2.2 Comparison of the spectrum of Yamamoto and Machida internal to the cavity (dashed line) with Equation (2.102) (solid line), for pump rates r of (a) 1000 and (b) 10000, and $Q_e = Q_h = 0$. The finely dashed line (which indicates the shot noise level) is included to illustrate that in (a) the area under the graph above zero is greater than that below zero, and vice versa for (b). 62

3.1 The different carrier populations to which the field modes couple are represented here by the different regions of the figure. The dark grey region is that referred to by the variables n_e, and n_h. The lighter grey region is referred to by the variables $\tilde{n}_e$, and $\tilde{n}_h$. The population represented by the white region is ignored in our analysis, since the intensity of the side modes is much smaller than that of the central mode. 68

3.2 The electrical circuit which models the pumping. 70

3.3 The equivalent circuit for the central part of Fig 3.2. . . 71

3.4 (a) Total intensity noise (Equation 3.21) in the absence of decorrelating mechanisms for $z = 10^{-9}$ and $\mu_1 = \mu_2 = \mu_3 = 1$. (b) Total intensity noise for $z = 10^{-2}$ and $\mu_1 = \mu_2 = \mu_3 = 1$. (c) Total intensity noise (dot-dashed line), central mode intensity noise (dotted line), and side mode intensity noise (dashed line), given by Equation (3.19), for $z = 10^{-2}$, $\mu_1 = 1$, and $\mu_2 = \mu_3 = 0.985$. The shot-noise level is indicated by the solid line. 79

3.5 Mode occupation for central (dotted line), and side (dashed line) modes as a function of $\log(1 - p)$. 81

3.6 Photon number as a function of pump strength, showing the lasing threshold for (a) the central mode, and (b) the side modes. 82

4.1 The function $f(m_1^0) = m_1$, depicted by the plotted points, shows an apparent discontinuity, and a regime in which the bisection algorithm could produce negative solutions. The lightly drawn solid line however, shows how the function can actually be continuous for some parameters. The dashed line is the function $f(m_1^0) = m_1^0$. 100

4.2 (a) Injected photon number (solid line), central mode photon number (dotted line), and $\beta_{1,+}^2/4 = m_1 \cos^2 \phi_1$ (dashed line), as a function of injected power, indicating the regime of injection locking. (b) Total intensity noise as a function of injected power. The dashed line indicates the shot-noise level. (c) Central mode intensity noise as a function of injected power. The dashed line indicates the shot noise level of the central mode intensity, normalised to the total intensity noise. (d) Side mode intensity noise as a function of injected power. The dashed line indicates the shot-noise level of the side mode intensity normalised to the total intensity noise. (e) Standard deviation of $\sin \phi_1$ as a function of injected power. 102

List of Tables

3.1 Eigenvectors and Eigenvalues describing energy exchange between the semiconductor and the field. 83
3.2 Eigenvectors and Eigenvalues describing energy exchange between the field modes. 84
3.3 Eigenvectors and Eigenvalues describing energy exchange between the carriers. 85

Glossary of Symbols

Chapter 2

b	The boson annihilation operator for the lasing mode.
$n_{e,k}, n_{h,k'}$	The electron and hole number operators respectively.
$c_{kk'}$	The dipole moment operator representing a transition of an electron from the conduction to the valence band.
$g_{kk'}$	The coupling constant between the field and the semiconductor.
$\sqrt{\kappa/(2\pi)}$	The coupling constant between the field and the reservoir.
$\sqrt{\mu_{kk'}/(2\pi)}$	The coupling constant between the dipole moment operator and the reservoir.
$\sqrt{\gamma_{kl}/(2\pi)}$	The coupling constant between the carrier population and a heat bath.
$\mathcal{L}_1$	The Liouvillian for the semiconductor subsystem.

$\mathcal{L}_2$ . . . . . The Liouvillian for the interaction between the field and the semiconductor.

$\mathcal{L}_3$ . . . . . The Liouvillian for the field subsystem.

$\bar{N}$ . . . . . The thermal photon number.

$\bar{N}^E_{kl}$ . . . . . The thermal electron number.

$\underline{n}$ . . . . . The vector of electron and hole numbers, $\underline{n} = (n_e, n_h)$.

$\mathcal{P}(\underline{n})$ . . . . . A projection operator which projects the system onto a subspace of solutions of $\dot{\rho} = \mathcal{L}_1\rho$.

$_T$ . . . . . This subscript refers to the thermal states of the system.

$p(\underline{n})$ . . . . . A projection operator which acts on the state vectors, to project out a state of definite $\underline{n}$.

$\rho_0(\underline{n})$ . . . . . The density operator for the subspace in which the field is fully quantized, but in which we deal with numbers of carriers. This is defined mathematically in Equation (2.18).

$F(\underline{n})$ . . . . . The transition probability for absorption of a photon in the master equation, given by Equation (2.48).

$G(\underline{n})$ . . . . . The transition probability for emission of a photon in the master equation, given by Equation (2.49).

$\epsilon_{kk'}$ . . . . . The frequency separation between the states in the conduction and valence bands.

$\bar{N}_{kk'}$	The mean occupation number of the reservoir to which non-lasing field modes couple.
$A(\underline{n})$	The transition probability for emission of a particle, given by Equation (2.53).
$B(\underline{n})$	The transition probability for the absorption of a particle, given by Equation (2.54).
C_i	A capacitor in the pump circuit.
R_i	A resistor in the pump circuit.
V_i	A voltage source in the pump circuit.
M	The number of fixed negative charges in the semiconductor.
Q_i	The charge on C_i.
I	The pump current.
T_i	The temperature of R_i.
ξ_i	The noise source associated with R_i.
I_{dc}	The dc component of the pump current.
k	Boltzmann's constant.
$\alpha_e, \beta_e, \beta_h, \alpha_h$	The coefficients of the pump contributions, given by Equations (2.79), (2.80), (2.82), and (2.83).

P_e, P_h . . . . . The electron and hole pump rates, given by Equations (2.81), and (2.84).

$\mathbf{X}$ . . . . . The vector of variables for the single mode system.

$\mathcal{C}(\mathbf{X})$ . . . . . The drift matrix for the linearised stochastic differential equations.

$\mathcal{B}(\mathbf{X})$ . . . . . The diffusion matrix for the linearised stochastic differential equations.

N^2 . . . . . The modifed square of the total number of states in the semiconductor, dependant on the spectral shape.

P . . . . . The pump rate.

P_{th} . . . . . The threshold pump rate.

a . . . . . The coefficient of the approximated transition probabilities $F(\underline{n})$ and $G(\underline{n})$, given by Equations (2.87), and (2.88).

d . . . . . The coefficient of the approximated transition probability $A(\underline{n})$, given by Equation (2.89).

r . . . . . The pump rate, defined as $r = (P - P_{th})/P_{th}$.

Chapter 3

j . . . . . The subscript j refers to the jth mode, where the central mode is denoted by $j = 1$, and the side modes by $j = 2, 3$.

Δ_j	The detuning of the jth mode from the central mode.
$\tilde{n}_e, \tilde{n}_h$	The additional electron and hole populations to which the central mode couples. All variables with a tilde refer to this population.
$\underline{n}, \underline{e}, \underline{\tilde{e}}$	Vectors as defined in Equations (3.7)-(3.9).
$\mathbf{Y}$	The vector of all variables in the multi-mode system, given by Equation (3.17).
$\mathcal{E}(\mathbf{Y}_0)$	The drift matrix in the linearised equation for $\mathbf{Y}$.
$\mathcal{F}(\mathbf{Y}_0)$	The diffusion matrix in the linearised equation for $\mathbf{Y}$.
p	The ratio of the side mode decay constants to the central mode decay constant, $p = \kappa_2/\kappa_1$.
η	The differential quantum efficiency.
μ_j	The detection efficiency of the jth mode.
$\tau^{(pe)}$	The lifetime due to output coupling losses.
$\tau^{(po)}$	The lifetime due to internal losses.
z	The ratio of the additional population, coupled to only by the central mode, to the common population coupled to by all the modes.

Chapter 4

ϵ	A c-number proportional to the amplitude of the injected signal.
$\beta_{1,+}$	The additional variable introduced into the injection locking system, given by $\beta_{1,+} = \beta_1 + \beta_1^*$.
$\beta_{1,-}$	An additional variable, which is eliminated due to the approximations made $\beta_{1,-} = -i(\beta_1 - \beta_1^*)$.
$\mathbf{Z}$	The vector of all variables in the injection locked system, given by Equation (4.16).
$\mathcal{H}(\mathbf{Z}_0)$	The drift matrix in the linearised stochastic differential equation for $\mathbf{z}$.
$\mathcal{I}(\mathbf{Z}_0)$	The diffusion matrix in the linearised stochastic differential equation for $\mathbf{z}$.
ϕ_1	The phase of the central mode.
$\sum_j v_{ij}^* d\eta_j^*, d\Xi_1^*, \tilde{v}_{11}^* d\tilde{\eta}^*$.	Noise terms as defined in Appendix E.

Chapter 1

Introduction

1.1 History

Lasing from a semiconductor was first demonstrated in 1962 by several groups [Hall 1962, Nathan 1962, Quist 1962, Holonyak 1962], after having been studied theoretically [Basov 1961, Bernard 1961, Dumke 1962] after the advent of the laser in 1958 [Schawlow 1958]. Since then, there has been great interest in semiconductor lasers because their small size, high efficiency, high reliability, compatibility with electronic systems, and relatively low cost, makes them ideal for use in optical communications. Because a semiconductor laser differs significantly from other types of laser in its operation however, progress in obtaining a theoretical description has been somewhat slower than progress for other laser systems.

The first difference between a gas or solid-state laser and a semiconductor laser is the existence of bands which contain a distribution of electronic states, rather than discrete levels of a definite energy. Electrons occupying a particular band interact with each other because of strong Coulombic forces and hence must be treated collectively. This complicates a theoretical analysis considerably, since an infinite number of electronic states are available within a band, to which a particular

state may couple.

Electrons and holes undergo spatial diffusion, which leads to a spatially inhomogeneous gain profile. This then affects the spatial variation of the mode through stimulated emission. In addition, the nature of the optical mode is different in a semiconductor laser to the modes found in other lasers. Most lasers have transverse electromagnetic modes, but because a heterostructure device acts as a dielectric waveguide, the modes in a semiconductor laser are transverse electric or transverse magnetic.

An effect unique to semiconductor lasers is the change in gain and refractive index of a mode with external pumping. This has an effect on the operating characteristics, such as a frequency shift in the longitudinal modes with pumping. These differences, and the complicated behaviour due to some of them, have led to rather phenomenological descriptions of the laser [Yamamoto 1987, Vahala 1983a, Vahala 1983b, Haug 1967a].

1.1.1 Single Mode Theories

The first quantum mechanical formulation of the semiconductor laser was the rate equation formulation [Haug 1967a]. This was effectively an analogous formulation to the theories which already existed for gas and solid state lasers [Lax 1966]. In this pioneering paper, second order perturbation theory was employed to include a quantum mechanical description of the pumping, spontaneous emission, and electron-electron scattering in the mean equations of motion for the semiconductor system, and a Langevin approach was also used to include noise.

Because the Langevin approach is based on a correspondence with the terms appearing in the equations of motion for the gas and solid-state lasers, the derivation is rather phenomenological, and has had some refinements since its original appearance [Haug 1967b, Vahala 1983a, Vahala 1983b]. The initial formulation has however

formed the basis of most current theories as can be seen in the references [Yamamoto 1983], [Meystre 1991], [Agrawal 1986], [Chow 1993] and [Haug 1993].

Haug and Haken were the first to develop a van der Pol description of the semiconductor laser in 1967 [Haug 1967b], in which the linewidth enhancement factor, an additional line broadening due to refractive index fluctuations, was discovered, but incorrectly assumed to have a small effect. Vahala and Yariv extended this analysis to include an intensity dependent refractive index [Vahala 1983a].

In 1969, the rate equation approach was extended to cover the full frequency range [Haug 1969], and a GHz resonance feature due to the interaction between carriers and the field was found. Vahala and Yariv also found this resonant peak within the Van der Pol description by taking the complex susceptibility to be an instantaneous function of carrier density rather than field intensity [Vahala 1983b]. The theoretical approach which is currently commonly used to describe semiconductor lasers is summarised in a paper by Yamamoto [Yamamoto 1983].

With the improvement of experimental techniques, it has become possible to excite semiconductor lasers on a time scale which is shorter than the electron scattering time. This is done by using a high intensity femtosecond pulsed laser to excite the semiconductor. In this case, a quasiequilibrium description, in which the motion of the carriers can be adiabatically eliminated is not valid, and alternative techniques must be used to describe the system. To do this non-equilibrium Green's function techniques have been employed, as have projection operator techniques [Haug 1985, Müller 1987, Schmitt-Rink 1988, Lindberg 1988, Herzel 1993]. For the systems we will be discussing however, a quasiequilibrium situation does apply, and thus these Green's function techniques are not of great importance to our work, and will not be discussed further here.

1.1.2 Pump Noise Suppression

Pump noise suppression is used in most semiconductor laser experiments in which noise properties are being examined. As such, it forms an important part of the history of noise in semiconductors, and is discussed in detail here. The idea of suppressing the pump noise in a laser in order to reduce the noise in the output light was first suggested in 1984 by Golubev and Sokolev [Golubev 1984]. The aim of this work was to try to reduce the noise due to spontaneous emission incident on photodetectors.

A system comprised of a doped crystal and a pulsed pump was considered, in which a fixed number of four-level atoms comprised the gain medium. The authors imposed conditions on the time scales of the various transitions in the system so that the presence of atoms in either level of the working transition could be controlled. From the Scully-Lamb master equation [Scully 1967] an expression for the two-time correlation function was obtained which showed an increasing probability with time of detecting a photon at time t, given an initial detection was registered at $t = 0$.

The spectral power of the photocurrent noise was also calculated and was found to approach zero at low frequencies. The authors showed that the noise reduction is due to anticorrelations between the shot-noise current fluctuations and the intensity fluctuations. In addition non-zero detunings and non-radiative losses from the upper lasing level were considered. Because they break down the regularity of the pumping scheme, these processes were found to degrade the antibunching and noise reduction in the system.

This work was followed in 1985 by experimental results [Teich 1985] in which sub-Poissonian light was generated in mercury vapour. This was the first stationary sub-Poissonian light source found, and the non-classical behaviour was attributed to the fact that the inelastic collisions which excite the mercury vapour are regulated by a space-charge

limited electron beam. The space-charge limited beams have reduced randomness below the usual Poisson limit and a quiet vacuum was thus seen. This regulation of the electrons due to Coulomb effects is transferred to the photons emitted from the excited mercury atoms, and thus sub-Poissonian statistics in the resultant light beams were obtained.

In the following year a second experimental scheme to generate sub-Poissonian statistics was proposed by Machida and Yamamoto [Machida 1986]. This scheme also involved the suppression of quatum fluctuations, in this case using a mechanism termed negative feedback. The phase-reversed photon detector output current was added to the laser dc-bias pump current, and a negative correlation was thus established between the photon flux fluctuation and the laser pump rate fluctuation. Two different feedback schemes were demonstrated to give sub-Poissonian statistics. The disadvantage of the negative feedback scheme, as noted by the authors, was the fact that a quantum non-demolition measurement had to be performed to extract the sub-Poissonian state from the negative-feedback loop, and so further new schemes continued to be sought.

In 1986 interest in pumping statistics in other coherent-radiation-producing systems began to be shown, and Filipowicz *et al.* [Filipowicz 1986] published two papers on the microscopic maser. In the first of these the authors found that the intracavity field of a microscopic maser was in general sub-Poissonian, and that the usual Poissonian statistics of lasers and macroscopic masers could only be recovered on introducing stochasticity into the system. The authors attributed their results to the fact that spontaneous emission is inhibited in the micromaser, but is unavoidable in optical resonators. In their second paper, Filipowicz *et al.* presented a microscopic theory and a Fokker-Planck theory of the microscopic maser. They included sources of stochasticity to show that the sub-Poissonian nature of the field can be destroyed.

High-Impedance Pump Noise Suppression

Later that year, Yamamoto, Machida, and Nilsson [Yamamoto 1986] published another new pump-noise suppression scheme which formed the basis for much of the work which followed in the area of pump-noise suppression. The authors performed a very thorough investigation of amplitude and phase fluctuations both internal and external to the laser cavity, and compared results for regular and Poisson pumped systems. They found that an amplitude squeezed state can be produced provided that pump amplitude fluctuations can be suppressed below the ordinary shot-noise limit. The noise correlations which arise out of the fluctuation-dissipation theorem were discussed and the power spectra of the photon-number amplitude and phase noise calculated.

It was shown that for the internal amplitude spectrum, half the noise power stems from pump fluctuations and internal losses, and the other half from incident vacuum fluctuations. It was shown that all other noise sources were either negligible or cancel each other out. The internal phase-noise spectrum was found to be contributed to by the dipole noise operator as well as by zero-point vacuum fluctuations.

For the external spectrum the amplitude noise was found to be due to pump fluctuations and the internal-loss noise operator below the cavity bandwidth, because the incident zero-point fluctuations of the internal field coupling out of the cavity interfere destructively with the reflected vacuum fluctuations outside the cavity. Above the cavity bandwidth the amplitude noise was found to stem only from reflected vacuum fluctuations. This is because above the cavity bandwidth, the internal amplitude noise is cut off, while incident zero-point fluctuations are simply reflected back from the mirror to constitute the higher frequency part of the amplitude noise. The external phase spectrum was found to differ from the internal phase spectrum only in that the reflected zero-point fluctuations also formed a part of the noise. The authors also included checks to ensure that Heisenberg's uncertainty

principle was not violated, and that commutators were still preserved for the internal and external fields if the pump noise was suppressed.

In addition the authors suggested possible experimental schemes for suppression of pump fluctuations. The first of these is based on the work of Teich and Saleh [Teich 1985], but is a stimulated emission version of the spontaneous process occuring in Teich and Saleh's experiment. The scheme involves suppressing the pump fluctuations by use of an electron beam in a space-charge limited vacuum tube, where the potential minimum between the cathode and the anode varies according to the electron emission rate. This has the effect of regulating the arrival of electrons at the anode. Sealing active atoms in the vacuum tube and exciting them with the sub-Poissonian electrons would certainly lead to a reduction below the shot-noise level of the laser amplitude fluctuations.

The second scheme involved the regulation of the carrier injection rate in an injection-current pumped semiconductor by a similar effect. Here, when the junction current of a diode changes, the junction voltage across the p-n junction changes to counteract the change in the current. This occurs due to the presence of a series resistance R_s, across which an increase or decrease in voltage manifests a corresponding decrease or increase respectively in the junction voltage. This process contributes to the regularization of the carrier injection process into the active layer of the semiconductor. The authors termed this scheme 'high-impedance pump suppression'.

Experimental results using high-impedance pump suppression soon followed. Machida, Yamamoto, and Itaya [Machida 1987] were the first to report amplitude squeezing using this noise suppression scheme. They found that the noise was reduced to 7.3% below the shot-noise level over a frequency range of 100 MHz, under conditions of constant-current operation (which occurs when the diode's series resistance is much greater than its differential resistance).

A full theoretical description of the high-impedance pump suppression effect was published in the same year [Yamamoto 1987, Yamamoto 1991]. Using equivalent circuits, and identifying the noise in the pumping process as a current noise, and the fluctuations in the population difference between the two levels of the semiconductor as a voltage noise, the authors derived expressions for the spectrum of the current noise. The reason for doing this was that the standard quantum mechanical theory assumed the pump mechanism could be treated as part of the reservoir, and the population difference as part of the system. This approach meant that the pump mechanism was also included as part of the system, and mutual interactions between the pump source and the population difference could be considered. The spectral expressions derived, indicated the condition already used in the previous experimental work, that the current noise is shot noise limited from above if the series resistance of the diode is much less than the diode's differential resistance, and that the current noise can go much lower than the shot-noise level if the source resistance is much greater than the differential resistance.

Using equivalent circuits an equation is obtained for the junction voltage fluctuations

$$\frac{dv_n}{dt} = \frac{-1}{C}\left[\frac{1}{R} + \frac{1}{R_s}\right] v_n - \frac{1}{C} i_L + \frac{1}{C} i - \frac{1}{CR_s} v_s, \qquad (1.1)$$

where i_L is the photon current fluctuation, i is the current noise source of the minority carriers, and v_s is the voltage noise source due to thermal fluctuations of the majority carrier. R, R_s, and C are the diode differential resistance, source resistance, and capacitance.

Using the correspondence (derived in the paper) that $\Delta N_c = v_n C/q$, a Langevin equation for the electron number fluctuations is derived where q is the fundamental charge, and ΔN_c is the fluctuating part of the electron number,

$$\frac{d\Delta N_c}{dt} = -\left(\frac{1}{\tau_n} + \frac{1}{\tau_{CR}}\right) \Delta N_c - (E_{cv} - E_{vc})\Delta S + f_N, \qquad (1.2)$$

in which

$$\tau_{CR} = CR_s, \tag{1.3}$$

$$f_N = \frac{i}{q} - \frac{v_s}{qR_s}, \tag{1.4}$$

$$\tau_n^{-1} = \left(\frac{1}{\tau_{st}} + \frac{1}{\tau_{sp}} + \frac{1}{\tau nr}\right)^{-1}, \tag{1.5}$$

where τ_{st} is the lifetime due to stimulated emission, τ_{sp} is the lifetime due to spontaneous emission, and τ_{nr} is the lifetime due to non-radiative recombination.

The noise source f_N does not include the usual shot-noise limited pump fluctuation seen in previous treatments, but is due to a thermal fluctuation generated in the source resistance R_s. The contribution of this term to the junction current fluctuation spectrum is the Nyquist expression $4k_BT/R_s$. The shot-noise level for the power spectrum of the junction current fluctuation of the majority carrier is shown to be

$$S_{i_n}(\Omega) \cong 2qI, \tag{1.6}$$

where I is the total current. Since $R = V_T/I$, where $V_T = k_BT/q$, this implies that the junction current fluctuations will be reduced to below the shot noise level provided the condition

$$\begin{aligned} & 2qI > \frac{4k_BT}{R_s} \\ \Rightarrow \quad & R_s > 2R \end{aligned} \tag{1.7}$$

is satisfied.

From this classical Langevin equation, and the corresponding field equation, which is unchanged from previous results, quantum mechanical equations were written down so as to describe the quantum mechanical interference between the transmitted internal laser field and the reflected vacuum field, and so obtain a spectral expression for the

external field noise. These power spectra for the amplitude fluctuations clearly showed the suppression of noise with suppressed pump fluctuations.

In 1988, Machida and Yamamoto [Machida 1988] reported squeezing over the broadest bandwidths ever observed, using constant-current driving (or high-impedance pump noise suppression). The range over which squeezing was found was from frequencies of 10 MHz to 1.1 GHz, and was limited only by the cut-off characteristics of the photodiode and the $1/f$ noise of the GaAs field effect transistor used in the detection process.

In addition, the effect on the amplitude squeezing of pump rate and optical loss was examined. As expected it was found that the amplitude squeezing decreased with decreasing quantum efficiency (in other words, increasing loss). With increasing pump strength the amplitude fluctuations were found to decrease further below the shot-noise level.

In 1989, Bergou *et al.* [Bergou 1989a] gave a method to incorporate the pump statistics in laser or maser dynamics, which allowed either regular injection or Poissonian statistics to be modelled. The approach, which was based on the master equation, predicted a 50% reduction below the shot-noise level in the photon number noise internal to the cavity for the maser and a 25% reduction for the laser. This work was soon generalised [Bergou 1989b] to describe a wide range of different pump mechanisms, and to calculate the effect of the pump noise on the phase fluctuations for both maser and laser. It was found that the pump noise has no effect on the phase fluctuations. In the following year a Langevin approach by the same authors [Benkert 1990] confirmed these predictions, and those of other authors [Yamamoto 1986, Machida 1987, Yamamoto 1987, Marte 1988b].

In 1990, Richardson and Shelby [Richardson 1990] measured the best squeezing ever reported for semiconductor lasers operated under pump-noise suppressed conditions. They achieved a noise reduction

of 11% below the shot-noise level by performing the experiment at a temperature of 4K, and predicted a result of 38% below the shot-noise level if weak optical feedback could be eliminated. This result was soon superseded however, by an experimental result of 85% amplitude noise reduction below the shot-noise limit [Richardson 1991]. This result was achieved by coupling the semiconductor 'face to face' with the detector, which has the effect of reducing optical feedback and increasing the light collection efficiency. The important point that the authors ascertained is that squeezing in semiconductor lasers is not limited by the current transfer efficiency from the laser injection current to the detector current, but only by the optical output coupling efficiency. This was shown by the fact that current division (which took place in their system) did not produce Poissonian partition noise, as is the case in optical systems. This result was explained by using Kirchoff's laws to obtain expressions for the low frequency current noise under high-impedance constant-current conditions. It was shown that if the series resistance is much greater than the differential resistance, then the current noise spectrum can become negligible compared with the shot-noise level, but in the opposite limit only 3dB of squeezing can be obtained.

Finally in 1993, Freeman *et al.* [Freeman 1993a] investigated pump noise suppression in index-guided quantum well lasers and obtained 2.9 dB of squeezing with close-coupled laser-detector measurements.

Squeezed Light as a Pump Source

In 1988 an interest emerged in using other quantum mechanical light sources, in particular squeezed light, to pump atomic lasers. In initial theoretical calculations, carried out by Marte and Walls [Marte 1988a], a reduction in the phase fluctuations was found, but not below the shot-noise limit. The work was extended by Marte, Ritsch and Walls [Marte 1988b], who examined the statistics of the output light for a

range of pump strengths and squeezing parameters. In this work it was found that amplitude fluctuations could become sub-Poissonian above threshold. These two papers generated a significant amount of further work on squeezed pump lasers by Marte, Walls and coworkers [Marte 1988c, Kennedy 1989, Marte 1989, Haake 1989, Marte 1990, Ritsch 1991], however to our knowledge, none of this theoretical work has been verified experimentally, as is the case for semiconductor lasers.

Among these papers, two exist which should be mentioned especially. These are the papers of Marte and Zoller [Marte 1989, Marte 1990]. In this work, a Scully-Lamb master equation approach is used to describe a laser with sub-Poissonian pumping. The work differs from the Scully-Lamb approach however, in the way that pumping is described.

The pump process is described quantum mechanically as unitary evolution of the pump field, with quantum jumps representing a change in the state of the pump system rather than by a simple classical atomic pump rate. An average-field density matrix is derived as for the usual Scully-Lamb approach. Such a probabilistic description of the quantum mechanical degrees of freedom of the pump field, in combination with a master equation description had never been given before, and is similar to the approach we will take in our work, in which we average over the carrier degrees of freedom, yet retain a fully quantum mechanical description of the field.

Noise Suppression via Coulomb Blockade

More recently, attention has been focussed on a new method of noise suppression in semiconductor lasers using Coulomb blockade of the electron emission process. The fact that electronic currents in small tunnel junctions can be blocked by Coulomb interactions so that a single electron tunnels through the junction per unit time and coherent oscillations of the voltage result, was discovered by Averin and Likharev

[Averin 1986] as early as 1986. The question as to whether some kind of maser effect could be possible was raised by these authors, but it was not until Imamoğlu, Yamamoto, and Solomon [Imamoğlu 1992a] discussed the idea of Coulomb-blockade with reference to *p-n* microjunctions in 1993, that this idea resurfaced. The authors showed that Coulomb-blockade type voltages as they were termed, existed in constant-current driven *p-n* microjunctions operated at tempertaures below 3K. The voltage oscillations occur because of the regulated single-electron thermionic emission events from the *n*-layer into the *p*-layer. This regulated process is explained as follows. If the capacitance of the depletion layer is such that the voltage drop across the junction following a single thermionic emission event is much greater than the voltage of the thermal fluctuations, the electrons 'feel' this change, and a second emission event is blocked until the junction voltage is restored to its original value. Under constant-current operation, the junction voltage increases monotonically over a time scale given by e/I. Thus, thermionic emission events occur at regular intervals e/I and the junction voltage exhibits single-electron thermionic emission oscillations with the same period. Provided the electrons, which are subsequently thermionically emitted into the *p*-layer, recombine quickly compared to e/I, the junction will generate a regulated single-photon stream.

In a further paper [Imamoğlu 1992b], the authors gave theoretical results which showed that Coulomb-blockade of resonant tunnelling creates correlations between single-charge tunnelling and single photon emission events leading to a regulated single-photon stream. This stream is generated by constant-current driving and when the system is also operated under constant-voltage the stream is antibunched and sub-Poissonian. This work constituted the first prediction of non-classical photon generation in a constant-voltage-driven semiconductor heterojunction.

A further theoretical paper in the following year [Imamoğlu 1993]

gave explicit conditions for when macroscopic squeezing (which is the type of squeezing obtained in a high-impedance pump noise suppressed system, in which the anticorrelation between successive photon emission events is very small, but becomes important for a large number of photons), and when Coulomb-blockade operation (the strict regulation of individual electronic injection events signifying a highly non-classical state) would occur. The critical parameter which determines the regime of operation was found to be the ratio of the single electron charging energy to the characteristic energy of the thermal energy fluctuations. If this ratio is much less than one, we are in the macroscopic high temperature limit and the injection process is sub-Poissonian. If the ratio is greater than one, we are in the mesoscopic low-temperature limit, and the individual injection process is regulated, so that a non-stochastic spike appears at the single-electron charging frequency, with a squeezed background noise.

The next proposal was to remove the requirement of a high-impedance constant-current source yet to retain sub-Poissonian statistics, since constant-current operation is hard to achieve in practice. The alternative to the high-impedance constant-current source is an alternating (ac) voltage source together with a dc-bias. The device which achieves this is called a turnstile device [Imamoğlu 1994]. It works as follows; if a dc-bias voltage is chosen so that the electron tunnelling is resonantly enhanced when the time-dependant part of the applied junction voltage is zero, then the applied square voltage pulses enable resonant hole-tunnelling while blocking electron tunnelling, due to quantum confinement. A second tunnelling event of the same carrier during the time interval where the junction voltage remains unchanged is prevented by Coulomb-blockade. Thus only one electron and one hole can tunnel into the i-GaAs layer within a single cycle of the applied voltage. If the radiative recombination occurs on a time scale short compared to the period of the ac-voltage, a single photon is gen-

erated in each cycle with a probability approaching unity.

Most recently a method has been proposed in which a constant voltage source is used, but in which the pump noise suppresses itself [Yamanishi 1996]. The mechanism, which applies to a *p-i-n* junction diode, relies on a non-zero response of the recombination coefficient to external fields in the *n*- and *p*-barriers. This means electrons and holes in the quantum well polarise and effectively form a capacitor.

The detailed mechanism can be explained as follows: electron and hole pumping events and recombination events lead to an increase in the electric field. Associated with this is a decrease in the radiative recombination coefficient. These events also induce current spikes in the external circuit. The charge in these spikes moves quickly to the *n*- and *p*-barriers and the potential difference across the diode is recovered. The electric field is then again decreased, and a corresponding increase in the recombination coefficient occurs.

Using some algebra, the authors show that the reduction of the recombination coefficient due to one electron and hole pump event, and one recombination event is completely compensated for by the associated charge transfer. The reduction in the recombination coefficient which occurs is expected to suppress the subsequent emission until the recovery of the coefficient is accomplished by the pump-induced charges. Monte-Carlo simulations are carried out which indicate a regulation of photons and pump events for increased non-zero response to external fields.

The area of pump-noise suppression is one of continued active interest. To our knowledge regulated pumping via Coulomb-blockade has not yet been achieved (with or without high-impedance suppression) and neither have any experimental results for atomic lasers with non-classical pump statistics appeared. The most promising area to date therefore, appears to be high-impedance pump-noise suppression and it is the results of this theory [Yamamoto 1986, Machida 1987,

Yamamoto 1987] that we use to compare with the results of our theory.

1.1.3 Injection Locking

Injection locking has a long and extensive history, and a multitude of papers exist on this topic. We concentrate here on those that deal with effects of injection locking on noise in laser systems. In 1946, Adler [Adler 1946] gave a theoretical account of locking phenomena in electrical oscillators, using a differential equation approach. The work accounted for many synchronization phenomena which had been previously observed. In the years that followed, injection locking was observed in many different laser systems such as helium-neon lasers [Stover 1966], CO_2 lasers [Buczek 1972], and semiconductor lasers [Lang 1980]. Classical theories describing noise in the system can be found in texts on semiconductor lasers [Stratonovich 1967, Siegman 1986, Yamamoto 1991].

It was only in 1984 that Haus and Yamamoto [Haus 1984] gave a quantum mechanical treatment of noise of an injection locked oscillator, although Haken *et al.* [Haken 1967] had studied the quantum theory of locking of modes in a laser oscillator, and Chow *et al.* [Chow 1975] had shown that injection locking would cause a narrowing of the laser spectrum. In an analysis using both a Fokker-Planck equation approach and a Langevin equation approach, the amplitude and phase noise of the injection locked oscillator were calculated, and used to calculate the uncertainty product. Phase and amplitude spectra were given for differing amounts of phase and amplitude noise of the injected signal. It was found that at low frequencies the higher the noise in the injected signal, the higher the noise in the output signal, but at high frequencies, the noise in the output signal was unaffected by that of the input signal. For large detunings of the injected signal frequency from the cavity frequency, the noise was found to increase.

Soon afterwards, the spectral power densities for the intensity and

frequency noise of single-mode injection locked semiconductor lasers were studied as a function of injected power and detuning between the master and slave lasers [Spano 1986]. It was found that as the injection power is increased, the frequency noise spectrum of the slave laser becomes identical to that of the master laser. Theoretical results for the intensity noise indicated a similar behaviour. Detuning was found to shift the frequency spectrum only slightly upwards for low frequencies, but the resonance peak of the slave laser was found to be enhanced substantially. These experimental results indicated good agreement with the theory.

A thorough quantum mechanical analysis of single mode injection-locked semiconductor lasers was given in 1990 [Gillner 1990]. The approach used was the Langevin approach characteristic of Yamamoto's work with semiconductor lasers [Yamamoto 1987]. The model included pump noise suppression and squeezing of the injected signal. Variable parameters in their model included characteristic time scales in the system, detuning, pump strength, squeezing factor, and injection strength. Results were given for the steady-state internal and external field amplitudes as a function of the injection strength for various time scales. A sudden increase in the internal field amplitude was seen as the injected signal began to dominate the system. This effect was also seen in the plot of the external field amplitude. The external field amplitude was also plotted as a function of the detuning, and it was found that the amplitude is greatest for large detunings. This is because for large detunings the injected signal ceases to be resonant with the cavity field, and so doesn't interfere destructively with it.

External amplitude and phase noise spectral densities (or correlation functions) were also calculated. It was found that the phase noise decreases as injection strength is increased, and that the amplitude noise increases (for low frequencies away from the resonance peak). The noises were also plotted as a function of the detuning, and were

shown to increase slightly until a particular detuning determined by the linewidth enhancement factor β was reached, at which point a sharp increase was observed. The effect of a squeezed injection signal on the noise was also investigated. It was found that for the phase noise the minimum noise occurs at a value of the squeezing factor which approximately equals the linewidth enhancement factor. For the amplitude noise, this minimum occurs for a coherent state. The authors also checked that the Heisenberg uncertainty principle was not violated.

In 1991 Agarwal and coworkers considered injection locking in which the injected signal enters from the side of the cavity [Agarwal 1991]. They found the results that for regular pumping the output light is amplitude squeezed for all injection strengths for the laser, and for some injection strengths (due to Rabi oscillations) for the maser. For random pumping, the results for the maser do not change much, but for the laser a squeezed output is no longer obtained.

In 1991, an injection locking scheme was proposed by Lai, Haus, and Yamamoto to prepare squeezed vacuum states from squeezed amplitude states [Lai 1991]. Two schemes were proposed, the first consisting of a laser diode which produces amplitude squeezed states and is phase locked to a coherent signal (the master laser), and the other system which consists of two phase-locked laser diodes which are injection locked.

Experimental results obtained by Wang, Freeman and Steel in 1993 [Wang 1993] reported that 3 dB of photon number squeezing was obtainable from a quantum well laser injection locked to a coherent signal. The results were taken at 10 K and 78 K. In each case an intensity noise reduction is reported compared to the free-running case. The authors discovered that a multi-mode analysis was required to explain this effect, since such an intensity noise reduction compared to the free-running case had not been predicted by a single-mode analysis (e.g. [Gillner 1990]). The authors' explanation was that since injec-

tion locking suppresses the side mode power by more than 10 dB, the contribution of the side modes to the total intensity noise would be significantly reduced.

A model of injection locking in a solid state laser was given in 1995 by Farinas *et al.* [Farinas 1995] based on laser equations for the laser field, atomic polarisation and population inversion. Frequency noise and intensity noise were also measured experimentally, and the frequency noise was found to be less in the injection locked laser than in the free-running slave laser, and about the same as the master laser. The intensity noise of the two cases (free-running and injection locked) were not found to differ much from each other. These experimental results were found to agree well with their model.

In 1995, Fontanelle and Davidovich [Fontanelle 1995] presented a model for the single-mode injection locked laser, which made no assumptions regarding the sizes of decay constants. As such, the model could be widely applied to a number of laser systems. A range of possible pumping schemes was considered and the photon number variance and homodyne spectra of the output were discussed. They found that injection improves amplitude squeezing and sub-Poissonian light generation close to threshold, but that quantum noise reduction is spoilt for very high pump rates. A Langevin approach was used and four regimes are identified.

The first of these is when the atomic polarisation and population decay rates are much greater than the field decay rate, such as in dye lasers. In this situation, one would normally adiabatically eliminate the atomic variables. It was found that for regular pumping, reduced amplitude fluctuations were obtained for the injected laser. The biggest reduction occurred close to threshold and for low frequencies.

In the second case, the atomic polarisation decay rate was much greater than the field decay rate, which is approximately equal to the atomic population decay rate, such as in helium-neon and argon-ion

lasers. In the third case, which involves the same approximations as in the second case as far as the spectral calculation goes, the atomic polarisation decay rate was much greater than the field decay rate, which is much greater than the atomic population decay rate. This is the situation in ruby, Nd:YAG, CO_2, and semiconductor lasers. In these cases squeezing was obtained for pump rates close to threshold, where uninjected lasers do not display squeezing. For higher pump rates however, the noise levels are increased.

The final case was when the field decay rate is much greater than the atomic population decay rate and polarisation decay rates which includes near infrared noble gas lasers and many far infrared gas lasers. The results here are similar to the previous two cases, where for lower pump rates, the injected laser produced squeezing, whereas the non-injected laser did not.

Most recently a linearised input/output method has been proposed to describe the intensity noise of injection locked lasers [Ralph 1996]. A four level atom model is given and three frequency regimes are found. At low frequencies the intensity fluctuations are simply the sum of fluctuations of the master and slave lasers (each scaled by their own intensities), at middle frequencies the master fluctuations are amplified in the same way as by a linear optical amplifier, where the slave noise source is suppressed, and at high frequencies the output is just master fluctuations scaled by the slave intensity. Experimental results are compared qualitatively with the theoretical results.

Thus extensive research in the area of injection locking has been undertaken. Some results indicate that a multi-mode analysis is required to fully explain the behaviour of the injection locked system compared to the free-running system, and we provide such a model in this thesis.

1.1.4 Multi-Mode Theories

More recently, attention has turned to describing multi-mode semiconductor lasers, and attempts have been made to understand the noise behaviour in these systems, as well as to try to reduce this noise.

The first multi-mode analysis of semiconductor lasers was given by Inoue *et al.* [Inoue 1992] in 1992. Using the standard Yamamoto equations (for example in [Yamamoto 1987]), but including two extra equations for the two additional modes considered, spectral densities are derived. The authors make four assumptions under which their theory is valid.

- They consider three lasing modes, as mentioned, one main mode, and two side modes.
- It is assumed that the stimulated emission gain of the main mode is slightly higher than those of the side modes because of a finite gain bandwidth, but the stimulated emission gains of the side modes are taken to be the same.
- All modes have the same internal and mirror losses.
- Ideal population inversion is created in the active layer, so the stimulated absorption rate is neglected.

The spectral densities calculated by the authors are the external intensity noise spectral densities for the individual modes and for the total intensity, as well as the cross-correlation spectral densities between the main mode and either one side mode, or the sum of the two side modes. The results are calculated as a function of pump strength.

For the intensity noise spectral densities, it is found that the total noise goes below the shot-noise limit, but that the individual noises do not. The cross-correlation spectral densities indicate a negative correlation between the central mode and the sum of the two side modes,

which suggests that anticorrelations between the mode noises lead to the observed noise reduction in the total intensity.

The authors attribute the observed negative correlation to cross-gain saturation. The increase of spontaneous emission coupling to the main mode makes the intensity of the main mode higher; then the gain of the side-mode is suppressed. The converse is also true. This only occurs in a homogeneously broadened medium however. If the gain medium is inhomogeneously broadened, the correlation disappears and the total intensity fluctuation is not reduced. This was verified by the authors.

In the same year further experimental results suggesting correlations between multiple modes in lasers were published [Harris 1992]. In this case, single-sideband and double-sideband intensity fluctuation spectra were measured for an argon-ion laser, and it was found that there was less noise in the double-sideband spectrum than in the single-sideband spectrum. The authors attributed the behaviour to anticorrelated sidebands.

In 1993 two experimental schemes appeared [Wang 1993, Freeman 1993b] in which attempts were made to suppress the noise in a multi-mode system by suppressing the side modes. The two methods involved injection locking and external grating stabilization respectively. In the first of these 3 dB of squeezing was reported, and in the second 1.8 dB.

The authors of the first paper felt that the system exhibited behaviour somewhere intermediate between homogeneous and inhomogeneous broadening, and thus, that if the side modes were suppressed, the total photon number fluctuation would be reduced.

In the second paper, no theoretical explanation of why noise suppression is achieved with a grating stabilised laser is given, although the fact that the approximations of Inoue [Inoue 1992] did not hold for the particular laser used by Freeman *et al.*, was a motivation for examining

the effect of suppressing the side modes, by using an external grating, on the noise of the system.

In 1994, Loudon *et al.* [Loudon 1994] extended their previous work and presented theoretical expressions for the correlation functions which were then used to explain their previous results. Gain measurements which showed similar correlations to the noise, were also given.

In 1995, Kitching *et al.* [Kitching 1995] produced amplitude squeezed states using a Fabry-Perot quatum well semiconductor laser, and in trying to match their results with theory, came to the conclusion that a multi-mode analysis should be used. Their results indicated that weak optical feedback led to a reduction of noise larger than that predicted by a single mode theory, which they attributed to an amplitude-phase correlation mechanism in combination with asymmetric cross-mode nonlinear gain saturation. Under these effects, the gain of one mode depends on the intensity of neighbouring longitudinal modes, which can lead to an increase of amplitude noise at low freuencies. This increase is accompanied by an increase in the carrier noise, which is strongly correlated with the total amplitude noise. The carrier fluctuation modulates the refractive index, which causes fluctuations in the phase of the main mode. Dispersive loss couples the phase fluctuations back into the main mode amplitude, and because of stronger correlations between the amplitude and the phase, the amplitude reduces by a larger amount than predicted by a single mode theory.

An alternative explanation, more in line with the predictions of Wang *et al.* [Wang 1993] was provided in 1995 by Marin *et al.* [Marin 1995]. The authors applied the theory of Inoue *et al.* [Inoue 1992], but modified the theory to include some inhomogeneity by adding a self-saturation of each mode due to its own fluctuations, since the purely homogeneous behaviour suggested by Inoue *et al.* implies perfect anticorrelations which were not always seen experimen-

tally. Comparing their theoretical results with experimental results, they showed that agreement was obtained.

1.2 Technical Aspects of Semiconductor Lasers

1.2.1 Introduction

Since this thesis discusses only semiconductor laser systems, and since this particular type of laser has complex aspects to both its design and operation, which are not relevant to other systems, it is worthwhile discussing here some of the more technical aspects of semiconductor lasers.

This section describes pertinent considerations for designing such a laser, such as mode confinement and hence laser structure, as well as features which appear when the laser is operated, such as linewidth enhancement and homogeneous and inhomogeneous broadening.

The material presented in this chapter could be found in any text on semiconductor lasers [Agrawal 1986, Saleh 1991], but we provide it here for the convenience of the reader, since much of the terminology is utilised throughout the body of this thesis.

1.2.2 General Features

Semiconductors consist basically of a forward-biassed p-n junction. The bias voltage lowers the potential barrier for the electrons, causing a current to flow and recombination to occur. The process is known as minority carrier injection. The gain is provided by electron-hole recombination in the depletion region of the junction, and the polished end facets of the semiconductor provide the optical feedback. Variations on the basic p-n junction take the form of layers of lower bandgap semiconductor sandwiched in between the p-layers and the n-layers. Such

devices are called heterostructure devices. For such heterostructure devices, careful matching of lattice constants is required to reduce the possibility of lattice defects.

A considerable number of semiconductor materials have exhibited lasing over a range of wavelengths from 0.3-100 μm. By varying the composition of the semiconducting elements in a particular material, the wavelength of the semicondutcor laser can be varied over a range of wavelengths.

A semiconductor laser differs from other types of lasers in several respects. Significant among these differences is the influence of external pumping on the gain and refractive index. This refractive index variation causes a shift in frequency of the modes with pumping.

Another difference is that in a semiconductor laser there are two contributions to the phase noise, whereas in other laser systems only spontaneous emission contributes. The additional contribution comes about in semiconductor lasers due to carrier number fluctuations which arise from the relaxation which occurs after a spontaneous emission event. These fluctuations affect the optical gain, which in turn changes the refractive index, and hence the phase. The linewidth enhancement factor gives a proportionality between the gain and index changes, and is defined by the ratio of the real part of the complex susceptibility of the medium to the imaginary part. The expression for the linewidth is modified by this process, such that the spectrum that would be obtained in the absence of this process is multiplied by the factor $(1 + \beta^2)$. The physical interpretation is that each spontaneous emission event gives rise to instantaneous and delayed phase fluctuations.

1.2.3 Modes and Mode Structure

The modes of a semiconductor laser differ from those of an optical oscillator, because they are confined to the gain medium in a direction perpendicular to the beam propagation. This means that in addition

to the longitudinal modes supported by the Fabry-Pérot cavity, transverse and lateral modes also exist. Generally, single mode operation is desired, and to achieve this, the mode must be controlled and confined.

Confinement of the transverse mode (which is in the direction perpendicular to the junction plane) occurs through dielectric waveguiding. The mechanism is called index guiding, because the higher refractive index of the cladding compared to the active layer causes total internal reflection and thus mode confinement. Lateral confinement (in the direction parallel to the junction plane but perpendicular to the longitudinal propagation direction) can be achieved either by index-guiding or by gain-guiding.

Gain-guiding is a mechanism by which the optical mode is confined by the variation in optical gain along the junction plane. This is usually achieved via some built-in feature which restricts current injection to a small region along the junction plane.

Although gain-guided lasers are easier to fabricate than index-guided lasers, they have several disadvantages compared with index guided lasers. A major disadvantage is that higher threshold currents are required to operate them. In addition, the light-current characteristic of a gain-guided laser often exhibits a non-linearity due to movement of the mode along the junction plane, or transition to another mode. This can severely alter the amount of light which couples into an optical fibre, and so limits the use of the laser in optical communications systems. Gain-guided lasers can also exhibit pulsations in the emitted light due to the non-uniformity of the carrier density along its length, and have low differential quantum efficiency. Thus index-guiding is almost invariably used.

In principle, several longitudinal modes could be supported by the cavity but in practice, only some reach threshold, and this is dictated by details of the gain spectrum, such as gain width, and the gain-broadening mechanism. In the presence of homogeneous broadening,

only one longitudinal mode reaches threshold, and the laser maintains single longitudinal mode operation. This occurs because when the laser is turned on, all modes for which the initial gain is greater than the loss begin to grow. Modes whose frequencies lie closest to the central transition frequency grow most quickly. These photons interact with the medium and reduce the gain by depleting the population difference. Because the gain coefficient is reduced uniformly, for modes sufficiently distant from the line centre, the loss exceeds the gain; the side modes lose power, while the more central modes continue to grow. In the end, only a single mode maintains a gain equal to the loss.

This simple text book definition however, does not agree with what we have observed in the detailed calculations of this thesis. Referring forward to Fig 3.6, we see that both the central and the side modes reach threshold. The side modes saturate however, for much lower pump rates than the central mode.

In practice, homogeneously broadened lasers can actually oscillate in multiple modes because the different modes occupy different spatial portions of the active medium. When oscillation on the most central mode is established, the gain coefficient can still exceed the loss coefficient where the standing wave electric field of the most central mode vanishes. The phenomenon is called spatial hole burning. Homogeneous broadening in semiconductor lasers is usually associated with electron-phonon collisional broadening.

The gain profile is largely homogeneously broadened for semiconductor lasers, but because many longitudinal modes oscillate simultaneously, a significant amount of power is carried out by the side modes, even above threshold. Spectral hole burning as well as spatial hole burning may contribute to the spectral features, despite the fact that spectral hole burning is an effect of inhomogeneous broadening.

In an inhomogeneous medium the gain is a composite envelope of the gains of different species. After laser turn-on, the situation is the

same as in the case of homogeneous broadening. Modes for which the gain is greater than the loss grow and the gain decreases.

If the mode frequency spacing is greater than the frequency spacing between the constituent lineshapes, different modes interact with different carriers. Carriers whose lineshapes do not coincide with any of the modes are ignorant of the presence of photons in the resonator. Their population difference is not affected and their gain contributes to the unsaturated gain. Carriers whose frequencies do coincide with the modes deplete their inverted population and the gain saturates, which leads to holes in the spectral profile. The process of saturation by hole burning progresses independently for the different modes until gain equals loss for each mode in steady-state. Modes do not compete because they draw power from different rather than shared atoms, and thus the many modes oscillate independently.

The spectral purity of a semiconductor laser is specified by the mode suppression ratio (MSR), which is the ratio of the main mode power to the power carried by the most intense side mode. An MSR value of twenty is generally considered large enough for a laser to be considered a single-mode laser. The results of Marin *et al.* [Marin 1995] and the results in this thesis however, indicate that even when the power of the most powerful sidemode is only one thousandth of the power of the central mode, a significant modification of the noise spectrum results compared to the situation in which there is truly only a single mode present.

1.2.4 Laser Structures

Different laser structures are essentially different ways of confining the lateral mode, with a view to producing a low threshold device which operates in the fundamental mode. Essentially, there are four different groups of lasers, classified by the method used to confine the lateral mode. The group for which the lateral mode is unconfined is called

the broad-area laser group, and for the confined mode there are gain-guided lasers, weakly-index-guided lasers, and strongly-index-guided lasers. These are now each discussed in turn.

Broad-Area Lasers

The broad-area laser is that in which there is no lateral confinement. As a result high threshold currents are required of ~ 1 A, which seriously limits the usefulness of such a laser. Some dependence does exist of the threshold current on parameters such as active layer thickness and doping concentration, however the threshold current cannot be reduced by amounts significant enough to make them useful, and so these lasers are not discussed further here.

Gain-guided lasers

The restriction of current injection to a small region along the junction plane provides several advantages over the broad-area laser. Firstly, continuous-wave operation is enabled with threshold currents which are 10-100 times smaller than those for broad-area lasers. In addition, fundamental-mode operation along the junction plane is allowed, which is necessary if the light is to be coupled out into something else, such as an optical fibre. Heat-sinking requirements are also considerably less severe than for a broad-area laser, and the lower operating current enables operation at higher temperatures and increases the operating life of the device.

The three basic gain-guided structures (of which variations exist), are the oxide-stripe laser, the proton-stripe or deuteron-stripe laser, and the junction-stripe laser. In the first of these a SiO_2 layer on the p-contact around an opening restricts injected current flow to this small opening. In the second, a similar restriction is provided by implanting protons or deuterons to create a region of high resistivity. The current then only flows where the protons and deuterons have not been

implanted. In the junction-stripe laser, Zn diffusion converts a small region of the top n-type layer into p-type, thus providing a current path. Undesirable characteristics of gain-guided lasers, as discussed previously, make index-guided lasers the preferred choice for many applications however.

Weakly-index-guided lasers

In weakly-index-guided lasers, the laser structure is modified so as to introduce an effective index step of about 10^{-2}. The optical mode along the junction plane is then essentially determined by the structure of the particular device. The design of a weakly index-guided lasers requires that the thickness of at least one layer be nonuniform in a lateral direction. The types of weakly index-guided lasers can be broadly grouped into two categories; ridge-waveguide structures, and rib-waveguide structures. In the ridge-waveguide, the use of a dielectric around the ridge prevents current spreading into the p-layer. In the rib-waveguide structure however, the thickness of the waveguide layer is varied, which prevents current spreading outside this region. Typical threshold currents for the ridge structure are 40-60 mA, and for the rib-structure 60-80 mA.

Strongly-index-guided lasers

In strongly-index-guided lasers, the active region is buried in higher bandgap layers on all sides, and thus these layers are called buried heterostructure lasers. The index step across the junction in the lateral direction is ~ 0.2 in these structures and is about two orders of magnitude larger than carrier-induced effects. Lasing characteristics of buried-heterostructure lasers are primarily determined by the rectangular waveguide that confines the mode inside the active region. Buried heterostructure lasers can be divided into two categories; planar-active-layer structures, and non-planar-active-layer structures, depending on

the shape of the active layer. Threshold currents for buried heterostructures are typically 10-15 mA, but these lasers have the disadvantage that they are more difficult to fabricate than other types of lasers.

Quantum well lasers

Another important class of semiconductor lasers which should be discussed is the quantum well laser. If the thickness of the active layer of a semiconductor laser is made sufficiently narrow, quantum effects begin to play a role. In a double-heterostructure laser (simply a device in which the active region is surrounded on both sides by cladding layers of higher band gap), the bandgap energy of the active layer is smaller than that of the surrounding layers, and so the structure acts as a quantum well. Because of the reduction in active layer thickness, the threshold current density for the single quantum well is much lower than for the types of lasers already discussed at ~ 0.5mA. Additional attractive features of quantum well lasers are the narrower gain coefficient spectrum, the smaller laser mode linewidth, and reduced temperature dependence. Semiconductor lasers fabricated in quantum wire and quantum dot configurations provide even lower threshold currents (less than 0.1mA).

Chapter 2

Master Equation Theory for a Single Mode Semiconductor Laser

2.1 Introduction

As mentioned in Chapter 1, the quatum theory of the semiconductor laser formulated by Haug [Haug 1967a] has formed the basis of nearly all treatments in which quantum statistical effects are of interest. The methodology which developed out of this paper is summarised in Chapter 1.

The motivation for the work in this chapter was the work of Yamamoto *et al.* [Yamamoto 1986, Machida 1987, Yamamoto 1987, Richardson 1991] on modelling the production of sub-Poissonian light by pumping the semiconductor laser with a sub-Poissonian electrical current.

Yamamoto used as the theoretical basis of his model the theory of Haug, however we feel that there is a reason to develop a somewhat more precise methodology, which does not rely so much on the mixture of phenomenological concepts with operator Langevin equations, and the rather intuitive replacement of operators with averages which are

factorized where necessary. The major problem we see in the present methodology is the lack of a clear *fundamental* understanding of the validity of the approximations made. We hasten to emphasize that the achievements of this methodology are significant, and the depth of physical understanding which workers in the field have of the systems they deal with almost invariably protects them from error. However, when dealing with subtle effects such as the production of nonclassical light, it would seem wise to attempt a more carefully formulated theoretical methodology.

Our aim is to present a new approach in deriving semiconductor laser equations using master equation methods, which are well known in quantum optics [Louisell 1974, Gardiner 1991]. Such a procedure has the advantage of being a systematic derivation, in which any approximations are clearly stated. Furthermore, because of the systematic nature of the derivation, further physical processes can easily be included in the description of a particular system if desired.

A master equation description of the full semiconductor system, describing both intra- and interband processes can easily be written down, but such a description is unfortunately not terribly useful, because of the coupling to every single state of the semiconductor introduced by intraband processes. Because of the different time scales on which intra- and interband motion occur, we will be able to formulate a description in which only the total number of electrons in each band is used, the actual distribution within the band being given by the Fermi distribution. We thus achieve a description which involves the full quantum statistics of the lasing mode of the electromagnetic field, but only requires the total numbers of electrons within each band. This description is *derived* as a result of the very different time scales involved and of course the Hamiltonian for the system.

2.2 Derivation of a Reduced Master Equation

2.2.1 Description of the System

The Hamiltonian for the semiconductor system is given as follows,

$$H = H_F + H_E + H_{EF} + H_{FB} + H_{EB_1} + H_{EB_2} \tag{2.1}$$

$$H_F = \hbar\omega b^\dagger b \tag{2.2}$$

$$H_E = \sum_k \hbar\omega_{p_k} p_k^\dagger p_k + \sum_{k'} \hbar\omega_{q_{k'}} q_{k'}^\dagger q_{k'} \tag{2.3}$$

$$H_{EF} = i\hbar \sum_{kk'} \left\{ g_{kk'} b c_{kk'}^\dagger + g_{kk'}^* b^\dagger c_{kk'} \right\} \tag{2.4}$$

$$H_{FB} = i\hbar \sqrt{\frac{\kappa}{2\pi}} \sum_i \left\{ b^\dagger \Gamma_i + \Gamma_i^\dagger b \right\} \tag{2.5}$$

$$H_{EB_1} = i\hbar \sum_{kk'} \sqrt{\frac{\mu_{kk'}}{2\pi}} \left\{ c_{kk'}^\dagger \Gamma_{kk'} + c_{kk'} \Gamma_{kk'}^\dagger \right\} \tag{2.6}$$

$$H_{EB_2} = i\hbar \sum_{kl} \sqrt{\frac{\gamma_{kl}}{2\pi}} p_k^\dagger p_l \Xi_{kl} + \sum_{k'l'} \sqrt{\frac{\gamma_{k'l'}}{2\pi}} q_{k'}^\dagger q_{l'} \Xi_{k'l'} + h.c. \tag{2.7}$$

The variables in these terms have the following meanings:

- ω is the lasing frequency.
- b is the boson annihilation operator for the lasing mode.
- The fermion annihilation operator for an electron in the conduction band of the semiconductor is denoted p_k, and $q_{k'}$ is the corresponding fermion annihilation operator for an electron in the valence band. We also define

$$n_{e,k} \equiv p_k^\dagger p_k, \text{ the electron number operator} \tag{2.8}$$

$$n_{h,k'} \equiv q_{k'} q_{k'}^\dagger, \text{ the hole number operator} \tag{2.9}$$

- ω_k ($\omega_{k'}$) corresponds to the frequency associated with the energy of a free electron in state k (k') of the conduction (valence) band.

- The process of an electron making a transition from one band to another is represented by the operators $c^\dagger_{kk'}$ and $c_{kk'}$ for upward and downward transitions respectively, where $c^\dagger_{kk'} = p^\dagger_k q_{k'}$ and $c_{kk'} = q^\dagger_{k'} p_k$.

- The strength of the interaction between the field and the semiconductor is described by the coupling constant $g_{kk'}$.

- Decay of the field to the reservoir is characterized by the coupling constant $\sqrt{\kappa/2\pi}$.

- The external modes to which the field is coupled are denoted Γ_i.

- Transitions of electrons between states occur in two ways. The first is by interband transitions in which there is an interaction with non-lasing field modes of the reservoir, described by $\Gamma_{kk'}$. This process is characterized by the coupling constant $\sqrt{\mu_{kk'}/2\pi}$. The second is by intraband scattering processes, where electrons scatter to states of different k and k'. We model this process by interacting with a heat bath [Gardiner 1991], denoted by Ξ_{kl}, and $\Xi_{k'l'}$, rather than the full coulombic interaction, because it is simpler to do so, and the final equations are not sensitive to the particular model used. This process is characterized by the coupling constants $\sqrt{\gamma_{kl}/2\pi}$.

- H_F and H_E describe the free parts of the Hamiltonian for the field and electrons respectively. We have chosen to deal here with a high-Q cavity, as is the case in whispering-gallery mode microdisk lasers [McCall 1992], and thus we may restrict our attention to one field mode in H_F. However, the description could easily be extended to a multi-mode system if desired.

- The dipole coupling of the electrons to the laser field is described by H_{EF}.

- H_{FB}, H_{EB_1}, and H_{EB_2} describe couplings of the internal modes to the external reservoir modes. H_{FB} describes the coupling of the internal light mode to the external light modes, in other words, irreversible damping. H_{EB_1} describes the coupling of the dipole moment operator to the external light modes, and H_{EB_2}, the coupling of the electron number operator to other electronic states, or thermal scattering.

2.2.2 Adiabatic Elimination

Each thermal state of the system is describable in terms of the variables for temperature, T, the total number of electrons in the conduction band, n_e, and the total number of holes in the valence band, n_h, where the total number in each band is a sum over numbers in all states of the band $n_i = \sum_k \langle n_{i,k} \rangle$. The adiabatic elimination must be carried out over all such states of the system.

In a semiconductor several different processes occur, as is evidenced by the many contributions to the Hamiltonian Eqns (2.1)-(2.7). These processes occur on different time scales. Interaction of the electrons with the cavity field mode resulting in an optical transition occurs on a relatively slow time scale ($\sim$ ns). This process is followed adiabatically by a thermal redistribution of the electrons within each band, so that quasi-equilibrium, or local equilibrium within the bands is obtained. The coulombic interactions which cause this scattering to take place are very strong, much stronger than the interaction between the semiconductor and the cavity field mode, and hence thermal equilibrium is reached very quickly ($\sim$ ps). This equilibration is only within a band, so the total numbers of electrons within each band are not disturbed; thus the quasi-equilibrium reached is characterized by two conserved quantities, the number of electrons in the conduction band and the number of holes in the valence band. Elimination of the variables which describe the momentum/energy distribution within the band is possible

using projection operator techniques [Gardiner 1991], but there will be a different projector for every possible number of electrons and holes. A method of multiple projectors will be needed to take care of this situation, and such a method has not to our knowledge been used before.

Liouvillians

The master equation for the full semiconductor system, which follows by standard techniques [Louisell 1974, Gardiner 1983] from the full Hamiltonian (2.1) including heat bath operators may be written as follows

$$\dot{\rho} = \mathcal{L}_1\rho + \mathcal{L}_2\rho + \mathcal{L}_3\rho, \tag{2.10}$$

where

$$\mathcal{L}_1\rho = \mathcal{L}_{\text{scatt}}\rho - \frac{i}{\hbar}\left[\sum_{kk'}\hbar\omega_{p_k}p_k^\dagger p_k + \hbar\omega_{q_{k'}}q_{k'}^\dagger q_{k'}, \rho\right], \tag{2.11}$$

$$\mathcal{L}_2\rho = \sum_{kk'}\left[g_{kk'}bc_{kk'}^\dagger + g_{kk'}^* b^\dagger c_{kk'}, \rho\right], \tag{2.12}$$

$$\begin{aligned}\mathcal{L}_3\rho = {} & \frac{\kappa}{2}\bar{N}(2b^\dagger\rho b - bb^\dagger\rho - \rho bb^\dagger) \\ & + \frac{\kappa}{2}(\bar{N}+1)(2b\rho b^\dagger - b^\dagger b\rho - \rho b^\dagger b),\end{aligned} \tag{2.13}$$

and

$$\begin{aligned}\mathcal{L}_{\text{scatt}} = {} & \sum_{kl}\bar{N}_{kl}^{\text{E}}\frac{\gamma_{kl}}{2}(2p_k^\dagger p_l\rho p_l^\dagger p_k - p_l^\dagger p_k p_k^\dagger p_l\rho - \rho p_l^\dagger p_k p_k^\dagger p_l) \\ & + \sum_{kl}(\bar{N}_{kl}^{\text{E}}+1)\frac{\gamma_{kl}}{2}(2p_l^\dagger p_k\rho p_k^\dagger p_l - p_k^\dagger p_l p_l^\dagger p_k\rho - \rho p_k^\dagger p_l p_l^\dagger p_k) \\ & + \sum_{k'l'}\bar{N}_{k'l'}^{\text{E}}\frac{\gamma_{k'l'}}{2}(2q_{k'}^\dagger q_{l'}\rho q_{l'}^\dagger q_{k'} - q_{l'}^\dagger q_{k'}q_{k'}^\dagger q_{l'}\rho - \rho q_{l'}^\dagger q_{k'}q_{k'}^\dagger q_{l'}) \\ & + \sum_{k'l'}(\bar{N}_{k'l'}^{\text{E}}+1)\frac{\gamma_{k'l'}}{2}(2q_{l'}^\dagger q_{k'}\rho q_{k'}^\dagger q_{l'} \\ & - q_{k'}^\dagger q_{l'}q_{l'}^\dagger q_{k'}\rho - \rho q_{k'}^\dagger q_{l'}q_{l'}^\dagger q_{k'})\end{aligned} \tag{2.14}$$

describes intraband scattering.

The $\mathcal{L}_1\rho$ term describes all electronic parts of the equations of motion which do not change the number of electrons within a band. It includes all intraband processes and hence all the motion which occurs on the fast time scale. The $\mathcal{L}_2\rho$ term describes the optical interaction with the electrons in the system (which takes place on a slower time scale) both with the lasing or cavity mode, and the reservoir field modes, and the $\mathcal{L}_3\rho$ term describes the cavity field part of the system including loss from the system.

Projection operators

The processes in the system, which occur on three different time scales characterized by the coupling constants γ_{kl} or $\gamma_{k'l'}, \kappa$, and $g_{kk'}$, have now been distinguished by writing the master equation in this form. Since $\mathcal{L}_1$ describes the fast motion of the system, and thus $\gamma_{kl}, \gamma_{k'l'} \gg \kappa, g_{kk'}$, the adiabatic elimination can be performed by projecting onto the stationary states of $\mathcal{L}_1$.

The projection operators $\mathcal{P}(\underline{n})$ acting on ρ, project the system onto a subspace of definite $\underline{n} = (n_e, n_h)$, in which each band is in quasi-equilibrium, and can be described by a temperature T—this is the space of stationary solutions of the equation of motion $\dot{\rho} = \mathcal{L}_1\rho$. The subspace (in the space of density operators) complementary to the union of *all* of these subspaces describes the deviation from quasi-equilibrium, which under the influence of the scattering is very rapidly damped to zero. The formal definition of the projection operator $\mathcal{P}(\underline{n})$ is

$$\mathcal{P}(\underline{n})\rho = \rho_{\mathrm{T}}(\underline{n}) \otimes \mathrm{Tr}_{\mathrm{T}}\{p(\underline{n})\rho\}, \tag{2.15}$$

where $p(\underline{n})$ is a projection operator on the state vectors, which projects out the part of the state vector with the definite value $\underline{n} = (n_e, n_h)$ of numbers of electrons and holes. The first factor in the definition of

Equation (2.15) is defined by

$$\rho_{\mathrm{T}}(\underline{n}) \equiv \rho_h(n_h) \otimes \rho_e(n_e), \tag{2.16}$$

where $\rho_e(n_e)$, $\rho_h(n_h)$ are thermal density operators corresponding to $\underline{n} = (n_e, n_h)$ electrons and holes.

The factorized nature of the density operator allows us to write

$$\langle (n_{ek} n_{hk'})(\underline{n}) \rangle \;=\; \langle n_{ek}(n_e) \rangle \langle n_{hk'}(n_h) \rangle. \tag{2.17}$$

Of course all information we need is contained in the second factor of Equation (2.15) so that it will be convenient to define

$$\rho_{\mathrm{o}}(\underline{n}) \equiv \mathrm{Tr}_{\mathrm{T}}\{p(\underline{n})\rho\}, \tag{2.18}$$

which is a density operator in the space of the operators $b, b^\dagger$, which describe the lasing mode, and is also a function of n_e and n_h.

Our aim is to find an equation of motion for $\rho_{\mathrm{o}}(\underline{n})$. The total numbers of electrons and holes present, $\underline{n}$, characterize the different possible stationary solutions of the equation $\dot{\rho} = \mathcal{L}_1 \rho$, and the optical part of the Hamiltonian causes a relatively slow evolution of the distribution of the observed state over these stationary states. The effect of the elimination is to yield an equation of motion in which we fully quantize the electromagnetic field, but describe the electrons and holes simply by the total numbers of each present.

In order to carry out the derivation, we must use the following properties of the projection operators which are easily checked, and are analogous to those which are essential for the adiabatic elimination of the normal kind (in which there is only one stationary solution to the equation $\dot{\rho} = \mathcal{L}_1 \rho$), to be possible [Gardiner 1991]:

- The $\mathcal{P}(\underline{n})$ project onto the stationary states of $\mathcal{L}_1$; therefore

$$\mathcal{P}(\underline{n})\mathcal{L}_1 = \mathcal{L}_1 \mathcal{P}(\underline{n}) = 0. \tag{2.19}$$

- Because the interaction has no diagonal elements in the bath representation,

$$\mathcal{P}(\underline{n})\mathcal{L}_2\mathcal{P}(\underline{m}) = 0. \tag{2.20}$$

for any $\underline{n}$, $\underline{m}$.

- Further, because $\mathcal{P}(\underline{n})$ and $\mathcal{L}_3$ operate in different subspaces.

$$\mathcal{P}(\underline{n})\mathcal{L}_3 = \mathcal{L}_3\mathcal{P}(\underline{n}). \tag{2.21}$$

Derivation of the reduced master equation

The elimination procedure is most conveniently carried out by using the Laplace transform, $\tilde{\rho}(s) = \int_0^\infty \rho(t)e^{-st}dt$. This gives

$$s\tilde{\rho}(s) - \rho(0) = (\mathcal{L}_1 + \mathcal{L}_2 + \mathcal{L}_3)\tilde{\rho}(s). \tag{2.22}$$

We introduce

$$\tilde{v}(\underline{n}, s) = \mathcal{P}(\underline{n})\tilde{\rho}(s), \tag{2.23}$$

and

$$\begin{aligned} \tilde{w}(s) &= \Big(1 - \sum_{\underline{m}} \mathcal{P}(\underline{m})\Big)\tilde{\rho}(s) \\ &\equiv \mathcal{Q}\tilde{\rho}(s), \end{aligned} \tag{2.24}$$

(which defines the complementary projector $\mathcal{Q}$) so that

$$\tilde{\rho}(s) = \sum_{\underline{n}} \tilde{v}(\underline{n}, s) + \tilde{w}(s). \tag{2.25}$$

We can use these relations in our transformed master equation to get

$$s\tilde{v}(\underline{n}, s) - v(\underline{n}, 0) = \mathcal{P}(\underline{n})\mathcal{L}_2\tilde{w}(s) + \mathcal{L}_3\tilde{v}(\underline{n}, s) \tag{2.26}$$

$$\begin{aligned} s\tilde{w}(s) - w(0) &= \Big(\mathcal{L}_1 + \mathcal{L}_3 + \mathcal{Q}\mathcal{L}_2\Big)\tilde{w}(s) \\ &\quad + \sum_{\underline{m}} \mathcal{Q}\mathcal{L}_2\tilde{v}(\underline{m}, s). \end{aligned} \tag{2.27}$$

Rearranging the equation for $\tilde{w}(s)$, and dropping the $w(0)$ term (which gives only transient terms, which we may neglect),

$$\tilde{w}(s) = \Big(s - \mathcal{L}_1 - \mathcal{L}_3 - \mathcal{Q}\mathcal{L}_2\Big)^{-1} \mathcal{Q}\mathcal{L}_2 \sum_{\underline{m}} \tilde{v}(\underline{m}, s). \tag{2.28}$$

Substituting into the equation for $\tilde{v}(s)$ leads to

$$\begin{aligned} s\tilde{v}(\underline{n}, s) - v(\underline{n}, 0) &= \sum_{\underline{m}} \mathcal{P}(\underline{n})\mathcal{L}_2 \Big(s - \mathcal{L}_1 - \mathcal{L}_3 - \mathcal{Q}\mathcal{L}_2\Big)^{-1} \mathcal{Q}\mathcal{L}_2 \tilde{v}(\underline{m}, s) \\ &\quad + \mathcal{L}_3 \tilde{v}(\underline{n}, s). \end{aligned} \tag{2.29}$$

We can now bring in the requirement that $\gamma_{kl}, \gamma_{k'l'} \gg \kappa, g$, i.e. that intraband relaxation is very fast. We thus drop all terms except the $\mathcal{L}_1$ term. This leads to a limiting equation of motion,

$$s\tilde{v}(\underline{n}, s) - v(\underline{n}, 0) = -\sum_{\underline{m}} \mathcal{P}(\underline{n})\mathcal{L}_2\mathcal{L}_1^{-1}\mathcal{Q}\mathcal{L}_2\tilde{v}(\underline{m}, s) + \mathcal{L}_3\tilde{v}(\underline{n}, s). \tag{2.30}$$

Inverting the Laplace transform and substituting for $\mathcal{Q}$ using Equation (2.24),

$$\frac{\partial v(\underline{n}, t)}{\partial t} = \mathcal{L}_3 v(\underline{n}, t) - \sum_{\underline{m}} \mathcal{P}(\underline{n})\mathcal{L}_2\mathcal{L}_1^{-1}\mathcal{L}_2 v(\underline{m}, t), \tag{2.31}$$

where a term

$$\sum_{\underline{m},\underline{l}} \mathcal{P}(\underline{n})\mathcal{L}_2\mathcal{L}_1^{-1}\mathcal{P}(\underline{l})\mathcal{L}_2\mathcal{P}(\underline{m})\rho(t) \tag{2.32}$$

has been dropped, because it is zero by condition (2.20).

Noting that

$$\begin{aligned} \mathcal{P}(\underline{n})\rho(t) &= \rho_{\mathrm{T}}(\underline{n}) \otimes \mathrm{Tr}_{\mathrm{T}}\{p(\underline{n})\rho(t)\} \\ &= \rho_{\mathrm{T}}(\underline{n}) \otimes \rho_{\mathrm{o}}(\underline{n}, t), \end{aligned} \tag{2.33}$$

we finally obtain

$$\begin{aligned} \frac{\partial \rho_{\mathrm{o}}(\underline{n}, t)}{\partial t} &= -\sum_{\underline{m}} \mathrm{Tr}_{\mathrm{T}}\Big\{p(\underline{n})\mathcal{L}_2\mathcal{L}_1^{-1}\mathcal{L}_2\{\rho_{\mathrm{T}}(\underline{m}) \otimes \rho_{\mathrm{o}}(\underline{m}, t)\}\Big\} \\ &\quad + \mathcal{L}_3\rho_{\mathrm{o}}(\underline{n}, t). \end{aligned} \tag{2.34}$$

Evaluation of terms

To evaluate the first part of the right hand side of Equation (2.34), we consider an example of the types of terms which can arise in

$$\sum_{\underline{m}} \mathrm{Tr}_{\mathrm{T}}\Big\{p(\underline{n})\mathcal{L}_2\mathcal{L}_1^{-1}\mathcal{L}_2\{\rho_{\mathrm{T}}(\underline{m})\otimes\rho_{\mathrm{o}}(\underline{m})\}\Big\}. \tag{2.35}$$

We consider one of the terms which arise upon substitution for the $\mathcal{L}_2$ terms.

$$\sum_{\underline{m}}\sum_{kk'}|g_{kk'}|^2\mathrm{Tr}_{\mathrm{T}}\Big\{p(\underline{n})\mathcal{L}_1^{-1}(b^\dagger c_{kk'}\rho_{\mathrm{T}}(\underline{m})\otimes\rho_{\mathrm{o}}(\underline{m}))bc_{kk'}^\dagger\Big\}. \tag{2.36}$$

We use first the cyclic properties of the trace, and then the fact that $\rho_{\mathrm{o}}(\underline{m})$ is independent of the thermal states to re-express this as

$$\sum_{\underline{m}}\sum_{kk'}|g_{kk'}|^2 b^\dagger\mathrm{Tr}_{\mathrm{T}}\Big\{c_{kk'}^\dagger p(\underline{n})\mathcal{L}_1^{-1}(c_{kk'}\rho_{\mathrm{T}}(\underline{m}))\Big\}\rho_{\mathrm{o}}(\underline{m})b. \tag{2.37}$$

We use the identity [Gardiner 1991]

$$\int_0^\infty dt\ \exp(\mathcal{L}_1 t) = \mathcal{Q}, \tag{2.38}$$

and an argument similar to that which leads to condition (2.20) to show that

$$\mathcal{Q}c_{kk'}\rho_{\mathrm{T}}(\underline{m}) = c_{kk'}\rho_{\mathrm{T}}(\underline{m}), \tag{2.39}$$

and thus make the replacement

$$\begin{aligned}(2.37) \;=\; &\sum_{\underline{m}}\sum_{kk'}|g_{kk'}|^2 b^\dagger\int_0^\infty dt\,\mathrm{Tr}_{\mathrm{T}}\Big\{c_{kk'}^\dagger p(\underline{n})\\ &\times\ \exp(\mathcal{L}_1 t)c_{kk'}\rho_{\mathrm{T}}(\underline{m},0)\Big\}\rho_{\mathrm{o}}(\underline{m})b.\end{aligned} \tag{2.40}$$

The operator $p(\underline{n})$ projects the density operator onto the particular value $\underline{n}$. In this case, the action of $c_{kk'}$ and $c_{kk'}^\dagger$ on $\rho_{\mathrm{T}}(\underline{m},0)$ leads to

the conclusion that the only value of $\underline{m}$ which can therefore contribute is $\underline{m} = \underline{n} + \underline{e}$, where

$$\underline{e} = (1, 1). \tag{2.41}$$

Thus we have

$$\begin{aligned}(2.37) \;=\; & \Big\{ \sum_{kk'} |g_{kk'}|^2 \int_0^\infty dt \, \mathrm{Tr}_\mathrm{T} \Big\{ c^\dagger_{kk'} \\ & \times \exp(\mathcal{L}_1 t) c_{kk'} \rho_\mathrm{T}(\underline{n} + \underline{e}, 0) \Big\} \Big\} b^\dagger \rho_\mathrm{o}(\underline{n} + \underline{e}) b. \end{aligned} \tag{2.42}$$

The traced part of the term can equivalently be written as a stationary two-time correlation function; thus we have

$$\begin{aligned}(2.37) \;=\; & \Big\{ \sum_{kk'} |g_{kk'}|^2 \int_0^\infty dt \, \langle c^\dagger_{kk'}(t) c_{kk'}(0)(\underline{n} + \underline{e}) \rangle_s \Big\} \\ & \times b^\dagger \rho_\mathrm{o}(\underline{n} + \underline{e}) b. \end{aligned} \tag{2.43}$$

The quantum regression theorem can now be used to evaluate the correlation function [Gardiner 1991]. This cannot be done exactly, but the results are not very sensitive to the exact form of these correlation functions so approximations can be made. Using a master equation description of the process occurring on a fast time scale, we can derive the equations of motion for $\langle c^\dagger_{kk'}(t) c_{kk'}(0)(\underline{n} + \underline{e}) \rangle_s$. If the resulting expression is factorized and we assume that $\langle n_{ek} \rangle$ and $\langle n_{hk'} \rangle$ are small, then in this degree of approximation we find

$$\begin{aligned} \frac{\partial \langle c^\dagger_{kk'}(t) c_{kk'}(0)(\underline{n} + \underline{e}) \rangle_s}{\partial t} \;=\; & (i\epsilon_{kk'} - \gamma_{kk'}) \\ & \times \langle c^\dagger_{kk'}(t) c_{kk'}(0)(\underline{n} + \underline{e}) \rangle_s, \end{aligned} \tag{2.44}$$

so that

$$\int_0^\infty dt \langle c^\dagger_{kk'}(t) c_{kk'}(0)(\underline{n} + \underline{e}) \rangle_s = - \frac{\langle c^\dagger_{kk'}(0) c_{kk'}(0)(\underline{n} + \underline{e}) \rangle_s}{i\epsilon_{kk'} - \gamma_{kk'}}, \tag{2.45}$$

and our full expression becomes

$$(2.37) = -b^\dagger \rho_o(\underline{n}+\underline{e})b \left\{ \sum_{kk'} |g_{kk'}|^2 \frac{\langle c^\dagger_{kk'}(0) c_{kk'}(0)(\underline{n}+\underline{e})\rangle_s}{i\epsilon_{kk'} - \gamma_{kk'}} \right\}. \quad (2.46)$$

Rationalising the denominator, and reorganising the terms we finally obtain

$$(2.37) = \left\{ b^\dagger \rho_o(\underline{n}+\underline{e})b \right\} \; G(\underline{n}+\underline{e}), \quad (2.47)$$

where we introduce the following definitions of terms

$$\begin{aligned} F(\underline{n}) &= F^{\mathrm{r}}(\underline{n}) + iF^{\mathrm{i}}(\underline{n}) \\ &= \frac{\sum_{kk'} |g_{kk'}|^2 (i\epsilon_{kk'} + \gamma_{kk'}) \langle (1-n_{hk'})(1-n_{ek})(\underline{n})\rangle_s}{\epsilon^2_{kk'} + \gamma^2_{kk'}} \quad (2.48) \\ G(\underline{n}) &= G^{\mathrm{r}}(\underline{n}) + iG^{\mathrm{i}}(\underline{n}) \\ &= \frac{\sum_{kk'} |g_{kk'}|^2 (i\epsilon_{kk'} + \gamma_{kk'}) \langle n_{ek} n_{hk'}(\underline{n})\rangle_s}{\epsilon^2_{kk'} + \gamma^2_{kk'}}. \quad (2.49) \end{aligned}$$

Thus, writing out the full first term of Equation (2.34) and explicitly writing in the $\mathcal{L}_3$ terms, we obtain an expression for the lasing part of the master equation

$$\begin{aligned} \left.\frac{\partial \rho_o(\underline{n})}{\partial t}\right|_{\mathrm{las}} &= \frac{\kappa \bar{N}}{2}(2b^\dagger \rho_o(\underline{n}) b - bb^\dagger \rho_o(\underline{n}) - \rho_o(\underline{n}) bb^\dagger) \\ &\quad + \frac{\kappa(\bar{N}+1)}{2}(2b\rho_o(\underline{n})b^\dagger - b^\dagger b \rho_o(\underline{n}) - \rho_o(\underline{n}) b^\dagger b) \\ &\quad + 2G^{\mathrm{r}}(\underline{n}+\underline{e}) b^\dagger \rho_o(\underline{n}+\underline{e}) b - G^{\mathrm{r}}(\underline{n}) [bb^\dagger, \rho_o(\underline{n})]_+ \\ &\quad + 2F^{\mathrm{r}}(\underline{n}-\underline{e}) b \rho_o(\underline{n}-\underline{e}) b^\dagger - F^{\mathrm{r}}(\underline{n}) [b^\dagger b, \rho_o(\underline{n})]_+ \\ &\quad - iG^{\mathrm{i}}(\underline{n}) [bb^\dagger, \rho_o(\underline{n})] - iF^{\mathrm{i}}(\underline{n}) [b^\dagger b, \rho_o(\underline{n})]. \quad (2.50) \end{aligned}$$

Equation (2.50) describes therefore a birth-death type master equation for the carriers, and thus has the form of a Scully-Lamb type master equation, as in the work of Marte and Zoller [Marte 1989, Marte 1990], yet the full quantum mechanical description of the field has been retained. The carrier processes can thus be described in terms of quantum jumps, and the form of the master equation lends itself particularly well to simulation of the wavefunction via quantum jump methods.

2.2.3 Inclusion of non-lasing modes and other losses

We now consider coupling of the dipole moment operator to other unspecified modes not associated with the lasing mode. Including non-lasing modes of the field requires a similar procedure to the above, but we trace over the field variables and treat them as a heat bath. We expect similar equations for a description of non-radiative transitions,

$$\begin{aligned}\left.\frac{\partial\rho}{\partial t}\right|_E &= \sum_{kk'}\bar{N}_{kk'}\frac{\mu_{kk'}}{2}(2c^\dagger_{kk'}\rho c_{kk'} - c_{kk'}c^\dagger_{kk'}\rho - \rho c_{kk'}c^\dagger_{kk'}) \\ &+\sum_{kk'}(\bar{N}_{kk'}+1)\frac{\mu_{kk'}}{2}(2c_{kk'}\rho c^\dagger_{kk'} \\ &-c^\dagger_{kk'}c_{kk'}\rho - \rho c^\dagger_{kk'}c_{kk'}). \qquad (2.51)\end{aligned}$$

The $\mu_{kk'}$ are the loss coefficients due to coupling to the field reservoir, the mean occupation number of which is described by $\bar{N}_{kk'}$. The analysis is essentially the same as for the lasing mode, but the absence of a cavity simplifies matters. We need the projection of Equation (2.51) which gives rise to a term which we call

$$\begin{aligned}\left.\frac{\partial\rho_o(\underline{n})}{\partial t}\right|_E &\equiv A(\underline{n}+\underline{e})\rho_o(\underline{n}+\underline{e}) - A(\underline{n})\rho_o(\underline{n}) \\ &+B(\underline{n}-\underline{e})\rho_o(\underline{n}-\underline{e}) - B(\underline{n})\rho_o(\underline{n}), \qquad (2.52)\end{aligned}$$

where

$$A(\underline{n}) = \sum_{kk'}\mu_{kk'}(\bar{N}_{kk'}+1)\langle(n_{ek}n_{hk'})(\underline{n})\rangle \qquad (2.53)$$

$$B(\underline{n}) = \sum_{kk'}\mu_{kk'}\bar{N}_{kk'}\langle(1-n_{ek})(1-n_{hk'})(\underline{n})\rangle. \qquad (2.54)$$

This expression corresponds to an ordinary birth-death process as expected.

2.2.4 Inclusion of Pumping

In a semiconductor laser the pumping is achieved by the creation of electron-hole pairs, but this may be done in a variety of different ways. The simplest method conceptually is optical pumping in which the pairs are created by the absorption of photons from a light source of one kind or another. If coherent light from a laser is used, the creation process can be modelled by a birth-death process such as

$$\left.\frac{\partial \rho_o(\underline{n})}{\partial t}\right|_{P1} = P\left[\rho_o(n_e-1, n_h+1) - \rho_o(n_e, n_h)\right]. \qquad (2.55)$$

Alternatively, the electrons and holes can be created by independent Poisson processes, for which a model would be

$$\begin{aligned}\left.\frac{\partial \rho_o(\underline{n})}{\partial t}\right|_{P2} = {} & P\left[\rho_o(n_e-1, n_h) - \rho_o(n_e, n_h)\right] \\ & + P\left[\rho_o(n_e, n_h-1) - \rho_o(n_e, n_h)\right]. \qquad (2.56)\end{aligned}$$

Finally there is also the possibility that electrons (and/or holes) can be introduced essentially noiselessly by the transport process of electrical conduction. Crudely speaking, this can be visualized as a flow of electrons across a boundary, in which the arrival times of the electrons are highly correlated, because of the requirement of electrical neutrality. Such a process cannot be represented as a simple birth-death process in the electron and hole numbers. Although the noise can be very low in principle, there is also the effect of thermal noise to be considered. Yamamoto and Machida have considered the noise which can occur due to such situations, and have shown that in effect the actual current noise can be extremely small [Yamamoto 1987].

In all the processes described so far, electrons and holes have been created or destroyed in pairs. The dynamics of pumping however, are such that electrons and holes can flow in and out of the semiconductor independently, and hence pairwise behaviour is not exhibited in this

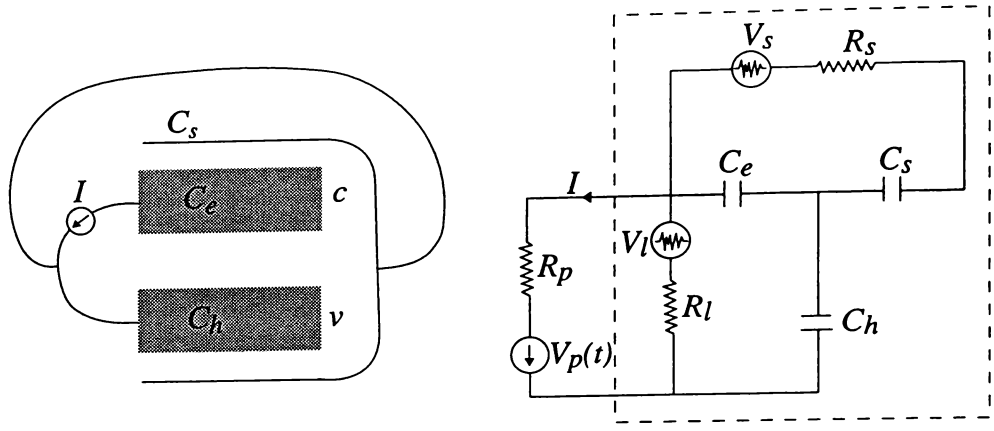


Figure 2.1: (a) A schematic of the pumping part of the semiconductor system. (b) An example of an equivalent circuit for the pumping part of the semiconductor system.

process. In other words, although we might expect electron and hole pump rates to be similar, they will not be the same at any given point in time.

Charge neutrality at any time is enforced by the electrostatic interaction between electrons and ions, and this has not yet been included in our theory. Such an electrostatic interaction could normally be included as an extra Hamiltonian term, and this would lead to a complicated description of the full quantum electrodynamics of the system. We would like to be able to treat the pumping process and the electrostatic interaction classically, and because we have a diagonalisation in the electrons and holes, it is possible to do this.

If we refer to Fig 2.1(a) we can get a picture of how charge neutrality is maintained. If the charges on the plates of C_e and C_h do not balance, then there is a net charge on the semiconductor. This charge can be viewed as the charge on a stray capacitance, C_s, which is very small. The basic situation in Fig 2.1(a) can be represented by an electrical circuit like that shown in Fig 2.1(b), which models the flow of electrons and holes under the effect of this stray capacitance. The dotted line

encompasses the lasing device, and the current I is the pump current. The resistance R_l is a leakage resistance, which for a laser system would be expected to be large. Some of the current is pumped into the capacitor C_e and out of C_h. These capacitors represent the storage of charge for the electrons and holes respectively, and are related to n_e and n_h by

$$Q_e = en_e \tag{2.57}$$

$$Q_h = e(n_h - M). \tag{2.58}$$

where M is the number of fixed negative charges in the semiconductor, and e is the fundamental electronic charge. The capacitance C_s represents the stray capacitance, and the resistance R_s ensures that the charge on C_s does not immediately dissipate. Each resistor has a Johnson noise source associated with it, and $V_p(t)$ also has a dc voltage component to provide the pumping. The size of the noise depends on the operating temperature of the semiconductor laser. The charge on the plates of C_s balances the sum of the charges on C_e and C_h, thus ensuring that charge neutrality is maintained. If C_s is small, this means that the charges on C_e and C_h are almost balanced. Note that this is a bare circuit describing the pumping processes only. We will add this to the lasing parts of our equations of motion.

We can now write down circuit equations, which when rearranged give equations of motion for n_e and n_h. The equations obtained through this procedure are

$$\begin{aligned}\dot{n}_e = & -\left(\frac{1}{C_eR_s}+\frac{1}{C_sR_s}+\frac{1}{C_eR_l}\right)n_e-\left(\frac{1}{C_hR_l}-\frac{1}{C_sR_s}\right)(n_h-M)\\ & +\frac{I_{\rm dc}}{e}+\sqrt{\frac{2kT_p}{e^2R_p}}\xi_p(t)-\sqrt{\frac{2kT_s}{e^2R_s}}\xi_s(t)-\sqrt{\frac{2kT_l}{e^2R_l}}\xi_l(t)\end{aligned} \tag{2.59}$$

$$\dot{n}_h = -\left(\frac{1}{C_eR_l}\right)n_e-\left(\frac{1}{C_hR_l}\right)(n_h-M)+\frac{I_{\rm dc}}{e}$$

$$+\sqrt{\frac{2kT_p}{e^2R_p}}\xi_p(t) - \sqrt{\frac{2kT_l}{e^2R_l}}\xi_l(t), \tag{2.60}$$

where $I_{\rm dc}$ is the dc component of the current I and the noise term $\sqrt{2kT_p/e^2R_p}\xi_p(t)$ results from the fluctuating component of the current I, where k is Boltzmann's constant. The other noise terms correspond to the voltage sources associated with Johnson noise on the other resistors.

We will include these equations as part of our stochastic differential equations later on, but for the moment will symbolically represent the pumping by

$$\left.\frac{\partial\rho_o(\underline{n})}{\partial t}\right|_P. \tag{2.61}$$

When we will later develop a small fluctuation limit of this description, it will be straightforward to include Equations (2.59) and (2.60) in a full description.

2.3 Solution of the Master Equation

The full master equation is given by

$$\frac{\partial\rho_o(\underline{n})}{\partial t} = \left.\frac{\partial\rho_o(\underline{n})}{\partial t}\right|_{\rm las} + \left.\frac{\partial\rho_o(\underline{n})}{\partial t}\right|_E + \left.\frac{\partial\rho_o(\underline{n})}{\partial t}\right|_P. \tag{2.62}$$

The particular choice of a pumping term depends on the kind of pumping used. This equation gives a description in terms of the full optical statistics and the electron number statistics. It is analogous to the equations of Marte and Zoller [Marte 1989], and is related to a Scully-Lamb type master equation [Scully 1967]. It is an equation which can be easily simulated using wavefunction stochastic differential equation methods [Gardiner 1992, Dum 1992, Mølmer 1993].

2.3.1 Deterministic Equations for Mean Values

We can check that these equations give the correct predictions for measurable quantities by calculating the mean photon number and the mean electronic occupation number and comparing with the literature [Haug 1967b, Haug 1969, Chow 1993]. These mean photon, electron and hole numbers are defined by

$$\langle \underline{n} \rangle = \sum_{\underline{n}} \mathrm{Tr}\,\{\underline{n}\rho_{\mathrm{o}}(\underline{n})\} \tag{2.63}$$

$$\langle m \rangle = \sum_{\underline{n}} \mathrm{Tr}\left\{b^{\dagger}b\rho_{\mathrm{o}}(\underline{n})\right\}. \tag{2.64}$$

If we neglect fluctuations and factorize all averages of products we get for the various contributions to the master equation, the following contributions to the equations for the time development of electron and hole numbers—N.B. in these equations for notational simplicity we write $\langle \underline{n} \rangle \to \underline{n}$, $\langle m \rangle \to m$,

$$\left.\frac{\partial \underline{n}}{\partial t}\right|_{\mathrm{las}} = -2\underline{e}\,[G^{\mathrm{r}}(\underline{n})(m+1) + F^{\mathrm{r}}(\underline{n})m] \tag{2.65}$$

$$\left.\frac{\partial \underline{n}}{\partial t}\right|_{E} = -\underline{e}\,[A(\underline{n}) - B(\underline{n})] \tag{2.66}$$

$$= \underline{e}\sum_{kk'} \mu_{kk'}\{\bar{N}_{kk'}\langle 1 - n_{hk'} - n_{ek}\rangle_{\underline{n}}\}$$

$$-\underline{e}\sum_{kk'} \mu_{kk'}\{\langle n_{ek}n_{hk'}\rangle_{\underline{n}}\} \tag{2.67}$$

$$\left.\frac{\partial \underline{n}}{\partial t}\right|_{P} = \underline{e}P, \tag{2.68}$$

where P is the carrier creation rate. There is only one contribution to the photon number equation of motion; it is

$$\frac{\partial m}{\partial t} = 2G^{\mathrm{r}}(\underline{n})(m+1) - 2F^{\mathrm{r}}(\underline{n})m + \kappa\bar{N} - \kappa m. \tag{2.69}$$

These expressions agree with those given by free-carrier theory treatments of the semiconductor laser [Chow 1993, Haug 1967a].

2.3.2 Stochastic equations for numbers of electrons, holes and photons

We wish to use our master equation to determine whether sub-Poissonian statistics can be obtained. Such behaviour has been predicted for the laser [Marte 1988c, Marte 1989], and in the low frequency region for the semiconductor laser, in the presence of supressed pump noise [Yamamoto 1987]. We will attempt to reproduce the results of Yamamoto and Machida [Yamamoto 1987].

We would like to calculate the photon statistics of the output field. Marte and Zoller [Marte 1989] relate this to the internal cavity spectrum by the expression

$$V(\omega) = 1 + \eta S(\omega), \tag{2.70}$$

where

$$S(\omega) = \frac{\kappa}{2\pi}\left[\int_{-\infty}^{\infty}\langle b^{\dagger}(0)b^{\dagger}(\tau)b(\tau)b(0)\rangle - \langle b^{\dagger}(0)b(0)\rangle^{2}\right], \tag{2.71}$$

η is the detection effeciency, which we take to be unity, and $V(\omega)$ is the variance in the fluctuations of the output light.

The simplest method by which we can calculate the internal spectrum from our master equation is to carry out the following procedure. We first rewrite the master equation as a diagonal equation in the photon number m. Defining

$$P(\underline{n}, m) = \langle m|\rho_o(\underline{n})|m\rangle \tag{2.72}$$

where $|m\rangle$ is a photon number state, this becomes

$$\begin{aligned}\frac{\partial P(\underline{n},m)}{\partial t} &= \kappa\bar{N}(mP(\underline{n},m-1) - (m+1)P(\underline{n},m)) \\ &\quad +\kappa(\bar{N}+1)((m+1)P(\underline{n},m+1) - mP(\underline{n},m)) \\ &\quad +2[G^{r}(\underline{n}+\underline{e})mP(\underline{n}+\underline{e},m-1) - G^{r}(\underline{n})(m+1)P(\underline{n},m)] \\ &\quad +2[F^{r}(\underline{n}-\underline{e})(m+1)P(\underline{n}-\underline{e},m+1) - F^{r}(\underline{n})mP(\underline{n},m)]\end{aligned}$$

$$
\begin{aligned}
&+(A(\underline{n}+\underline{e})P(\underline{n}+\underline{e},m) - A(\underline{n})P(\underline{n},m)) \\
&+B(\underline{n}-\underline{e})P(\underline{n}-\underline{e},m) - B(\underline{n})P(\underline{n},m)) \\
&+ \left.\frac{\partial \rho_o(\underline{n})}{\partial t}\right|_P .
\end{aligned} \tag{2.73}
$$

Since the fluctuations are in practice small, we can apply a Kramers-Moyal expansion [Gardiner 1983] to derive a Fokker-Planck equation; this takes the form

$$
\begin{aligned}
\frac{\partial P(\underline{n},m)}{\partial t} &= -\sum_{\alpha} \frac{\partial}{\partial X_\alpha}\Big[\mathcal{A}_\alpha(\underline{n},m)P(\underline{n},m)\Big] \\
&\quad +\frac{1}{2}\sum_{\alpha,\beta} \frac{\partial}{\partial X_\alpha}\frac{\partial}{\partial X_\beta}\Big[\mathcal{D}_{\alpha,\beta}(\underline{n},m)P(\underline{n},m)\Big],
\end{aligned} \tag{2.74}
$$

where

$$
\mathbf{X} = \begin{pmatrix} n_e \\ n_h \\ m \end{pmatrix},
$$

$$
\mathcal{A}(\mathbf{X}) = \begin{pmatrix} -A(\underline{n}) + B(\underline{n}) - 2G^r(\underline{n})(m+1) + 2F^r(\underline{n})m + P_e(\underline{n}) \\ -A(\underline{n}) + B(\underline{n}) - 2G^r(\underline{n})(m+1) + 2F^r(\underline{n})m + P_h(\underline{n}) \\ \kappa\bar{N}(m+1) - \kappa(\bar{N}+1)m + 2G^r(\underline{n})(m+1) - 2F^r(\underline{n})m \end{pmatrix},
$$

and

$$
\mathcal{D}(\mathbf{X}) = \begin{pmatrix} A(\underline{n}) + B(\underline{n}) & A(\underline{n}) + B(\underline{n}) & -2G^r(\underline{n})(m+1) \\ +2G^r(\underline{n})(m+1) & +2G^r(\underline{n})(m+1) & -2F^r(\underline{n})m \\ +2F^r(\underline{n})m + D_e(\underline{n}) & +2F^r(\underline{n})m + D_{eh}(\underline{n}) & \\ \\ A(\underline{n}) + B(\underline{n}) & A(\underline{n}) + B(\underline{n}) & -2G^r(\underline{n})(m+1) \\ +2G^r(\underline{n})(m+1) & +2G^r(\underline{n})(m+1) & -2F^r(\underline{n})m \\ +2F^r(\underline{n})m + D_{he}(\underline{n}) & +2F^r(\underline{n})m + D_h(\underline{n}) & \\ \\ -2G^r(\underline{n})(m+1) & -2G^r(\underline{n})(m+1) & \kappa\bar{N}(m+1) \\ -2F^r(\underline{n})m & -2F^r(\underline{n})m & +\kappa(\bar{N}+1)m \\ & & +2G^r(\underline{n})(m+1) \\ & & +2F^r(\underline{n})m \end{pmatrix}.
$$

The quantities $P_e(\underline{n})$ and $P_h(\underline{n})$, represent the rates of injection of electrons and holes into the active volume, while the quantities $D_e(\underline{n})$, $D_h(\underline{n})$, $D_{eh}(\underline{n})$, and $D_{he}(\underline{n})$ represent the noises in these processes. We assume that the two injection processes are statistically independent, so that optical pumping as above is excluded.

In the steady-state, and hence in the linearized limit, it is necessary that $P_e(\underline{n}) = P_h(\underline{n})$, but there is no such constraint on the $D(\underline{n})$'s. We can use the expressions (2.59) and (2.60) to make the following correspondences

$$P_e(\underline{n}) = P_e - \alpha_e n_e - \beta_e(n_h - M) \tag{2.75}$$

$$P_h(\underline{n}) = P_h - \beta_h n_e - \alpha_h(n_h - M) \tag{2.76}$$

$$D_e(\underline{n}) = \frac{2kT_L}{e^2 R_s} + \frac{2kT_L}{e^2 R_l} + \frac{2kT_p}{e^2 R_p} \tag{2.77}$$

$$D_h(\underline{n}) = D_{eh}(\underline{n}) = D_{he}(\underline{n}) = \frac{2kT_L}{e^2 R_l} + \frac{2kT_p}{e^2 R_p}, \tag{2.78}$$

where

$$\alpha_e = \frac{1}{C_e R_s} + \frac{1}{C_s R_s} + \frac{1}{C_e R_l} \tag{2.79}$$

$$\beta_e = \frac{1}{C_h R_l} - \frac{1}{C_s R_s} \tag{2.80}$$

$$P_e = \frac{I_{\rm dc}}{e} \tag{2.81}$$

$$\beta_h = \frac{1}{C_e R_l} \tag{2.82}$$

$$\alpha_h = \frac{1}{C_h R_l} \tag{2.83}$$

$$P_h = \frac{I_{\rm dc}}{e}, \tag{2.84}$$

and where we have taken $T_l = T_s = T_L$, the operating temperature of the laser. It can be seen from the above equations that $D_e(\underline{n})$ will always be greater than $D_h(\underline{n})$. Hence it is not possible to make $D_e(\underline{n})$ sub-Poissonian without also making $D_h(\underline{n})$ sub-Poissonian.

From this the following Ito stochastic differential equations can be obtained in their most general form,

$$d\mathbf{X} = \mathcal{A}(\mathbf{X})dt + \mathcal{B}(\mathbf{X})d\mathbf{W}(t) \tag{2.85}$$

where $d\mathbf{W}$ is a five-fold white noise increment, and

$$\mathcal{B}(\mathbf{X}) = \begin{pmatrix} c_1 & c_2 & 0 & -c_4 & c_5 & -c_6 \\ c_1 & c_2 & 0 & 0 & c_5 & -c_6 \\ 0 & -c_2 & c_3 & 0 & 0 & 0 \end{pmatrix}, \tag{2.86}$$

in which

- $c_1 = \sqrt{A(\underline{n}) + B(\underline{n})}$
- $c_2 = \sqrt{2F_r(\underline{n})m + 2G_r(\underline{n})(m+1)}$
- $c_3 = \sqrt{\kappa[\bar{N}(m+1) + (\bar{N}+1)m]}$
- $c_4 = \sqrt{2kT_L/e^2R_s}$
- $c_5 = \sqrt{2kT_L/e^2R_l}$
- $c_6 = \sqrt{2kT_p/e^2R_p}$.

Simplified equations

We make the following assumptions which simplify our equations somewhat. We assume that $\bar{N} = \bar{N}_{kk'} = 0$, which is a valid assumption at optical frequencies. This means that $B(\underline{n}) = 0$, and that $A(\underline{n})$ will be simplified. We assume that $\gamma_{kk'} \gg \epsilon_{kk'}$. This means that the real parts of $G(\underline{n})$ dominate the imaginary parts, and that we can write

$$G(\underline{n}) = \sum_{kk'} \frac{|g_{kk'}|^2}{\gamma_{kk'}} \langle n_{ek} n_{hk'}(\underline{n}) \rangle.$$

If we assume that we have a broadband spectrum, $G(\underline{n})$ can be written as a constant multiplied by $n_e n_h$ after the summation is carried out.

We can use an analogous argument for $A(\underline{n})$ and $F(\underline{n})$ to obtain the following substitutions for these terms,

$$F(\underline{n}) = aN^2 \tag{2.87}$$

$$G(\underline{n}) = an_e n_h \tag{2.88}$$

$$A(\underline{n}) = dn_e n_h \tag{2.89}$$

$$B(\underline{n}) = 0, \tag{2.90}$$

where N^2 is the square of the total number of states in the semiconductor in the very broadband limit, but is a modified total number of states, (having a value less than $n_e n_h$) if the spectrum is sharper.

The substitutions (2.87)-2.90) are used throughout this entire thesis. For a more complete semiconductor laser theory, details of the particular bandstructure need to be included, and these details would be expected to have an effect on the results obtained. We have used the simpler approach here however, since we wish to compare with the more phenomenological results of others, and thus, such detail is not necessary.

Linearized equations

In order to compare with the equations of Yamamoto [Yamamoto 1987], we require Equations (2.85) in their linearized form. If we write $\mathbf{X}(t) = \mathbf{X}_0 + \mathbf{x}(t)$ and then linearize, we get

$$d\mathbf{x} = -\mathcal{C}(\mathbf{X}_0)\mathbf{x}(t)dt + \mathcal{B}(\mathbf{X}_0)d\mathbf{W}(t) \tag{2.91}$$

where we have

$$\mathcal{C}(\mathbf{X}_0) = \begin{pmatrix} (d+c_1)n_h^0 + \alpha_e & (d+c_1)n_e^0 + \beta_e & c_2 \\ (d+c_1)n_h^0 + \beta_h & (d+c_1)n_e^0 + \alpha_h & c_2 \\ -c_1 n_h^0 & -c_1 n_e^0 & -c_2 + \kappa \end{pmatrix}$$

$$\mathcal{B}(\mathbf{X}_0) = \begin{pmatrix} c_3 & c_4 & 0 & -c_5 & c_6 & -c_7 \\ c_3 & c_4 & 0 & 0 & c_6 & -c_7 \\ 0 & -c_4 & \sqrt{\kappa m^0} & 0 & 0 & 0 \end{pmatrix},$$

in which

- m^0, n_e^0, and n_h^0 are the steady-state photon, electron and hole numbers respectively,
- $c_1 = 2a(m^0 + 1)$
- $c_2 = -2aN^2 + 2an_e^0 n_h^0$
- $c_3 = \sqrt{dn_h^0 n_e^0}$
- $c_4 = \sqrt{2cN^2 m^0 + 2cn_e^0 n_h^0 (m^0 + 1)}$
- $c_5 = \sqrt{2kT_L/(e^2 R_s)}$
- $c_6 = \sqrt{2kT_L/(e^2 R_l)}$
- $c_7 = \sqrt{2kT_p/(e^2 R_p)}$.

Steady-state solutions can be obtained by setting the deterministic parts of the stochastic differential equations equal to zero,

$$\begin{aligned} 0 &= -dn_e^0 n_h^0 - 2an_e^0 n_h^0 (m^0 + 1) + 2N^2 am^0 \\ &\quad + P_e - \alpha_e n_e^0 - \beta_e (n_h^0 - M) \qquad (2.92) \\ 0 &= -dn_e^0 n_h^0 - 2an_e^0 n_h^0 (m^0 + 1) + 2N^2 am^0 \\ &\quad + P_h - \beta_h n_e^0 - \alpha_h (n_h^0 - M) \qquad (2.93) \\ 0 &= -\kappa m^0 + 2an_e^0 n_h^0 (m^0 + 1) - 2aN^2 m^0. \qquad (2.94) \end{aligned}$$

From this, solutions can be obtained in two different limits, when different terms dominate. In the small or zero photon limit, we can drop all terms containing m^0 and we obtain

$$m^0 = n_e^0 n_h^0 = 0. \qquad (2.95)$$

This leads to the equations

$$0 = P_e - \alpha_e n_e^0 - \beta_e(n_h^0 - M) \tag{2.96}$$

$$0 = P_h - \beta_h n_e^0 - \alpha_h(n_h^0 - M). \tag{2.97}$$

Now, m^0 will be zero when $P_e = P_h = 0$. Also, we have that $n_e^0 n_h^0 = 0$, and because n_e^0 is the minority carrier we set $n_e^0 = 0$. This leaves

$$0 = -\beta_e(n_h^0 - M) = -\alpha_h(n_h^0 - M).$$

Hence for $\beta_e \neq 0$ and $\alpha_h \neq 0$, n_h^0 must equal M.

In the large photon limit, we replace $m^0 + 1$ with m^0 in all three equations. The last equation then gives

$$n_e^0 n_h^0 = N^2 + \frac{\kappa}{2a}. \tag{2.98}$$

This can be substituted in the remaining equations, and subtracting one resulting equation from the other we obtain the following relationship between n_e^0 and n_h^0,

$$n_e^0 = (n_h^0 - M)\frac{(\alpha_h - \beta_e)}{(\alpha_e - \beta_h)}. \tag{2.99}$$

We can use the expression for the $n_e^0 n_h^0$ product to solve simultaneously for n_e^0 and n_h^0, and the solutions of the quadratic which give positive values are

$$n_e^0 = \left[-\frac{M}{2} + \sqrt{\frac{M^2}{4} + \frac{(\alpha_e - \beta_h)}{(\alpha_h - \beta_e)}\left(\frac{\kappa}{2a} + N^2\right)}\right] \times \frac{(\alpha_h - \beta_e)}{(\alpha_e - \beta_h)} \tag{2.100}$$

$$n_h^0 = \frac{M}{2} + \sqrt{\frac{M^2}{4} + \frac{(\alpha_e - \beta_h)}{(\alpha_h - \beta_e)}\left(\frac{\kappa}{2a} + N^2\right)}. \tag{2.101}$$

It can be seen that the values of n_e^0 and n_h^0 are independent of the size of the current pumping the semiconductor. One can use these expressions

then to obtain in the limit that $C_s \ll C_e, C_h$, and $n_h^0 \gg n_e^0$ the result for m^0,

$$m^0 = \frac{P - P_{\text{th}}}{\kappa},$$

where

$$\begin{aligned} P &= \frac{I_{\text{dc}}}{e} \\ P_{\text{th}} &= \left(d + \frac{1}{\kappa M R_l}\left[\frac{1}{C_e} + \frac{1}{C_h}\right]\right)\left(\frac{\kappa}{2a} + N^2\right). \end{aligned}$$

The algebra leading to the above result is given in Appendix A.

Values of parameters

Parameters are chosen to match up with those given by Yamamoto and Machida [Yamamoto 1987], and are as follows:

- $\kappa = 5 \times 10^{11}$ s^{-1}. This is chosen to agree exactly with the parameter given in the paper by Yamamoto and Machida [Yamamoto 1987].
- N^2. This can be shown, by using the expression for the population inversion parameter n_{sp} from the Yamamoto and Machida paper [Yamamoto 1987], to be given by $N^2 = n_e n_h/2$.
- $n_e^0 = 4.5 \times 10^8$. This corresponds to the value given by Yamamoto and Machida [Yamamoto 1987].
- d. Assuming that n_h^0 will be an order of magnitude greater than n_e^0 (since it is the majority carrier), we use the value in the Yamamoto and Machida paper [Yamamoto 1987] for the inverse spontaneous emission lifetime to obtain $d = 7.5 \times 10^{-2}$ s^{-1}.
- a. If C_e and C_h are large, then P_{th} can be approximated by $P_{\text{th}} = d(N^2 + \kappa/2a)$. Using substitutions from the Yamamoto and

Machida paper [Yamamoto 1987] we find $d = 2a/\beta$, where β is the spontaneous emission coefficient. This leads to $a = 3.75 \times 10^{-7}$ s^{-1}.

- n_h^0. Now, from Equation (2.98), and the fact that $N^2 = n_e n_h/2$, we can get a consistent value of $n_h = 2.692 \times 10^9$. We thus also deduce $N = 6.6 \times 10^{17}$.

- The pump noises can be chosen so that they are Poissonian, sub-Poissonian, or a mixture of sub-Poissonian and Poissonian. Changing the pump noise statistics of the majority carrier (in our case, the holes), has no effect on the resulting spectrum. This is because the majority carrier fluctuations are so small compared to the majority carrier number, that no effect of the fluctuations can be seen in the spectrum. The plotted results we present in this chapter are for the situation in which the pump noise is perfectly sub-Poissonian.

Squeezing spectrum of output light

From the stochastic differential equations (2.91), the photon number correlation function $\langle m(\tau)m(0)\rangle$ can be calculated, which we need to manipulate somewhat in order to arrive at the internal cavity spectrum. The procedure for carrying out this manipulation is given in Appendix B. The spectrum (2.71) can thus be obtained numerically by calculating

$$\begin{aligned} S(\omega) &= \frac{\kappa}{2\pi}\Big\{(\mathcal{C}(\mathbf{X}_0)+i\omega)^{-1}\mathcal{B}(\mathbf{X}_0)\mathcal{B}(\mathbf{X}_0)^T(\mathcal{C}(\mathbf{X}_0)^T-i\omega)^{-1} \\ &\quad -\langle b^\dagger(0)b(0)\rangle\left[(\mathcal{C}(\mathbf{X}_0)+i\omega)^{-1}U\right. \\ &\quad \left.+\,U(\mathcal{C}(\mathbf{X}_0)^T-i\omega)^{-1}\right]\Big\}, \end{aligned} \tag{2.102}$$

where

$$U = \begin{pmatrix} 0 & 0 & 0 \\ 0 & 0 & 0 \\ 0 & 0 & 1 \end{pmatrix}. \tag{2.103}$$

The result is compared with the spectra of [Yamamoto 1987]. The equation (2.102) is thus programmed, and the result is compared with the spectra of Yamamoto and Machida [Yamamoto 1987].

The comparisons between our spectrum and that of Yamamoto and Machida [Yamamoto 1987] are shown in Fig. 2.2, for two different values of the parameter $r = (P - P_{\rm th})/P_{\rm th} >\sim 10$. It can be seen that the two results agree very well, and that for increasing r, the output light is increasingly sub-Poissonian. For values of $r <\sim 10$ the output light is completely Poissonian in nature. Thus calculation of the Mandel Q-parameter will yield a positive result for smaller r, and a negative result for large r. Yamamoto and Machida predict sub-Poissonian statistics for low frequencies [Yamamoto 1987]. What is suggested therefore, is that if a low-band pass filter were used on the output light, sub-Poissonian statistics would be obtained.

We expect that the shape of the spectrum might depend on the values of $\alpha_e, \beta_e, \alpha_h$, and β_h chosen. We have found that for the parameters considered above, and a pump rate of one thousand times $P_{\rm th}$, the spectrum is only altered for values of $\alpha_e > 5 \times 10^{10}$ s^{-1}, and does not depend on the values of β_e, β_h or α_h. The inverses of the other time constants in this system are

$$\begin{aligned} \tau_{\rm sp}^{-1} &= 2.2 \times 10^8 {\rm s}^{-1} \\ \tau_{\rm st}^{-1} &= 4.4 \times 10^{11} {\rm s}^{-1}. \end{aligned}$$

Thus, the value of α_e, at which changes in the spectrum become apparent falls between these two values.

It is also possible to reduce the pump noise in the electrons and holes individually. We have carried out tests to check the effect of making one or both of these noises sub-Poissonian. We find that making the hole pump noise sub-Poissonian has no effect when compared to both noises being Poissonian. Thus, any effect on the statistics of the output field is due solely to the nature of the electronic pump noise.

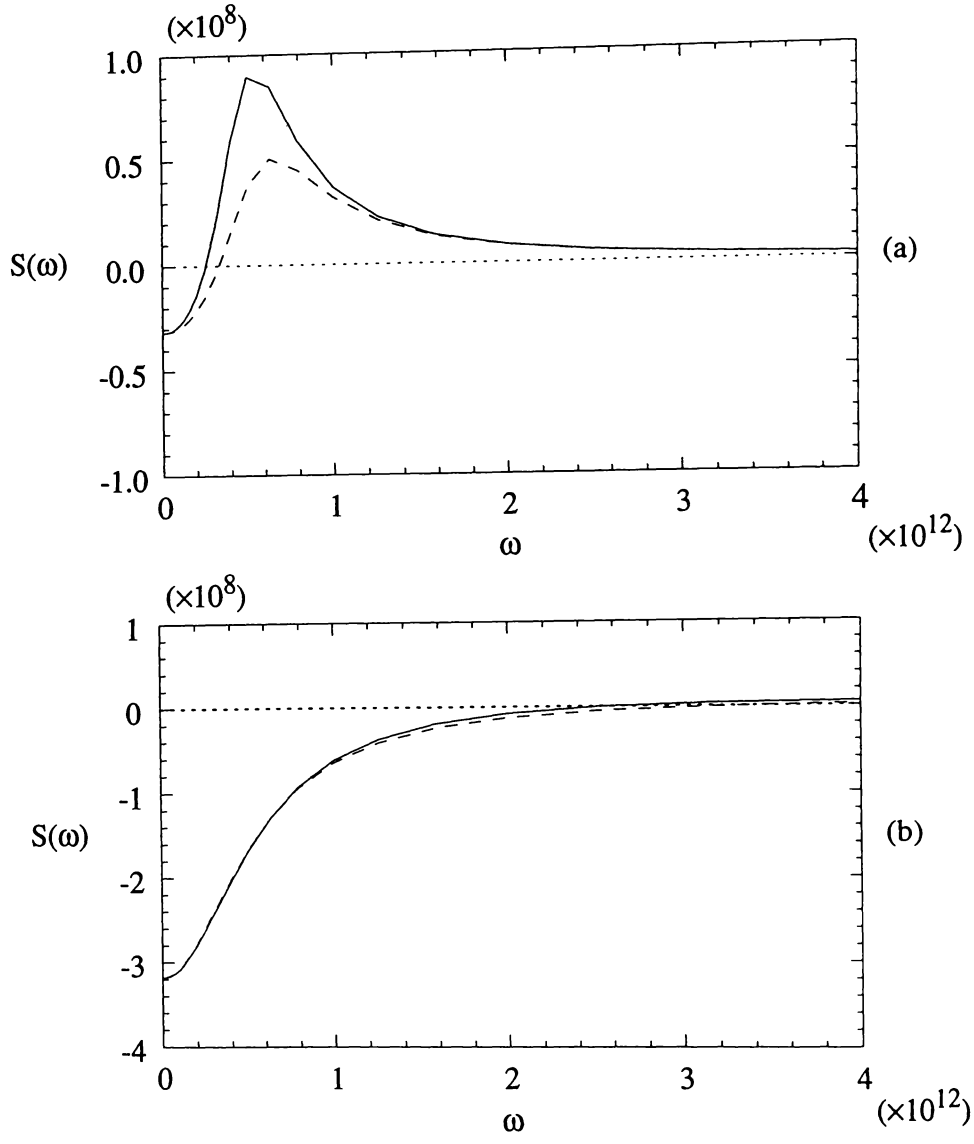


Figure 2.2: Comparison of the spectrum of Yamamoto and Machida internal to the cavity (dashed line) with Equation (2.102) (solid line), for pump rates r of (a) 1000 and (b) 10000, and $Q_e = Q_h = 0$. The finely dashed line (which indicates the shot noise level) is included to illustrate that in (a) the area under the graph above zero is greater than that below zero, and vice versa for (b).

Chapter 3

Master Equation Theory of Multi-Mode Semiconductor Lasers

3.1 Introduction

The experiment of Marin *et al.* and the accompanying theoretical explanation provided the impetus for the work of this chapter. It became apparent to us that an extension of our work to describe multi-mode situations was required to explain some experimental results that were beginning to be seen. The work of Marin *et al.* was briefly introduced in Chapter 1, but we give a more detailed discussion here of the results obtained by them.

Marin *et al.* investigated squeezing experimentally in three different laser systems, a free-running laser, an injection locked laser, and a grating stabilised laser [Marin 1995]. The three systems have different amounts of side mode suppression, and by investigating the noise properties of the individual modes, as well as the total noise, the effect of the side modes on the total noise could be deduced.

They found that for the free-running system, all noises measured are above the shot-noise level. The intensity noises of the individual

modes are much higher than the intensity noise of the main mode. In the injection-locked system, the side-mode and central-mode intensity noises are above the shot-noise level, and the total intensity noise is now squeezed, hence, in this case, the squeezing is not single mode squeezing. For the external grating system, the total intensity noise and the intensity noise of the central mode alone are below the shot-noise level and practically the same. The noise in the side modes is too low to be detected and hence there is true single mode squeezing in this case.

Marin *et al.* refute the implications made by others that the size of the side modes is solely responsible for a reduction in the (total) noise measured [Wang 1993, Freeman 1993b]. They believe rather, that anticorrelations between the side modes and the main mode (as suggested by Inoue *et al.* [Inoue 1992]) also play a role in the total intensity noise. Their results are explained by proposing a multi-mode model which assumes homogeneous behaviour [Inoue 1992], but with some inhomogeneity built in [Wang 1993]. The inhomogeneity prevents the perfect anticorrelations between the modes that would be expected of a fully homogeneous gain medium.

The approach of Marin *et al.* is a Langevin one similar to that of Inoue *et al.* [Inoue 1992], but with a small self-saturation of each mode by its own fluctuations, built in to model the inhomogeneous behaviour. The theory relies upon the experimental results as its basis however, and as such, is not of much use for predictions of what could happen in a slightly different system, unless the experiment has already been performed. In this chapter we extend the master equation theory for the single mode semiconductor laser to the multi-mode case, and show that we obtain similar predictions to those of Marin *et al.* for the free-running and external grating cases. We model the effect of the external grating theoretically by using a value of the central mode decay constant which is less than the free-running value, thus less central-mode photons

escape the cavity per unit time than side-mode photons, enhancing the mode selectivity of the laser. The injection-locked system considered by Marin *et al.* is not considered in this chapter, since it is treated slightly differently, and will be dealt with in Chapter 4.

The advantage of our approach is that the calculation is from first principles and does not require any *a priori* knowledge of the behaviour of the system. We do not use a self-saturation term to model the inhomogeneous effects. Rather, these are modelled by physical effects which are believed to occur in semiconductor lasers. The theory could also be extended to calculate other effects, such as phase effects and the effects of refractive index shifts.

3.2 Hamiltonian

We consider here a system in which we have three modes, although there would be no difficulty (at least in principle) in putting in more. The central mode is the resonant dominant mode and the other two modes are on either side at frequencies given approximately by $\omega_1 \pm c/(2L)$, where ω_1 is the frequency of the central mode, c is the speed of light, and L is the cavity length.

For brevity only those parts of the single mode Hamiltonian which are modified with the addition of further modes are given here. The reader is referred to Equations (2.1)-(2.7) for the full original expression. Three parts of the single mode Hamiltonian need to be modified, H_F, H_{EF}, and H_{FB} (Equations (2.2),(2.4), and(2.5) respectively). These become

$$H_F = \sum_j \hbar\omega_j b_j^\dagger b_j \tag{3.1}$$

$$H_{EF} = i\hbar \sum_{kk'} \sum_j \{g_{kk'}^j b_j e^{i\omega_j t} c_{kk'}^\dagger + g_{kk'}^{j*} b_j^\dagger e^{-i\omega_j t} c_{kk'}\} \tag{3.2}$$

$$H_{FB} = \sum_{i,j} i\hbar \sqrt{\frac{\kappa_j}{2\pi}} \{b_j^\dagger \Gamma_{ij} + \Gamma_{ij}^\dagger b_j\}, \tag{3.3}$$

where the summation j is over the three field modes ($j = 1$ referring to the central mode, and $j = 2, 3$ referring to the side modes), and all symbols describe the same physical processes (for the particular mode by which they are indexed) as in the single mode case.

3.3 Master Equation

Using the procedures of Chapter 2, one finds that the contribution to the master equation of these elements is as follows;

$$\begin{aligned}\left.\frac{\partial \rho_0(\underline{n})}{\partial t}\right|_{\text{las}} = & \sum_j \Big\{ \frac{\kappa_j}{2} \bar{N}_j (2b_j^\dagger \rho_0(\underline{n}) b_j - b_j b_j^\dagger \rho_0(\underline{n}) - \rho_0(\underline{n}) b_j b_j^\dagger) \\ & + \frac{\kappa_j}{2} (\bar{N}_j + 1)(2b_j \rho_0(\underline{n}) b_j^\dagger - b_j^\dagger b_j \rho_0(\underline{n}) - \rho_0(\underline{n}) b_j^\dagger b_j) \\ & + \sum_{lj} \{ -G_{lj}(\underline{n}) b_l b_j^\dagger \rho_0(\underline{n}) + G_{lj}(\underline{n} + \underline{e}) b_j^\dagger \rho_0(\underline{n} + \underline{e}) b_l \\ & - F_{jl}^*(\underline{n}) b_l^\dagger b_j \rho_0(\underline{n}) + F_{jl}^*(\underline{n} - \underline{e}) b_j \rho_0(\underline{n} - \underline{e}) b_l^\dagger \\ & - F_{lj}(\underline{n}) \rho_0(\underline{n}) b_j^\dagger b_l + F_{lj}(\underline{n} - \underline{e}) b_l \rho_0(\underline{n} - \underline{e}) b_j^\dagger \\ & - G_{jl}^*(\underline{n}) \rho_0(\underline{n}) b_j b_l^\dagger + G_{jl}^*(\underline{n} + \underline{e}) b_l^\dagger \rho_0(\underline{n} + \underline{e}) b_j \\ & - i\Delta_j [b_j^\dagger b_j, \rho_0(\underline{n})] \} \Big\}, \end{aligned} \tag{3.4}$$

where Δ_j is the detuning of the jth mode from the central mode, $\Delta_j = \omega_j - \omega_1 = \pm c/(2L)$ ($\Delta_1 = 0$), where c is the speed of light, and L is the length of the semiconductor cavity. Here

$$G_{lj}(\underline{n}) = \sum_{kk'} g_{kk'}^l g_{kk'}^{j*} \frac{\text{Tr}\{c_{kk'}^\dagger c_{kk'} \rho_T(\underline{n})\}}{i\epsilon_{kk'} - \gamma_{kk'}} \tag{3.5}$$

and $G_{jl}^*(\underline{n})$ is its conjugate transpose, and a similar modification of the single mode $F(\underline{n})$ term leads to $F_{lj}(\underline{n})$.

3.4 Coupling of the Field to the Semiconductor

The three-mode system consists of one dominant mode, and two side modes of lower intensity. Since the modes will have different spatial distributions[1], they couple to slightly different populations, provided that carrier diffusion effects are insignificant, as is the case for the index-guided lasers used in the experiments of Marin *et al.* In a realistic multi-mode model this effect must be included. The fact that the carrier diffusion is insignificant means that there is a definite independent carrier population to which each mode couples. If the effects of carrier diffusion are significant however, there are no such independent carrier populations and the following model does not apply.

All modes have a common carrier population to which they couple, and each mode couples to an additional carrier population, to which the other modes do not couple. Since the intensity of the side modes is rather small however, the additional population to which it couples is ignored in our analysis, and only the additional population to which the central mode couples is included. In the master equation and Hamiltonian terms above, we have assumed that all three modes couple to the same carrier population. To account for the additional population we now include for the central mode, we introduce the new carrier numbers $\tilde{n}_e$ and $\tilde{n}_h$, which represent the additional carrier population to which only the central mode couples. This situation is illustrated in Fig 3.1. Since the field-carrier interaction is predominantly through the central mode, and only parasitic effects between the field modes with little carrier involvement result in population of the side modes[2], we neglect the additional population to which the side modes couple. The number of variables in our system is thus increased from five to seven, three

[1]The reader is referred to Section 3.10 for a discussion of this statement.
[2]See section 3.9 for a further discussion of this.

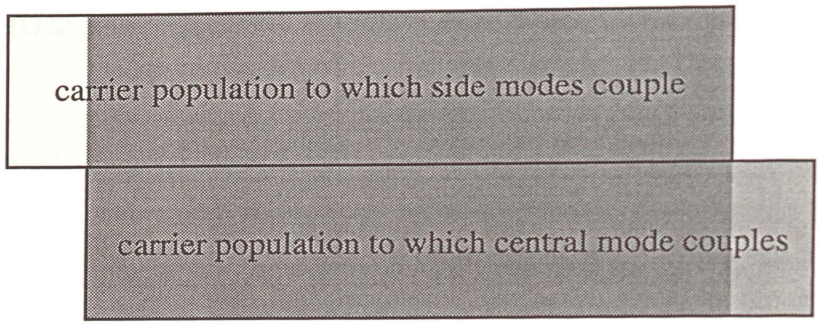


Figure 3.1: The different carrier populations to which the field modes couple are represented here by the different regions of the figure. The dark grey region is that referred to by the variables n_e, and n_h. The lighter grey region is referred to by the variables $\tilde{n}_e$, and $\tilde{n}_h$. The population represented by the white region is ignored in our analysis, since the intensity of the side modes is much smaller than that of the central mode.

representing the field, and four representing the semiconductor.

The coupling between the additional population, and lasing and non-lasing modes, leads to additional terms in the master equation. These take the same form as previous terms describing the interaction of the common population with the lasing and non-lasing modes. These additional terms are

$$\begin{aligned}
\left.\frac{\partial \rho_0(\underline{n})}{\partial t}\right|_{\text{pop}} = & \left\{-\tilde{G}_{11}(\underline{n}) b_1 b_1^\dagger \rho_0(\underline{n}) + \tilde{G}_{11}(\underline{n}+\tilde{\underline{e}}) b_1^\dagger \rho_0(\underline{n}+\tilde{\underline{e}}) b_1 \right. \\
& -\tilde{F}_{11}^*(\underline{n}) b_1^\dagger b_1 \rho_0(\underline{n}) + \tilde{F}_{11}^*(\underline{n}-\tilde{\underline{e}}) b_1 \rho_0(\underline{n}-\tilde{\underline{e}}) b_1^\dagger \\
& -\tilde{F}_{11}(\underline{n}) \rho_0(\underline{n}) \rho_0(\underline{n}) b_1^\dagger b_1 + \tilde{F}_{11}(\underline{n}-\tilde{\underline{e}}) b_1 \rho_0(\underline{n}-\tilde{\underline{e}}) b_1^\dagger \\
& \left. -\tilde{G}_{11}^*(\underline{n}) \rho_0(\underline{n}) b_1 b_1^\dagger \right\} + \tilde{G}_{11}^*(\underline{n}+\tilde{\underline{e}}) b_1^\dagger \rho_0(\underline{n}+\tilde{\underline{e}}) b_1 \\
& +\tilde{A}(\underline{n}+\tilde{\underline{e}}) \rho_0(\underline{n}+\tilde{\underline{e}}) - \tilde{A}(\underline{n}) \\
& +\tilde{B}(\underline{n}-\tilde{\underline{e}}) \rho_0(\underline{n}-\tilde{\underline{e}}) - \tilde{B}(\underline{n}) \rho_0(\underline{n}), \qquad (3.6)
\end{aligned}$$

where $\underline{n}$ is now

$$\underline{n} = \begin{pmatrix} n_e \\ n_h \\ \tilde{n}_e \\ \tilde{n}_h \end{pmatrix}, \tag{3.7}$$

$$\underline{e} = \begin{pmatrix} 1 \\ 1 \\ 0 \\ 0 \end{pmatrix}, \tag{3.8}$$

$$\underline{\tilde{e}} = \begin{pmatrix} 0 \\ 0 \\ 1 \\ 1 \end{pmatrix}, \tag{3.9}$$

and

$$\tilde{G}_{lj}(\underline{n}) = \sum_{kk'} \tilde{g}^{l}_{kk'} \tilde{g}^{j*}_{kk'} \mathrm{Tr} \frac{\{\tilde{c}^{\dagger}_{kk'} \tilde{c}_{kk'} \rho_{\mathrm{T}}(\underline{n})\}}{i\epsilon_{kk'} - \gamma_{kk'}} \tag{3.10}$$

$$\tilde{A}(\underline{n}) = \sum_{kk'} (\tilde{\bar{N}}_{kk'} + 1) \langle (\tilde{n}_{ek} \tilde{n}_{hk'})(\underline{n}) \rangle. \tag{3.11}$$

3.5 Pumping

The pump model given in the previous chapter did not treat electrons and holes in quite the same way. We consider here a more realistic pump model than that considered in the single mode case, in which the electrons and holes are treated equivalently. Since there are two different carrier populations in this model, the pump circuit must also be modified so that both populations are pumped and become inverted.

An equivalent circuit for such a pumping process is shown in Fig 3.2. The left hand side of the circuit describes the pump mechanism for the carriers which couple only to the central mode, and the right

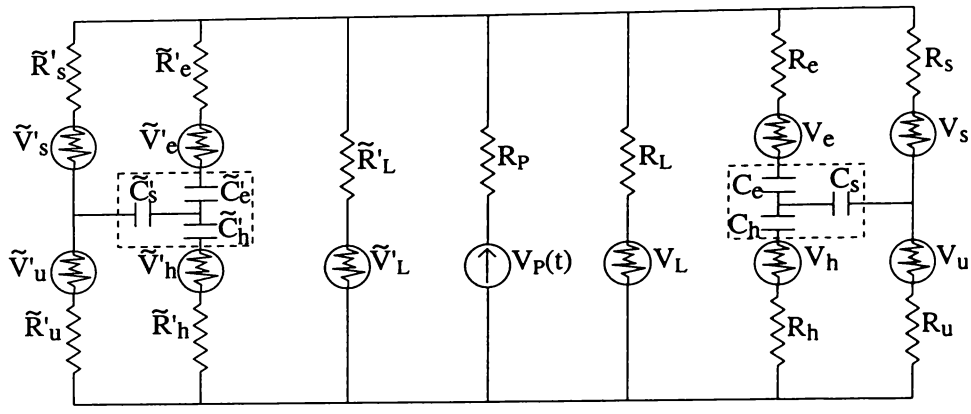


Figure 3.2: The electrical circuit which models the pumping.

hand side of the circuit gives the pumping for carriers which couple to all modes. The pump current is provided by the dc voltage component of $V_p(t)$. R_L and $\tilde{R}_L$ are leakage resistances. Associated with each resistance R, is a Johnson noise voltage source of the form $\sqrt{2kTR}\xi(t)$. The dashed lines encompass the lasing device. It is within this area that coupling between the carriers and the field takes place (which is not described by this circuit). The capacitors with subscripts e and h represent storage of charge for the electrons and holes respectively, and the capacitor with subscript s allows C_e and C_h to store independent charges, while ensuring that overall charge neutrality is maintained.

The central part of the circuit can be written as an equivalent circuit (shown in Fig 3.3), and Kirchoff's laws can be applied. Rearranging leads to equations of motion for $n_e, n_h, \tilde{n}_e, \tilde{n}_h$ which can be added to the quantum mechanical contributions which will be derived in Section 3.7. Although these equations look complicated, the use of an equivalent circuit gives a complete physical description of the pumping processes in a semiconductor laser. The parameters in the resulting equations are all ones which could be measured by an experimentalist, and as such provide a means of direct comparison between the results of experiment and theory. We believe that this work is the first which allows such

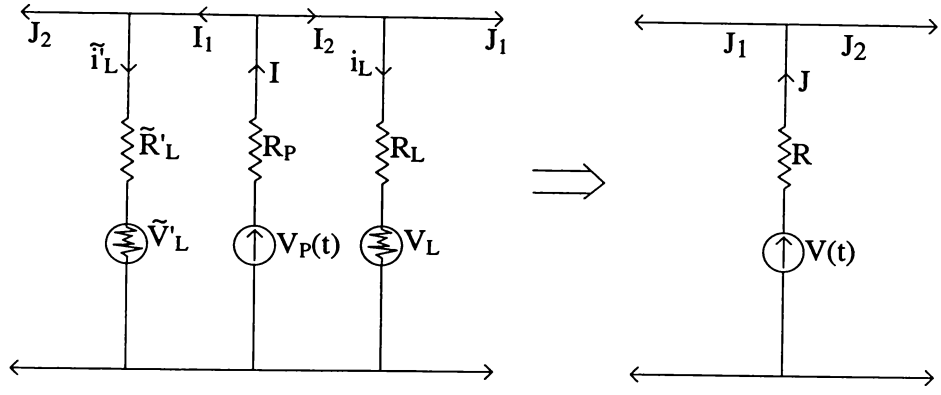


Figure 3.3: The equivalent circuit for the central part of Fig 3.2.

a comparison to be made. Since the resulting equations are rather complicated, they are given in Appendix C.

3.6 Transformation to a Fokker Planck Equation

The full master equation for the multi-mode case is thus

$$\frac{\partial \rho_0(\underline{n})}{\partial t} = \left.\frac{\partial \rho_0(\underline{n})}{\partial t}\right|_{\text{las}} + \left.\frac{\partial \rho_0(\underline{n})}{\partial t}\right|_{\text{pop}} + \left.\frac{\partial \rho_0(\underline{n})}{\partial t}\right|_{E} + \left.\frac{\partial \rho_0(\underline{n})}{\partial t}\right|_{P}, \quad (3.12)$$

where $\left.\frac{\partial \rho_0(\underline{n})}{\partial t}\right|_E$ is given by Equation (2.52), and $\left.\frac{\partial \rho_0(\underline{n})}{\partial t}\right|_P$ refers to the pump contribution to the master equation. Because of the fact that we have more than one mode, we cannot take the master equation into a diagonal representation and perform the Kramers-Moyal expansion to obtain a Fokker-Planck equation as we have done in the single mode case, since the master equation in the diagonal representation couples to off-diagonal elements and we do not have a closed system.

Instead, we convert to the positive-P representation using operator correspondences [Gardiner 1991], which relate the field operators $b_i, b_i^\dagger$ to c-number amplitudes β_i, β_i^*. Since we then have c-numbers rather

than quantum mechanical operators there is no longer a coupling to off-diagonal states of the semiconductor, and it is possible to carry out a Kramers-Moyal expansion on the terms which couple to the neighbouring states of $\underline{n}$ of the semiconductor. Because we work in the positive-P representation, higher order noise terms are obtained, which can be shown to be small by scaling arguments. The resulting Fokker-Planck equation for the full three mode system (including all processes common to the single- and multi-mode cases) is

$$\begin{aligned}\frac{\partial P(\mathbf{X})}{\partial t} &= -\sum_{\alpha}\frac{\partial}{\partial X_{\alpha}}[\mathcal{A}_{\alpha}(\mathbf{X})P(\mathbf{X})] \\ &\quad +\frac{1}{2}\sum_{\alpha,\gamma}\frac{\partial}{\partial X_{\alpha}}\frac{\partial}{\partial X_{\gamma}}[\mathcal{D}_{\alpha,\gamma}(\mathbf{X})P(\mathbf{X})],\end{aligned} \tag{3.13}$$

where

$$\mathbf{X} = \begin{pmatrix} n_e \\ n_h \\ \tilde{n}_e \\ \tilde{n}_h \\ \beta_1 \\ \beta_2 \\ \beta_3 \\ \beta_1^* \\ \beta_2^* \\ \beta_3^* \end{pmatrix}, \tag{3.14}$$

and the β_i, β_i^* terms are the c-number field amplitudes corresponding to the quantum mechanical field operators $b_i, b_i^\dagger$. Due to their complexity, the drift and diffusion matrices, $\mathcal{A}(\mathbf{X})$ and $\mathcal{D}(\mathbf{X})$, as well as the mathematics of the above argument, are given in Appendix D.

3.7 Linearised Stochastic Differential Equations

From the Fokker-Planck equation, one can write down Ito stochastic differential equations for $n_e, n_h, \tilde{n}_e, \tilde{n}_h, \beta_l$, and β_l^* directly. Using

$$d(\beta_l^*\beta_l) = d(\beta_l^*)\beta_l + \beta_l^* d(\beta_l) + d(\beta_l^*)d(\beta_l), \tag{3.15}$$

the Ito stochastic differential equations for the field modes can be replaced by Ito stochastic differential equations for the photon numbers. This gives equations in the same variables as in the single mode case, where we take $\beta_l^*\beta_l = m_l$.

To simplify the subsequent analysis, the stochastic differential equations are simplified by use of the rotating wave approximation, which removes all terms of the form $\beta_l^*\beta_j$ for which $l \neq j$. It is valid to do this here because these are non-stationary terms which should average to zero over the long times considered in the theory and experiment of Marin *et al.* In addition, since we have an unknown band structure, the same broadband assumptions are made as in the single mode case (Equations (2.87)-(2.90)), which leads to considerable simplification of the terms $G_{jl}(\underline{n}), \tilde{G}_{jl}(\underline{n}), F_{jl}(\underline{n}), \tilde{F}_{jl}(\underline{n}), A(\underline{n}), \tilde{A}(\underline{n}), B(\underline{n})$, and $\tilde{B}(\underline{n})$. The reader is referred to Appendix E for the intermediate results of the above procedure, and for a more detailed discussion of the simplifications made.

Steady-state solutions are obtained by solving the deterministic parts of the simplified equations numerically. We have found it far from simple to obtain accurate stable solutions. The method we have found which does give satisfactory results is a bisection algorithm which is detailed in Appendix F.

The steady-state solutions are used for substitution in the linearised stochastic differential equations stochastic differential equations, which are required to calculate the spectrum. The stochastic differential equa-

tions are linearised about the steady-state solutions,

$$d\mathbf{y} = -\mathcal{E}(\mathbf{Y}_0)\mathbf{y}(t)dt + \mathcal{F}(\mathbf{Y}_0)d\mathbf{W}(t), \tag{3.16}$$

where

$$\mathbf{Y} = \begin{pmatrix} n_e \\ n_h \\ \tilde{n_e} \\ \tilde{n_h} \\ m_1 \\ m_2 \\ m_3 \end{pmatrix}, \tag{3.17}$$

and

$$\mathbf{Y}(t) = \mathbf{Y}_0 + \mathbf{y}(t). \tag{3.18}$$

The matrices $\mathcal{E}(\mathbf{Y}_0)$ and $\mathcal{G}(\mathbf{Y}_0) = \mathcal{F}(\mathbf{Y}_0)\mathcal{F}^T(\mathbf{Y}_0)$, are given in Appendix G.

3.8 Calculation of the Spectrum

Marin *et al.* have plotted intensity noises as a function of $\log(1-p)$, where p is the ratio of the side mode decay constant to the central mode decay constant. This is done because the ratio p represents the degree to which the side modes are suppressed. For the purposes of comparison, we also plot the results for the two laser systems considered in this chapter as a function of $\log(1-p)$.

For a range of decay constant ratios $p = \kappa_2/\kappa_1$, we calculate the normalised variance of intensity fluctuations in mode j external to the cavity

$$V_{jj}(\omega) = 1 + \frac{\eta\mu_j S_{jj}(\omega)}{\langle b_j^\dagger(0)b_j(0)\rangle}, \tag{3.19}$$

similarly to [Marte 1989], and where

$$S_{jj}(\omega) = \kappa_j[(\mathcal{E}(\mathbf{Y}_0) + i\omega)^{-1}\mathcal{G}(\mathbf{Y}_0)(\mathcal{E}^T(\mathbf{Y}_0) - i\omega)^{-1}]_{jj} \tag{3.20}$$

is the diagonal element of the spectral matrix corresponding to mode j, η is the quantum efficiency, and μ_j is the detection efficiency of the jth mode. In addition, the variance for the total intensity $I_1 + I_2 + I_3$ was calculated, and is given by

$$V_{\rm tot}(\omega) = 1 + \sum_{ij} \frac{\eta \mu_i \mu_j S_{ij}(\omega)}{\langle \mu_1 b_1^\dagger(0) b_1(0)\rangle + \langle \mu_2 b_2^\dagger(0) b_2(0)\rangle + \langle \mu_3 b_3^\dagger(0) b_3(0)\rangle} \tag{3.21}$$

where $\sum_{ij} S_{ij}(\omega)$ is a sum over all purely optical elements of the spectral matrix, and

$$S_{ij}(\omega) = \sqrt{\kappa_i \kappa_j}[(\mathcal{E}(\mathbf{Y}_0) + i\omega)^{-1} \mathcal{G}(\mathbf{Y}_0)(\mathcal{E}^T(\mathbf{Y}_0) - i\omega)^{-1}]_{ij}. \tag{3.22}$$

We now turn to a discussion of parameter sizes used for the spectral calculation. The effect of the external diffraction grating is to select out a mode of one frequency (the frequency of the central mode), which is reflected back into the cavity. The modes at other frequencies (the side modes) do not reflect back into the cavity. The way that we have modelled this theoretically is to assign a smaller decay constant to the central mode than the value for a free-running laser. If we calculate the central mode spectrum, side mode spectrum, and total spectrum for a range of values of κ_1, then at some point we must obtain agreement with the experimental results of Marin *et al.* for the laser with an external diffraction grating, that is, essentially single mode squeezing. Similarly, for κ_1 near the free-running value, we must obtain agreement with the free-running experimental results of Marin *et al.*, that is, anti-correlated noises in the central and side modes leading to a substantially smaller total noise, which is however still above the shot-noise.

In their Langevin formulation of the problem, Marin *et al.* have not decreased κ_1 however, but rather, increased the decay constants of the side modes. We feel that this is fundamentally incorrect however, since the presence of the grating does not affect the rate at which the side modes couple out of the laser system. The side modes behave in the

same way (from the point of view of the cavity), with or without the grating.

Hence, although we plot intensity noises as a function of $\log(1-p)$ as Marin *et al.* do, different variables are being varied in each case. Marin *et al.* give a value for $\kappa_1 = 1/\tau^{(pe)} + 1/\tau_1^{(po)}$ (in their notation) of 2.45×10^{11} s^{-1}. We use this value for κ_2 and κ_3, and vary κ_1.

Other parameters appearing in the matrices $\mathcal{E}(\mathbf{Y}_0)$ and $\mathcal{G}(\mathbf{Y}_0)$, which we have matched exactly with those of Marin *et al.* are the differential quantum efficiency η, of 66%, the ratio of the side mode to the central mode coupling constant, which is 0.9995. We also apply a pump strength which is eight times above the Marin *et al.* threshold of 18mA.

Some terms appearing in our linearised equations can be matched with terms appearing in the equations of Marin *et al.*, but even so, there are a large number of additional parameters in our system, so that exact correspondence is not possible. For many of our parameters numerical results are unavailable, although we see no reason why in principle they could not be measured experimentally. In order to match our spectra with those of Marin *et al.* therefore, a significant amount of guesswork is required in choosing parameters. We hasten to add however, that it seems that for any pumping resistances and capacitances, the coupling constants can be varied to give the desired threshold.

For the spectra presented in this chapter, we have chosen what we believe to be reasonable parameters for the electrical circuit, and have adjusted other parameters to obtain results which are in agreement with those of Marin *et al.* The parameters for the electrical circuit are as follows

$$T_l = T_s = T_u = T_p = T_e = T_h = 293K \tag{3.23}$$

$$\tilde{T}_l = \tilde{T}_s = \tilde{T}_u = \tilde{T}_p = \tilde{T}_e = \tilde{T}_h = 293K. \tag{3.24}$$

We choose all temperatures to be at room temperature since the experiments of Marin *et al.* were carried out at room temperature. The

remaining parameters are

$$\begin{aligned}
R_s &= 30\,\Omega & \tilde{R}_s &= R_s/z \\
R_l &= 10\,\Omega & \tilde{R}_l &= R_l/z \\
R_p &= 1000\,\Omega & \tilde{R}_p &= R_p/z \\
R_u &= 1000\,\Omega & \tilde{R}_u &= R_u/z \\
R_e &= 0\,\Omega & \tilde{R}_e &= R_e/z \\
R_h &= 0\,\Omega & \tilde{R}_h &= R_h/z \\
C_s &= 0.1 \times 10^{-12}\,\mathrm{F} & \tilde{C}_s &= zC_s \\
C_e &= 10 \times 10^{-12}\,\mathrm{F} & \tilde{C}_e &= zC_e \\
C_h &= 10 \times 10^{-12}\,\mathrm{F} & \tilde{C}_h &= zC_h.
\end{aligned}$$

The parameter z is the ratio of the coupling to the additional carrier population by the central mode, to the coupling to the common carrier population coupled to by all modes. Its value is discussed overleaf.

Ballpark figures for resistances and capacitances in a laser are approximately tens of ohms for resistances, and picofarads for capacitances. We choose R_p and R_u to be large. The former is large because it is the pump resistance, and the latter is chosen large to ensure that some current travels through one of the capacitive branches of the circuit. R_e and R_h are not expected to have a great influence, since they are in branches containing capacitors, and hence are chosen to be zero. C_s is chosen to be somewhat smaller than C_e and C_h, since this capacitor is only expected to store small amounts of charge to balance the charges stored on C_e and C_h.

The remaining parameters are chosen to obtain the best possible results which agree with Marin *et al.* These parameters have the values

$$\begin{aligned}
a_{11} &= 8.7 \times 10^{-6}\mathrm{s}^{-1} & \tilde{a}_{11} &= za_{11} \\
d &= 6.8 \times 10^{-1}\mathrm{s}^{-1} & \tilde{d} &= zd \\
N &= \sqrt{(n_e n_h)/200} & \tilde{N} &= zN \\
M &= n_h - \frac{(\alpha_e - \beta_h)n_e}{(\alpha_h - \beta_e)} & \tilde{M} &= \tilde{n}_h - \frac{(\tilde{\alpha}_e - \tilde{\beta}_h)\tilde{n}_e}{(\tilde{\alpha}_h - \tilde{\beta}_e)}.
\end{aligned}$$

The values of n_e and n_h chosen to calculate N and M are not particularly important, since N and M are both constants and thus have no actual n_e and n_h dependence as such. The values we use are obtained by finding approximate steady-state solutions for n_e and n_h where some simplifications have been made. These values are

$$\begin{aligned} n_e &= 1.136 \times 10^8 \qquad \tilde{n}_e = z n_e \\ n_h &= 20 n_e \qquad\qquad\ \tilde{n}_h = z n_h. \end{aligned}$$

The remaining parameters c_{11}, d, and the denominator of N are varied to give the experimental threshold of Marin *et al.*

The purpose in choosing a value of z (since we know nothing about z we must choose a value) is to obtain noise levels which show agreement with previous experimental and theoretical results. Thus for small values of $\log(1-p)$ we expect a noise level which has values above the shot noise level, and for values of $\log(1-p)$ closer to zero, we expect a sub-shot noise level value.

We chose a variety of z values and calculated intensity noises, but could not find a regime in which agreement with experimental results was obtained. A slight shift in the position of the plot of intensity noises (given by Eqn (3.21)) towards positive values was found for increasing values of z as shown in Figs 3.4(a) and 3.4(b), but this shift was not found to be great enough for the shot noise level to be crossed, and thus for agreement with experimental results to be obtained.

For another set of parameters however (which did not match up to the parameters of Marin *et al.*), z was found to have a significant influence on the noise, and the shift in the noise level with increasing values of z was found to bring the noise above the shot noise level.

Since the value of z does not seem to have a large influence on the noise level for the parameters we have chosen here, the choice of a value remains rather arbitrary. We chose a value of $1/100$, since this indicates a 1% difference in the populations to which the central and side modes couple, and as such, is consistent with the discussion which

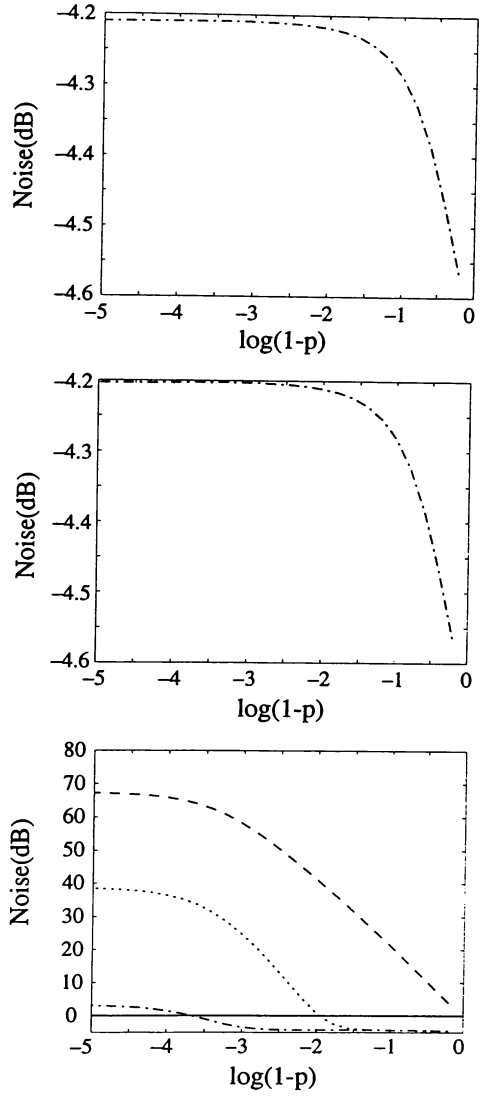


Figure 3.4: (a) Total intensity noise (Equation 3.21) in the absence of decorrelating mechanisms for $z = 10^{-9}$ and $\mu_1 = \mu_2 = \mu_3 = 1$. (b) Total intensity noise for $z = 10^{-2}$ and $\mu_1 = \mu_2 = \mu_3 = 1$. (c) Total intensity noise (dot-dashed line), central mode intensity noise (dotted line), and side mode intensity noise (dashed line), given by Equation (3.19), for $z = 10^{-2}$, $\mu_1 = 1$, and $\mu_2 = \mu_3 = 0.985$. The shot-noise level is indicated by the solid line.

will be given in Section 3.10.

Other mechanisms must exist then, which for the parameters here, give a total intensity noise above the shot-noise level for some values of $\log(1-p)$. One such mechanism, which we have included here, involves the detection efficiency of the central mode compared to the side mode. We expect that since the central and side modes have different spatial distributions[3], then in propagating between the cavity and the detector, the modes will be affected slightly differently by the medium in which they propagate. For example, the location of the scattering centres could be such that photons from the central mode are scattered, but photons from the other modes are not, or vice versa. We have therefore introduced a detection efficiency for the side modes μ_2, μ_3, which is slightly less than the detection efficiency of the central mode μ_1, which has a value of 1. In our case, a value of $\mu_2 = \mu_3 = 0.985$ gives results which agree best with experiment.

The total intensity noise for this situation is plotted in Fig 3.4(c), where $\mu_2 = \mu_3 = 0.985$. We now have the situation of Marin *et al.*, in that squeezing is destroyed for the regime which corresponds to the free-running laser. On this plot, we have included the intensity noise spectra for the central and side modes (Equation (3.19)), which do not change significantly for the three cases. The left hand side of the graph represents ratios of the decay constants which are close to 1, and hence correspond to the free-running laser. As can be seen from this figure, the intensity noise in the central and side modes is large, and the total intensity noise is small and not squeezed. The right hand side of Fig 3.4 represents ratios of the decay constants which are less than 1, in other words, the external grating laser. Here we see that the total noise, and the noise in the central mode are the same. The side mode noise is somewhat higher, as in the Langevin model of Marin *et al.*, but has negligible intensity as indicated in the plot of main mode and side mode

[3]See Section 3.10.

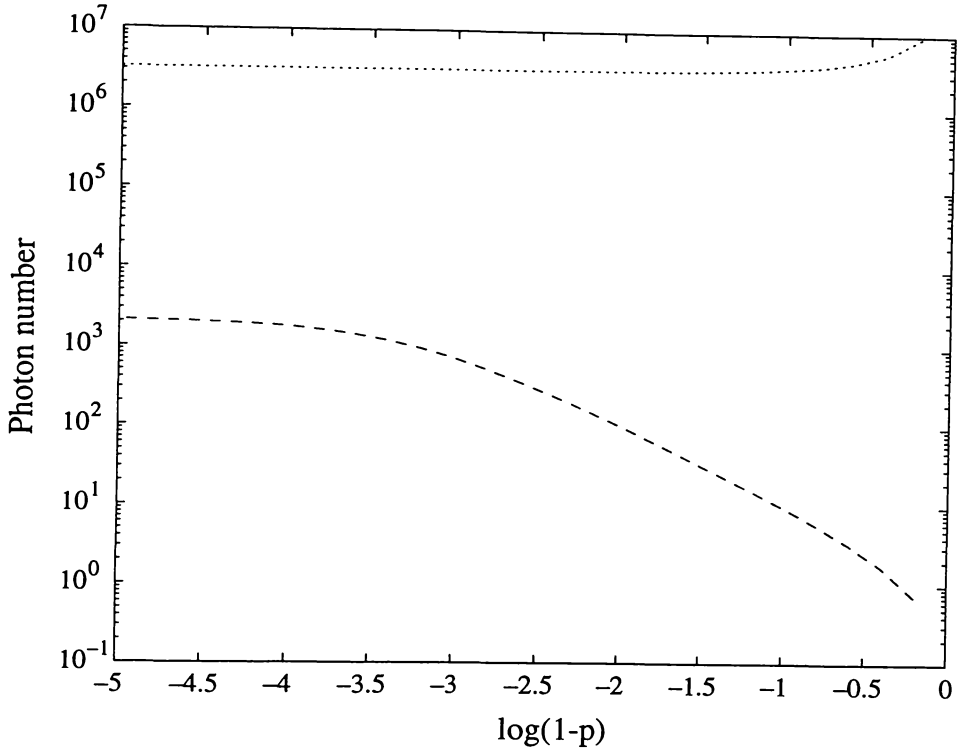


Figure 3.5: Mode occupation for central (dotted line), and side (dashed line) modes as a function of $\log(1-p)$.

photon numbers in Fig 3.5, indicating that in this regime, we have true single mode squeezing.

Fig 3.6 shows the photon number as a function of pump strength. From this figure we can see that the lasing threshold is the same as the experimental value of 18mA of Marin *et al.*

3.9 Eigenvectors and Eigenvalues

Examination of the eigenvectors and eigenvalues of the drift matrix allows us to gain some insight into the physical and dynamic processes occuring in the semiconductor. A typical example of these eigenvalues

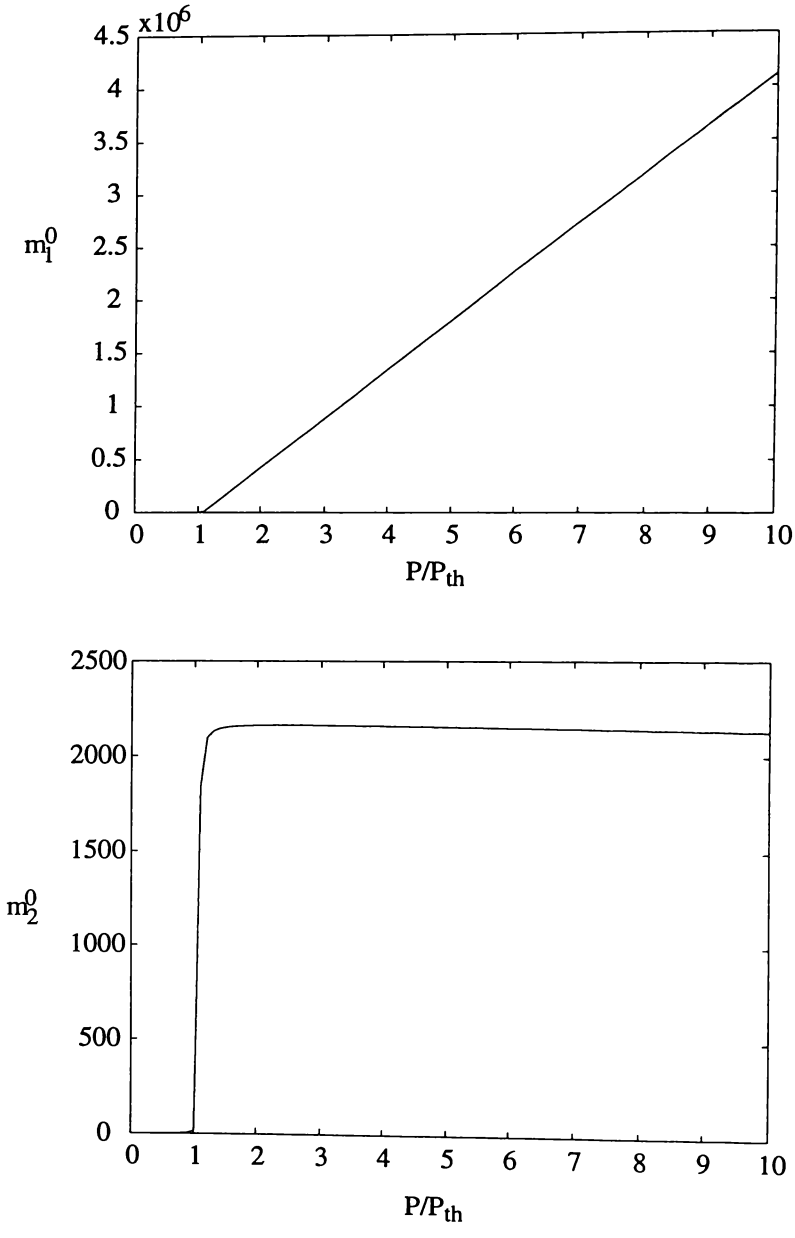


Figure 3.6: Photon number as a function of pump strength, showing the lasing threshold for (a) the central mode, and (b) the side modes.

and eigenvectors is given, so that features of the system may be discussed. The example given corresponds to a value of $\log(1-p)$ of -5. The eigenvectors and eigenvalues are given in three separate tables, so that the following discussion may be more easily followed.

n_e	0.1-0.7i	0.1+0.7i
n_h	0.1-0.7i	0.1+0.7i
$\tilde{n}_e$	~ 0	~ 0
$\tilde{n}_h$	~ 0	~ 0
m_1	0.2+0.1i	0.2-0.1i
m_2	~ 0	~ 0
m_3	~ 0	~ 0
λ	$(2+7i) \times 10^{10}$	$(2-7i) \times 10^{10}$

Table 3.1: Eigenvectors and Eigenvalues describing energy exchange between the semiconductor and the field.

Table 3.1 gives the eigenvectors and eigenvalues representing the coupling between the field and the semiconductor. These describe the principal lasing effect. The eigenvalues are complex conjugates, and their complex nature arises due to parasitic oscillations in the semiconductor. The eigenvectors describe the interaction of the central optical mode with the carriers in the semiconductor. It is interesting to note here that the side modes have negligible interaction with the carriers compared to the central mode.

Table 3.2 indicates the eigenvectors and eigenvalues (denoted by the symbol λ) for the processes in which only the field modes exchange energy. These processes occur over the longest time scales. The first describes the exchange of energy between the central mode and the side modes, and the second describes energy exchange between the side modes. These two situations can be considered as symmetric and antisymmetric modes of the coupled field system respectively. These eigenvalues are found to vary significantly with a change in $\log(1-p)$.

n_e	~ 0	~ 0
n_h	~ 0	~ 0
$\tilde{n}_e$	~ 0	~ 0
$\tilde{n}_h$	~ 0	~ 0
m_1	-0.8	~ 0
m_2	0.4	-0.7
m_3	0.4	0.7
λ	1×10^8	1×10^8

Table 3.2: Eigenvectors and Eigenvalues describing energy exchange between the field modes.

For $\log(1-p) = -0.2$, these eigenvalues are found to have values of 1.5×10^{11}. This means that in the case where mode selectivity is enhanced by having significantly different decay constants, energy transfer between the field modes occurs on a much faster time scale. For this value of $\log(1-p) = -0.2$, there is no longer strictly the situation of symmetric and antisymmetric modes however, since the symmetric eigenvector includes some feeding into the carriers populations n_e and n_h. It is thus the effects described by these two eigenvalues in which the carriers play little part which result in side mode population.

These eigenvectors in Tables 3.1 and 3.2 give us information about how noise in the system arises. If the carriers coupled only to the central mode, one would expect perfect squeezing to be obtained. This is not the case, however the eigenvectors indicate that the resultant noise is not due to partitioning noise of the carriers dividing themselves up among the modes either. The mechanism indicated by the eigenvectors is rather that essentially all the carrier population is fed into the central mode, and is then distributed into the side modes from the central mode, with very little contribution from the carriers. It is this process which introduces noise into the system.

Table 3.3 gives the eigenvalues describing energy exchange amongst

n_e	1	~ 0	~ 0
n_h	0.03	~ 0	~ 0
$\tilde{n}_e$	~ 0	0.6	-0.7
$\tilde{n}_h$	~ 0	0.8	-0.7
m_1	0.07	~ 0	~ 0
m_2	~ 0	~ 0	~ 0
m_3	~ 0	~ 0	~ 0
λ	3×10^{11}	3×10^{11}	2×10^{12}

Table 3.3: Eigenvectors and Eigenvalues describing energy exchange between the carriers.

the carriers. The eigenvalues are the largest and thus describe processes which occur on the shortest time scales. The contributions to the eigenvectors are essentially all carrier contributions and as such, these eigenvalues and eigenvectors describe carrier relaxation effects, which occur on a very fast time scale.

3.10 Mode Spatial Distributions

Experimentalists working with semiconductor lasers have to the best of our knowledge, not yet attempted to measure any differences in the spatial distribution of the modes in a semiconductor. It is generally believed that any differences which may exist will be beyond the finite resolution of the detection equipment, and are thus negligible.

We have found it impossible to match our results with those of experiment without introducing differing detection efficiencies which arise due to a difference in spatial mode distributions. However, the values we have used to obtain agreement with experiment are of the order of 1% difference in the external detection efficiencies between the central mode and the side modes. This translates into a tiny difference internal to the laser system, and would thus quite likely be beyond

detection limits. In terms of the differences in carrier populations to which the different modes couple, we have introduced an additional carrier population for the central mode which is also 1%.

A preliminary literature search into theoretical work on differing spatial distributions of the multiple modes in a semiconductor laser (or indeed in any laser), have not revealed any published results on the subject. In work by Ballagh and coworkers [McCord 1990, Ballagh 1992], coupled Maxwell-Bloch equations, describing the propagation of σ^+ and σ^- beams in a gas of atoms, are solved numerically. Results indicate that self-induced separation of the components of the beam can occur, and interesting beam intensity profiles can result [McClelland 1991, Wilson 1992]. In the case of semiconductor lasers, effects such as phase-amplitude coupling and the resultant refractive index shifts of the modes (by differing amounts for the different frequency modes), certainly make differing mode shapes for the different modes seem plausible, although this needs to be proved theoretically. If this were done, then one could use the noise rise observed in our results as the difference in efficiencies and carrier populations is increased, as an experimental verification of the different mode shapes.

3.11 The use of Electrical Circuits to Describe Pumping

The reader may have reservations regarding the use of the electrical circuits in a pumping model, which leads to a large number of free parameters. These parameters however, are in principle physically measurable, though this has not yet been done. To a greater or lesser extent, all are necessary for a description of the phenomena observed experimentally. The values chosen for the parameters are what we believe to be reasonable values, as discussed in the body of this chapter. The spectra are sensitive to the sizes of some parameters, but to others

are fairly insensitive. Hence, R_e and R_h can be set to zero, and the sizes of R_s and R_u have no effect on the spectra, although if they are set to zero, problems with the computations occur. The remaining parameters have a noticeable effect on the spectrum (causing an upwards or downwards shift) and thus must be chosen more carefully.

The resulting mathematics does become rather messy, but this is the price one has to pay for an attempt at a realistic model – and the rather simple equivalent circuit we have given does provide such a realistic model. It is our belief that further experimental progress in this field will require careful and detailed measurement of the kind of electrical properties of the lasers which we have used, as well as the more interesting optical measurements. If this is done, we believe that our methodology provides a basis for genuine quantitative modelling.

Chapter 4

Injection Locking of Multi-Mode Semiconductor Lasers

4.1 Introduction

In the last chapter, we considered the free-running and external grating laser theoretically, using a master equation description for the multi-mode semiconductor laser. We found results which agreed with those of Marin *et al.*; for the free-running case, there is no squeezing, and for the external grating case, single-mode squeezing is obtained.

In this chapter we focus our attention on the other situation considered by Marin *et al.* of injection locking, which completes a comparison with their work. In this case Marin *et al.* found that although there was squeezing of the total intensity noise, the individual mode noises were unsqueezed. Thus squeezing in the sense of single mode squeezing is not obtained, but squeezing of the total intensity noise arises as the result of anticorrelated fluctuations of the individual modes in the semiconductor. In addition to examining this intensity noise theoretically, we also examine the phase noise of the system, to see whether a reduction in noise occurs as locking takes place.

4.2 Inclusion of Injection Locking

Injection locking involves feeding a stable coherent signal into the system. This serves the purpose of locking the frequency of the dominant mode of the system to that of the injected signal, the effect of which is to stabilise the system with regard to fluctuations in the frequency.

Mathematically this process is written in terms of a Hamiltonian which introduces a coupling between the dominant mode and the injected signal.

$$H_{\text{inj}} = i\hbar(b_1^\dagger \epsilon - b_1 \epsilon^*), \tag{4.1}$$

where $|\epsilon|$ is proportional to the amplitude of the coherent injected signal, and b_1 is the annihilation operator for a photon in the dominant mode. Using standard input-output theory arguments, the injected power in units of photons per second can be found in terms of $|\epsilon|$ to be $4|\epsilon|^2/\kappa$. All other Hamiltonian contributions are the same as in Section 2.2 and Section 3.2.

Standard techniques [Louisell 1974] can be used to write down the injection locking contribution to the master equation.

$$\left.\frac{\partial \rho_0(\underline{n})}{\partial t}\right|_{\text{inj}} = \frac{-i}{\hbar}[H_{\text{inj}}, \rho] = b_1^\dagger \epsilon \rho - b_1 \epsilon^* \rho - \rho b_1^\dagger \epsilon + \rho b_1 \epsilon^* \tag{4.2}$$

The remaining master equation contributions are given in Equation (2.52) and Section 3.4. Using operator correspondences [Gardiner 1991] to convert to the positive-P representation, the contribution to the Fokker-Planck equation obtained due to injection locking is

$$\left.\frac{\partial P(\mathbf{X})}{\partial t}\right|_{\text{inj}} = \left[-\frac{\partial}{\partial \beta_1}\epsilon - \frac{\partial}{\partial \beta_1^*}\epsilon^*\right] P(\mathbf{X}), \tag{4.3}$$

where $\mathbf{X}$ is defined in Equation (3.14). This contribution leads to additional terms in two of the stochastic differential equations, Equations (E.1)-(E.6). For clarity and completeness, these altered equations

(Equations (E.5)-(E.6)) are given here in full.

$$\begin{aligned} d(\beta_1) &= \Big\{ \sum_j [G^*_{j1}(\underline{n})\beta_j - F^*_{j1}(\underline{n})\beta_j] - \frac{\kappa_1\beta_1}{2} - i\Delta_1\beta_1 \\ &\quad + \tilde{G}^*_{11}(\underline{n})\beta_1 - \tilde{F}^*_{11}(\underline{n})\beta_1 + \epsilon \Big\} dt \\ &\quad - \sum_j v_{1j} d\eta_j + \sqrt{\kappa_1 \bar{N}_1}\, d\Xi_1 - \tilde{v}_{11} d\tilde{\eta} \qquad (4.4) \\ d(\beta_1^*) &= \Big\{ \sum_j [G_{1j}(\underline{n})\beta_j^* - F_{1j}(\underline{n})\beta_j^*] - \frac{\kappa_1\beta_1^*}{2} + i\Delta_1\beta_1^* \\ &\quad + \tilde{G}_{11}(\underline{n})\beta_1^* - \tilde{F}_{11}(\underline{n})\beta_1^* + \epsilon^* \Big\} dt \\ &\quad - \sum_j v^*_{1j} d\eta^*_j + \sqrt{\kappa_1 \bar{N}_1}\, d\Xi^*_1 - \tilde{v}^*_{11} d\tilde{\eta}^*, \qquad (4.5) \end{aligned}$$

where all symbols have the same definitions as in Chapters 2 and 3. Since we wish to calculate the photon number fluctuations, we need a stochastic differential equation for the central mode photon number, $m_1 = \beta_1^*\beta_1$, and such an expression can be obtained from Equations (4.4) and (4.5) using Ito calculus,

$$\begin{aligned} d(m_1) &= \Big\{ \sum_j [G^*_{j1}(\underline{n})\beta_1^*\beta_j - F^*_{j1}(\underline{n})\beta_1^*\beta_j] \\ &\quad + \sum_j [G_{1j}(\underline{n})\beta_j^*\beta_1 - F_{1j}(\underline{n})\beta_j^*\beta_1] \\ &\quad + [\tilde{G}^*_{11}(\underline{n}) + \tilde{G}_{11}(\underline{n})]m_1 - [\tilde{F}^*_{11}(\underline{n}) + \tilde{F}_{11}(\underline{n})]m_1 \\ &\quad - \kappa_1 m_1 + \beta_1^*\epsilon + \beta_1\epsilon^* \Big\} dt + \sqrt{\kappa_1 \bar{N}_1}[\beta_1^* d\Xi_1 + \beta_1 d\Xi_1^*] \\ &\quad - \sum_j [\beta_1^* v_{1j} d\eta_j - \beta_1 v^*_{1j} d\eta^*_j] - \beta_1^* \tilde{v}_{11} d\tilde{\eta} - \beta_1 \tilde{v}^*_{11} d\tilde{\eta}^* \\ &\quad + \Big\{ 2G^r_{11}(\underline{n}) + \kappa_1 \bar{N}_1 + 2\tilde{G}^r_{11}(\underline{n}) \Big\} dt. \qquad (4.6) \end{aligned}$$

Equation (4.6) can be simplified somewhat by applying the rotating wave approximation as done in Section 3.7, and setting the phase of

the injected field equal to zero. We obtain

$$\begin{aligned} d(m_1) &= \Big\{2G^r_{11}(\underline{n})(m_1+1) - 2F^r_{11}(\underline{n})m_1 - \kappa_1 m_1 + |\epsilon|(\beta_1+\beta_1^*) \\ &\quad +2\tilde{G}^r_{11}(\underline{n})(m_1+1) - 2\tilde{F}^r_{11}(\underline{n})m_1 + \kappa_1\bar{N}_1\Big\}\,dt \\ &\quad -\sum_j [v_{1j}d\eta_j\beta_1^* + v^*_{1j}d\eta^*_j\beta_1] + \sqrt{\kappa_1\bar{N}_1}[d\Xi_1\beta_1^* + d\Xi_1^*\beta_1] \\ &\quad -(\beta_1^*\tilde{v}_{11}d\tilde{\eta} + \beta_1\tilde{v}^*_{11}d\tilde{\eta}^*) \end{aligned} \tag{4.7}$$

The remaining equations describing the system are unaltered by the presence of injection locking and so are not repeated here. The reader is referred to Equations (E.30)-(E.34) for these, where $l = 2, 3$ in Equation (E.34). We can see that the system of equations for the injection locked system is now no longer closed, since Equation (4.7) couples to the field amplitudes β_1 and β_1^*. A closed system can be retained however, at the expense of introducing a further variable to our system,

$$\beta_{1,+} = \beta_1 + \beta_1^*. \tag{4.8}$$

The variable $\beta_{1,+}$ has the Ito SDE

$$\begin{aligned} d(\beta_{1,+}) &= \Big\{\sum_j [G^*_{j1}(\underline{n})\beta_j + G_{1j}(\underline{n})\beta_j^* - F^*_{j1}(\underline{n})\beta_j - F_{1j}(\underline{n})\beta_j^*] \\ &\quad +\beta_{1,+}\tilde{G}^r_{11}(\underline{n}) + \beta_{1,-}\tilde{G}^i_{11}(\underline{n}) - \beta_{1,+}\tilde{F}^r_{11}(\underline{n}) - \beta_{1,-}\tilde{F}^i_{11}(\underline{n}) \\ &\quad -\frac{\kappa_1}{2}\beta_{1,+} + \epsilon + \epsilon^*\Big\}dt - \sum_j [v_{1j}d\eta_j + v^*_{1j}d\eta^*_j] \\ &\quad +\sqrt{\kappa_1\bar{N}_1}[d\Xi_1 + d\Xi_1^*] - \tilde{v}_{11}d\tilde{\eta} - \tilde{v}^*_{11}d\tilde{\eta}^*, \end{aligned} \tag{4.9}$$

where

$$\beta_{1,-} = -i(\beta_1 - \beta_1^*). \tag{4.10}$$

Making the same approximations as those made in arriving at Equation (4.7), and assuming that the imaginary part of G_{lj} and F_{lj} is much less than the real part (this amounts to assuming that the dephasing

time is much less than the inverse of the frequency separation between states in the conduction and valence bands, and as such is a realistic assumption), the new variable $\beta_{1,-}$ appearing in the above equation can be eliminated, and the above expression can be simplified to

$$\begin{aligned} d(\beta_{1,+}) &= \Big\{G^r_{11}(\underline{n})\beta_{1,+} - F^r_{11}(\underline{n})\beta_{1,+} + \beta_{1,+}\tilde{G}^r_{11}(\underline{n}) - \beta_{1,+}\tilde{F}^r_{11}(\underline{n}) \\ &\quad -\frac{\kappa_1}{2}\beta_{1,+} + 2|\epsilon|\Big\}dt - \sum_j [v_{1j}d\eta_j + v^*_{1j}d\eta^*_j] \\ &\quad +\sqrt{\kappa_1\bar{N}_1}(d\Xi_1 + d\Xi^*_1) - \tilde{v}_{11}d\tilde{\eta} - \tilde{v}^*_{11}d\tilde{\eta}^*, \end{aligned} \tag{4.11}$$

which couples only to $\beta_{1,+}$, and thus a closed system is recovered.

The phase noise of the system is also worth calculating, since it would be interesting to see whether this decreases as the injection strength is increased, and phase locking begins to occur. The easiest correlation to measure the spectrum of, in order to gain information about the phase noise, is the $\langle\beta_{1,-}(t)\beta_{1,-}(0)\rangle$ correlation. Since $\beta_{1,-}$ is proportional to the sine of the phase, a reduction in the noise of $\beta_{1,-}$ translates directly into a reduction in the noise of the phase. This is not the case for the variable $\beta_{1,+}$, which is proportional to the cosine of the phase, and hence the phase noise would increase for decreasing noise in $\beta_{1,+}$. Hence, in order to consider the phase noise, we include the stochastic differential equation for $\beta_{1,-}$ in our system.

The equation of motion for $\beta_{1,-}$ can be written down from Equations (4.4) and (4.5),

$$\begin{aligned} d(\beta_{1,-}) &= \Big\{ \sum_j [-iG^*_{j1}(\underline{n})\beta_j + iG_{1j}(\underline{n})\beta^*_j + iF^*_{j1}(\underline{n})\beta_j - iF_{1j}(\underline{n})\beta^*_j] \\ &\quad +i\beta_{1,+}\tilde{G}^i_{11}(\underline{n}) + \beta_{1,-}\tilde{G}^r_{11}(\underline{n}) - i\beta_{1,+}\tilde{F}^i_{11}(\underline{n}) - \beta_{1,-}\tilde{F}^r_{11}(\underline{n}) \\ &\quad -\frac{\kappa_1}{2}\beta_{1,-} - i(\epsilon - \epsilon^*)\Big\}dt + i\sum_j [v_{1j}d\eta_j - v^*_{1j}d\eta^*_j] \\ &\quad -i\sqrt{\kappa_1\bar{N}_1}[d\Xi_1 - d\Xi^*_1] + i(\tilde{v}_{11}d\tilde{\eta} + \tilde{v}^*_{11}d\tilde{\eta}^*). \end{aligned} \tag{4.12}$$

Making the rotating wave approximation, setting the phase of the injected field to zero, and assuming that the imaginary parts of the F_{ij} and G_{ij} terms are much less than the real parts, the above expression simplifies to

$$\begin{aligned} d(\beta_{1,-}) &= \Big\{G^r_{11}(\underline{n})\beta_{1,-} - F^r_{11}(\underline{n})\beta_{1,-} + \beta_{1,-}\tilde{G}^r_{11}(\underline{n}) - \beta_{1,-}\tilde{F}^r_{11}(\underline{n} \\ &\quad -\frac{\kappa_1}{2}\beta_{1,-})\Big\}dt + i\sum_j [v_{1j}d\eta_j - v^*_{1j}d\eta^*_j] \\ &\quad -i\sqrt{\kappa_1\bar{N}_1}(d\Xi_1 - d\Xi^*_1) + i(\tilde{v}_{11}d\tilde{\eta} + \tilde{v}^*_{11}d\tilde{\eta}^*). \end{aligned} \tag{4.13}$$

4.3 Linearised Equations

Calculation of the spectrum requires use of the drift and diffusion matrices of the system of equations linearised about their steady-state values. These linearised equations are

$$d\mathbf{z} = -\mathcal{H}(\mathbf{Z}_0)\mathbf{z}(t)dt + \mathcal{I}(\mathbf{Z}_0)d\mathbf{W}(t), \tag{4.14}$$

where

$$\mathbf{Z}(t) = \mathbf{Z}_0 + \mathbf{z}(t), \tag{4.15}$$

$$\mathbf{Z} = \begin{pmatrix} n_e \\ n_h \\ \tilde{n}_e \\ \tilde{n}_h \\ \beta_{1,+} \\ \beta_{1,-} \\ m_1 \\ m_2 \\ m_3 \end{pmatrix}, \tag{4.16}$$

and the following definitions,

$$r_j = 2a_{jj}(m^0_j + 1) \tag{4.17}$$

$$s_{jj} = 2a_{jj}(N^2 - n_e n_h) \tag{4.18}$$

$$\tilde{r}_1 = 2\tilde{a}_{11}(m_1^0 + 1) \tag{4.19}$$

$$\tilde{s}_{11} = 2\tilde{a}_{11}(\tilde{N}^2 - \tilde{n}_e\tilde{n}_h), \tag{4.20}$$

and

$$t(m_j^0) = 2m_j^0 a_{jj} n_e^0 n_h^0 \tag{4.21}$$

$$u(m_j^0) = t(m_j^0 + 1) + 2m_j^0 a_{jj} N^2 + d n_e^0 n_h^0 \tag{4.22}$$

$$\tilde{t}(m_1^0) = 2m_1^0 \tilde{a}_{11} \tilde{n}_e^0 \tilde{n}_h^0 \tag{4.23}$$

$$\tilde{u}(m_1^0) = \tilde{t}(m_1^0 + 1) + 2m_1^0 \tilde{a}_{11} \tilde{N}^2 + \tilde{d}\tilde{n}_e^0 \tilde{n}_h^0, \tag{4.24}$$

are used in the matrices

$$\mathcal{H}_{cc}(\mathbf{Z}_0) = \begin{pmatrix} \sum_j (r_j + d) n_h^0 + \alpha_e & \sum_j (r_j + d) n_e^0 + \beta_e & 0 & 0 \\ \sum_j (r_j + d) n_h^0 + \beta_h & \sum_j (r_j + d) n_e^0 + \alpha_h & 0 & 0 \\ 0 & 0 & (\tilde{r}_1 + \tilde{d})\tilde{n}_h^0 & (\tilde{r}_1 + \tilde{d})\tilde{n}_e^0 \\ 0 & 0 & (\tilde{r}_1 + \tilde{d})\tilde{n}_h^0 & (\tilde{r}_1 + \tilde{d})\tilde{n}_e^0 \end{pmatrix} \tag{4.25}$$

$$\mathcal{H}_{cf}(\mathbf{Z}_0) = \begin{pmatrix} 0 & 0 & -s_{11} & -s_{22} & -s_{33} \\ 0 & 0 & -s_{11} & -s_{22} & -s_{33} \\ 0 & 0 & -\tilde{s}_{11} & 0 & 0 \\ 0 & 0 & -\tilde{s}_{11} & 0 & 0 \end{pmatrix} \tag{4.26}$$

$$\mathcal{H}_{fc}(\mathbf{Z}_0) = \begin{pmatrix} -a_{11}\beta_{1,+}^0 n_h^0 & -a_{11}\beta_{1,+}^0 n_e^0 & -\tilde{a}_{11}\beta_{1,+}^0 \tilde{n}_h^0 & -\tilde{a}_{11}\beta_{1,+}^0 n_e^0 \\ -a_{11}\beta_{1,-}^0 n_h^0 & -a_{11}\beta_{1,-}^0 n_e^0 & -\tilde{a}_{11}\beta_{1,-}^0 \tilde{n}_h^0 & -\tilde{a}_{11}\beta_{1,-}^0 n_e^0 \\ -r_1 n_h^0 & -r_1 n_e^0 & -\tilde{r}_1 \tilde{n}_h^0 & -\tilde{r}_1 \tilde{n}_e^0 \\ -r_2 n_h^0 & -r_2 n_e^0 & 0 & 0 \\ -r_3 n_h^0 & -r_3 n_h^0 & 0 & 0 \end{pmatrix} \tag{4.27}$$

$$\mathcal{H}_{ff}(\mathbf{Z}_0) = \begin{pmatrix} \frac{1}{2}(s_{11}+\tilde{s}_{11}+\kappa_1) & 0 & 0 & 0 & 0 \\ 0 & \frac{1}{2}(s_{11}+\tilde{s}_{11}+\kappa_1) & 0 & 0 & 0 \\ -\epsilon & 0 & s_{11}+\tilde{s}_{11}+\kappa_1 & 0 & 0 \\ 0 & 0 & 0 & -s_{22}+\kappa_2 & 0 \\ 0 & 0 & 0 & 0 & s_{33}+\kappa_3 \end{pmatrix} \tag{4.28}$$

$$\mathcal{I}_{cc}(\mathbf{Z}_0) = \begin{pmatrix} \sum_j u(m_j^0)+D_e & \sum_j u(m_j^0)+D_{eh} & 0 & 0 \\ \sum_j u(m_j^0)+D_{he} & \sum_j u(m_j^0)+D_h & 0 & 0 \\ 0 & 0 & \tilde{u}(m_1^0)+\tilde{D}_e(\underline{n}) & \tilde{u}(m_1^0)+\tilde{D}_{eh}(\underline{n}) \\ 0 & 0 & \tilde{u}(m_1^0)+\tilde{D}_{he}(\underline{n}) & \tilde{u}(m_1^0)+\tilde{D}_h(\underline{n}) \end{pmatrix} \tag{4.29}$$

$$\mathcal{I}_{cf}(\mathbf{Z}_0) = \begin{pmatrix} -t(\beta_{1,+}^0) & -t(\beta_{1,-}^0) & -2t(m_1^0) & -2t(m_2^0) & -2t(m_3^0) \\ -t(\beta_{1,+}^0) & -t(\beta_{1,-}^0) & -2t(m_1^0) & -2t(m_2^0) & -2t(m_3^0) \\ -\tilde{t}(\beta_{1,+}^0) & -\tilde{t}(\beta_{1,-}^0) & -2\tilde{t}(m_1^0) & 0 & 0 \\ -\tilde{t}(\beta_{1,+}^0) & -\tilde{t}(\beta_{1,-}^0) & -2\tilde{t}(m_1^0) & 0 & 0 \end{pmatrix} \tag{4.30}$$

$$\mathcal{I}_{fc}(\mathbf{Z}_0) = \begin{pmatrix} -t(\beta^0_{1,+}) & -t(\beta^0_{1,+}) & -\tilde{t}(\beta^0_{1,+}) & -\tilde{t}(\beta^0_{1,+}) \\ -t(\beta^0_{1,-}) & -t(\beta^0_{1,-}) & -\tilde{t}(\beta^0_{1,-}) & -\tilde{t}(\beta^0_{1,-}) \\ -2t(m^0_1) & -2t(m^0_1) & -2\tilde{t}(m^0_1) & -2\tilde{t}(m^0_1) \\ -2t(m^0_2) & -2t(m^0_2) & 0 & 0 \\ -2t(m^0_3) & -2t(m^0_3) & 0 & 0 \end{pmatrix} \tag{4.31}$$

$$\mathcal{I}_{ff}(\mathbf{Z}_0) = \begin{pmatrix} 2t(1) & 0 & t(\beta^0_{1,+}) & 0 & 0 \\ +2\tilde{t}(1) & & +\tilde{t}(\beta^0_{1,+}) & & \\ 0 & 2t(1) & t(\beta^0_{1,-}) & 0 & 0 \\ & +2\tilde{t}(1) & +\tilde{t}(\beta^0_{1,-}) & & \\ t(\beta^0_{1,+}) & t(\beta_{(1,-)^0}) & 2t(m^0_1) & 0 & 0 \\ +\tilde{t}(\beta^0_{1,+}) & +\tilde{t}(\beta^0_{1,-}) & +2\tilde{t}(m^0_1) & & \\ 0 & 0 & 0 & 2t(m^0_2) & 0 \\ 0 & 0 & 0 & 0 & 2t(m^0_3) \end{pmatrix}, \tag{4.32}$$

which make up the matrices

$$\mathcal{H}(\mathbf{Z}_0) = \begin{pmatrix} \mathcal{H}_{cc}(\mathbf{Z}_0) & \mathcal{H}_{cf}(\mathbf{Z}_0) \\ \mathcal{H}_{fc}(\mathbf{Z}_0) & \mathcal{H}_{ff}(\mathbf{Z}_0) \end{pmatrix}, \tag{4.33}$$

and

$$\mathcal{I}(\mathbf{Z}_0) = \begin{pmatrix} \mathcal{I}_{cc}(\mathbf{Z}_0) & \mathcal{I}_{cf}(\mathbf{Z}_0) \\ \mathcal{I}_{fc}(\mathbf{Z}_0) & \mathcal{I}_{ff}(\mathbf{Z}_0) \end{pmatrix}, \tag{4.34}$$

and $\mathbf{Z}_0$ is the vector of steady-state values of $\mathbf{Z}(t)$. We have made the same approximations for the $G^r_{ij}(\underline{n})$ and $F^r_{ij}(\underline{n})$ as in Chapter 3 (Equations (E.22)-(E.29)) in the matrices above. In the diffusion matrix we have dropped terms of the form $2G^r_{k1}(\underline{n})\beta_{k,+}$ where $k = 2, 3$ in the off-diagonal elements where they appear. This can be done for the same reasons as we make the rotating wave approximation.

Although the variable $\beta_{1,-}$ does not couple to any of the other stochastic differential equations under the approximations we have made, we have included its linearised stochastic differential equation in the drift and diffusion matrices, since it is required for the phase noise description. However, for the calculations of intensity noise, the stochastic differential equation for $\beta_{1,-}$ is ignored, and we deal with 8×8 matrices rather than 9×9, where the sixth row and column of $\mathcal{H}(\mathbf{Z}_0)$ and $\mathcal{I}(\mathbf{Z}_0)$ (which are those corresponding to the equation for $\beta_{1,-}$) are deleted, as is the sixth element of the vector $\mathbf{Z}(t)$.

4.4 Steady-State Solutions

Steady-state solutions must be found for the system of equations describing injection locking if the matrices (4.33) and (4.34) are to be used to calculate the spectrum. Since the variable $\beta_{1,-}$ does not couple into any of the other equations of the system, its steady-state solution can readily be found from Equation (4.13). Dropping the noise terms and setting $d(\beta_{1,-}) = 0$, we obtain

$$0 = [G^r_{11}(\underline{n}) - F^r_{11}(\underline{n}) - \frac{\kappa_1}{2} + \tilde{G}^r_{11}(\underline{n}) - \tilde{F}^r_{11}(\underline{n})]\beta_{1,-}. \tag{4.35}$$

The term in the square brackets is non-zero, so in the steady-state $\beta_{1,-}$ will be zero.

The remainder of the system of equations is given by Equations (4.7) and (4.11) of this chapter, and Equations (E.30)-(E.34), where $l = 2, 3$ in (E.34). Because of the complexity of this system of equations however, steady-state solutions must be found numerically, using an iterative procedure. This involves making some initial guess for the central mode photon number, and using it to calculate a new value of the central mode photon number.

If the noise terms in the system of equations are dropped, and the left hand sides set to zero, then for $P_e = P_h$, the equations (E.30)-(E.34)

can be rearranged to give equations (F.1)-(F.4) and (F.6), (F.7), and equations (4.7) and (4.11) can be rearranged to give the equation

$$m_1 = \frac{4|\epsilon|^2 + 2a_{11}n_e n_h(\kappa_1 + 2a_{11}N^2 - 2a_{11}n_e n_h)}{(\kappa_1 + 2a_{11}N^2 - 2a_{11}n_e n_h)^2}. \tag{4.36}$$

Equations (F.1)-(F.4) use an input value of the central mode photon number, which we call m_1^0, to generate values for $n_e, n_h, \tilde{n}_e$, and $\tilde{n}_h$. These values can then be substituted into Equation (4.36) to generate a new value of the central mode photon number m_1. Thus, for a range of values of m_1^0, m_1 can be said to be a function of m_1^0, $m_1 = f(m_1^0)$.

When the calculated value m_1, equals (or becomes close enough to) the input value m_1^0, a solution has been found. Referring to Fig 4.1, we are finding the point at which the function $f(m_1^0) = m_1$ intersects the line $f(m_1^0) = m_1^0$. The procedure used is similar to the bisection approach used in Appendix F, except because of the added complication of the injection locking, one must take extra care in choosing the boundaries of the interval to be bisected at each step.

The plot of the generated value m_1 versus the input value m_1^0 shown in Fig 4.1 illustrates this point.

The plot shows that $m_1 = f(m_1^0)$ can be negative for some values of m_1^0. In addition it appears that $m_1 = f(m_1^0)$ is discontinuous. However, careful magnification of $m_1 = f(m_1^0)$ reveals that the function is in fact continuous for some choices of parameters (notably, high injection powers). This continuity gives rise to two possible solutions, however the solutions which give rise to positive values of the eigenvalues of the drift matrix (in other words, stable solutions) lie on the part of the curve $f(m_1^0)$ with negative slope.

We must be careful to consider these two properties of the function and shift boundaries accordingly. It is important that in finding solutions for m_1, we do not inadvertantly shift the boundaries so that our bisection interval spans only negative solutions, or the regime of positive solutions where the slope of $f(m_1^0)$ is positive (in which an unstable

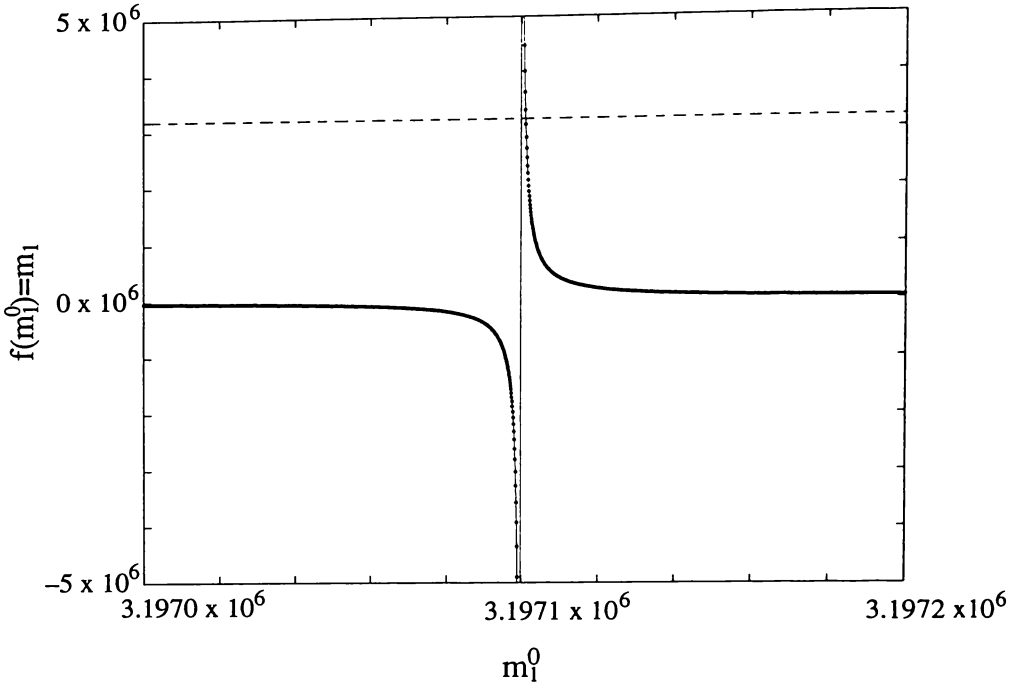


Figure 4.1: The function $f(m_1^0) = m_1$, depicted by the plotted points, shows an apparent discontinuity, and a regime in which the bisection algorithm could produce negative solutions. The lightly drawn solid line however, shows how the function can actually be continuous for some parameters. The dashed line is the function $f(m_1^0) = m_1^0$.

solution lies), but which lies beyond (to the left of) the stable solution.

The way in which we choose new upper and lower boundaries therefore differs from that used in the previous case. The first thing to check is whether the value of $m_1 = f(m_1^0)$ obtained is negative. If so, then we shift the lower boundary upwards and re-bisect the interval until a positive $m_1 = f(m_1^0)$ is obtained. Secondly, given that we have a positive value of $m_1 = f(m_1^0)$, we need to check the slope in the region of m_1. If it is positive, then we can shift the lower boundary to this point. If we have a positive solution for m_1, and are on the strictly decreasing portion of the curve, then we use the same procedure as in

Chapter 3.

Introducing these extra features was found to have no perceptible effect on the running time of the program.

4.5 Results

The variances of the individual and total intensity fluctuations, given by Equations (3.19) and (3.21) were calculated, where in this case, the matrices $\mathcal{E}(\mathbf{Y}_0)$ and $\mathcal{G}(\mathbf{Y}_0)$ appearing in Equations (3.20) and (3.22) are replaced with $\mathcal{H}(\mathbf{Z}_0)$ and $\mathcal{I}(\mathbf{Z}_0)$ (Equations (4.33) and (4.34), where the sixth column and row are ignored), and the intensity fluctuations in the individual modes are normalised with respect to the total shot-noise rather than the individual shot-noises. Results were obtained for the total, central and side mode intensity noise as a function of injection strength. The values of the decay constants used were $\kappa_1 = \kappa_2 = \kappa_3 = 2.45 \times 10^{11}\text{s}^{-1}$, which corresponds to the free-running laser when $\epsilon = 0$. All other parameter sizes are exactly the same as those used in Chapter 3.

Before we give the spectral results, we first examine the photon number, the injected photon number, and the variation of the phase of the central mode. Referring to Fig 4.2(a), the injected photon number, the central mode photon number, and the quantity $\beta_{1,+}^2/4$ are plotted as a function of the injection power.

It can be seen that $\beta_{1,+}^2/4$ approaches the central mode photon number for an injection power of about 10^7 photons/second. Since $\beta_{1,+}^2/4 = m_1 \cos^2 \phi_1$, this means that at an injection power of 10^7 photons/second, the phase ϕ_1 becomes zero, and phase locking has occured. Thus we expect to begin to see any effects on the spectra due to injection locking around this point.

The injected photon number becomes equal to the central mode photon number for an injection power of about 10^{19} photons/second.

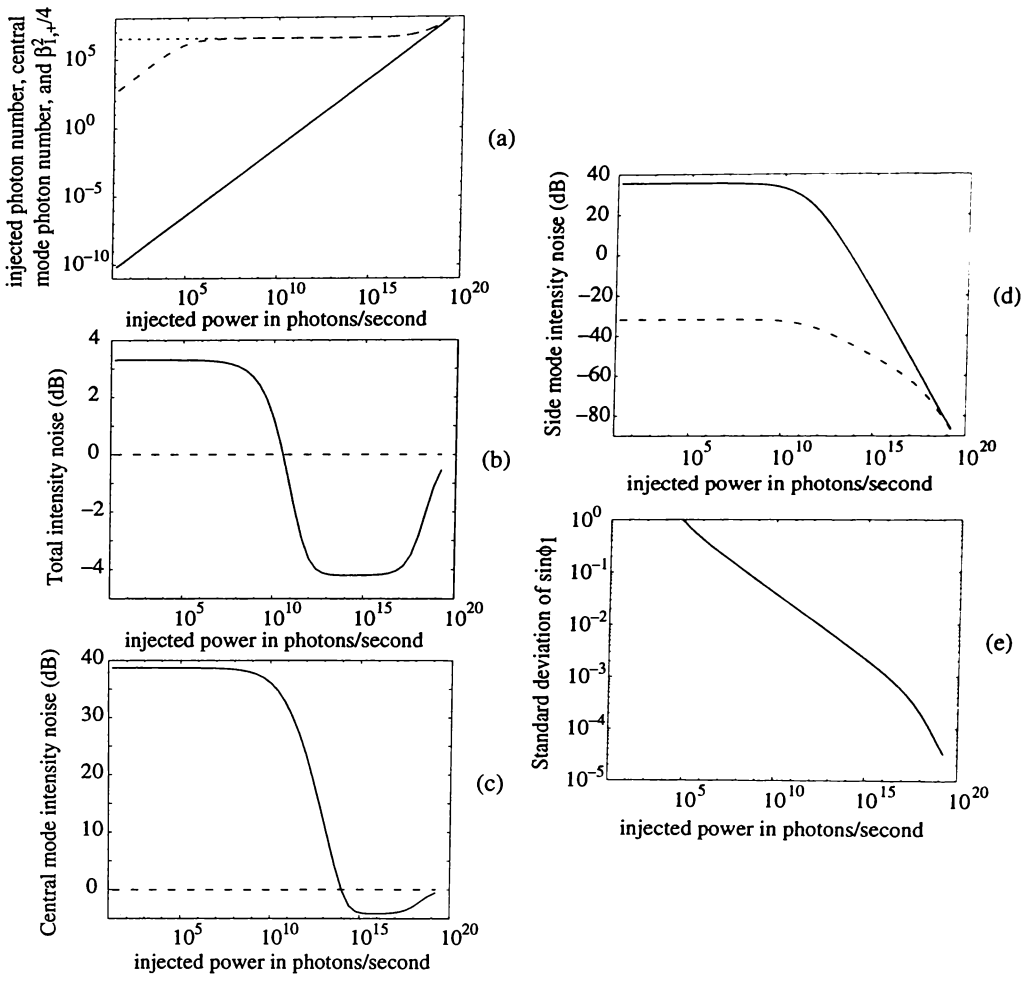


Figure 4.2: (a) Injected photon number (solid line), central mode photon number (dotted line), and $\beta_{1,+}^2/4 = m_1 \cos^2 \phi_1$ (dashed line), as a function of injected power, indicating the regime of injection locking. (b) Total intensity noise as a function of injected power. The dashed line indicates the shot-noise level. (c) Central mode intensity noise as a function of injected power. The dashed line indicates the shot noise level of the central mode intensity, normalised to the total intensity noise. (d) Side mode intensity noise as a function of injected power. The dashed line indicates the shot-noise level of the side mode intensity normalised to the total intensity noise. (e) Standard deviation of $\sin \phi_1$ as a function of injected power.

At this point the injection signal is so strong that it dominates any lasing processes occuring in the cavity, so essentially, all we see is the bare injected signal. In fact, the dominance of the injected signal can be seen in the sudden increase in m_1 for injection powers greater than about 10^{16} photons/second.Thus it would be undesirable to work in this regime. The region of interest in terms of seeing effects of injection locking on the spectra is therefore between injection powers of 10^7 photons/second and about 10^{16} photons/second.

The intensity noises are plotted as a function of injected power in Figs 4.2(b)-(d). It can be seen in all three figures that a reduction in the noise occurs as injection power is increased beyond 10^7 photons/second, the point at which locking occurs. The increase in noise for higher injection strengths is due to the injection power beginning to dominate the system , and thus beyond injection powers of about 10^{16} or 10^{17} photons/second the system becomes rather uninteresting. In the regime of interest, the reduction of the noise with increasing injection strength seen in each case, agrees with the results of the Langevin approach of Marin *et al.* The graphs indicate a regime in which there is squeezing in the total intensity, but the side and central modes are unsqueezed, which has been observed experimentally by Marin *et al.*, and a regime in which true single mode squeezing occurs. Due to technical problems arising at higher injection powers [Poizat 1996], this single mode squeezing has not been seen in this system to date. The spectra, which are all normalised with respect to the total noise in the system show particularly well the noise cancellation due to anti-correlated fluctuations. Thus, the intensity noises of the individual modes are almost the same, and their difference gives the total noise which is very small.

In calculating the phase noise, the real quantity of interest is the standard deviation of $\sin\phi_1$. If this is significantly less than one, we know that the phase is defined to within a revolution. The standard

deviation is calculated from the variance as follows,

$$\sqrt{\langle \sin\phi_1(0), \sin\phi_1(0)\rangle} = \sqrt{\frac{1}{2\pi}\int_{-\infty}^{\infty} S_{6,6}(\omega)d\omega}, \tag{4.37}$$

where

$$S_{6,6}(\omega) = \frac{[(\mathcal{H}(\mathbf{Z}_0) + i\omega)^{-1}\mathcal{I}(\mathbf{Z}_0)(\mathcal{H}^T(\mathbf{Z}_0) - i\omega)^{-1}]_{6,6}}{(\beta_{1,+})^2 + (\beta_{1,-})^2} \tag{4.38}$$

is the spectrum of the correlation function $\langle \sin\phi_1(t), \sin\phi_1(0)\rangle$. The standard deviation is plotted in Fig 4.2(e). The axes have been chosen so that standard deviations greater than one do not appear, since this means that the phase is random. It can be seen that the standard deviation decreases steadily as locking is achieved. Beyond a locking strength of 10^{16} photons/second, the phase noise is extremely small, corresponding to the dominance of the injected signal. For injection powers lower than 10^5 photons/second, there is no locking, and the fluctuations in the phase are too large for our linearised analysis to be valid.

Chapter 5

Conclusion

In Chapter 2 a master equation approach to the semiconductor laser was presented, in which a description in terms of numbers of electrons and holes, combined with a fully quantum mechanical treatment of light, was derived on the basis of an analysis of relaxation time scales. The description corresponds closely to an intuitive description of semiconductor lasers, but is in fact equivalent in its results to the phenomenological operator equations more traditionally used. Indeed the statistics of the output light were investigated, and the results shown to be essentially the same as those of Yamamoto and Machida [Yamamoto 1987]. The formalism which has been developed, since it is based on master equations, lends itself naturally to simulation using wavefunction stochastic differential equation methods, although these were not carried out here.

In practice however, semiconductor lasers are rarely purely single mode, so in the next chapter we extended the theory of Chapter 2 to explore the effect of side modes on the intensity spectrum.

We presented a master equation approach for treating semiconductor laser systems in which there is more than one mode present. Pumping was treated by the somewhat more phenomenological approach of writing down Kirchoff's equations from an equivalent circuit for the pumping process, and from these finding the pump contributions to

the equations of motion, as had been done in Chapter 2. In Chapter 3 however, the model was modified so that the two bands of the semiconductor were treated equivalently, and additional processes were also included.

We calculated the total intensity noise, the intensity noise in the main mode and the intensity noise in the side modes as a function of $\log(1-p)$, using a set of reasonable parameter values. Three regimes were found, the first, for small values of $\log(1-p)$, with no squeezing in any of the noises, the second, for intermediate values of $\log(1-p)$, with squeezing in the total noise only, and no individual mode squeezing, and the final regime, for large values of $\log(1-p)$, with squeezing in the central and total modes, and negligible intensity in the side modes. Comparison with the results of Marin *et al.* showed good agreement with the experimental results for the squeezing, and with the theoretical results obtained using the Langevin model.

Finally in Chapter 4, we adapted the master equation approach for the multi-mode semiconductor laser to the case of an injection locked laser and examined intensity and phase noise. We found that the injection locking caused a decrease in the noise in both the intensity and phase, and that in principle, either true single mode squeezing, or squeezing only in the total intensity were obtainable. The type of squeezing obtained depended on the injected power, single mode squeezing being obtained for higher injection strengths, and squeezing only in the total intensity for lower strengths.

The analysis of Chapter 4 completed a comparison with the results of Marin *et al.*, and excellent agreement was found to be obtained. The additional complications brought about by a description of injection locking indicate that our model can be easily adapted to describe more complicated and interesting systems than the bare laser.

We give now a brief discussion of future work concerned with our master equation model. Such work can be divided into two broad

groups. The first of these involves further refinements to the model which would lead to new possible calculations, and the second involves calculations which could be carried out with the model in its current form.

Our approach has several shortcomings which should be addressed. The most major of these is the assumption in the multi-mode theory that the spatial distributions of the central mode and the side modes differ. It is most important that this be established as true, since our theoretical results cannot be matched to other results [Marin 1995], both theoretical and experimental, without it. The theoretical procedure to follow in order to calculate the mode spatial distributions would be to solve the non-linear Schrödinger equation numerically for a given set of parameters.

Secondly, the theory assumes a broadband distribution which allows us to average over the carrier populations to obtain expressions for the terms $G(\underline{n})$, $F(\underline{n})$, and $A(\underline{n})$, in which only the total carrier numbers appear. It would be interesting to relax this approximation and examine other distributions of the carriers. In order to do this, knowledge of the particular bandstructure of the semiconductor would be required, and thus the methods of solid-state physics would be needed.

Although our theory has the capacity to predict the well-known semiconductor effects of frequency-pulling and refractive index shifts, the assumption that the real parts of $G(\underline{n})$, $F(\underline{n})$, and $A(\underline{n})$ dominate the imaginary parts, means that we do not see these effects in the results that we have given in this thesis. Retaining the imaginary parts of these terms is straightforward and will lead to the effects mentioned above, although the number of variables in the system may increase for the free-running and external grating systems.

There are also some calculations which could be carried out with the model under its current approximations. The first of these has already been mentioned above. The resultant master equation is of a form

suited to wavefunction simulation methods, and these could be used to find out information about the quantum statistics of the system.

Variations on the schemes considered in this thesis could also be modelled, for example, injecting a grating-stabilised laser signal into the cavity could be modelled using a cascaded systems approach [Gardiner 1993, Carmichael 1993], and is a system currently being considered by experimentalists in France.

Appendix A

Simplification of Steady-State Solutions

The algebra in this appendix gives a simplification of the steady-state photon number, and the corresponding threshold pump rate for the single-mode semiconductor laser system considered in Chapter 2.

We wish to simplify the expression for m^0,

$$\begin{aligned} m^0 &= -\frac{d}{2a} - \frac{dN^2}{\kappa} + \frac{P_e}{\kappa} \\ &\quad -\frac{1}{\kappa}\left[\frac{-M}{2} \pm \sqrt{-\frac{M^2}{4} + \frac{(\alpha_e - \beta_h)}{(\alpha_h - \beta_e)}\left(\frac{\kappa}{2a} + N^2\right)}\right] \frac{(\alpha_e\alpha_h - \beta_e\beta_h)}{\alpha_e - \beta_h}. \end{aligned}$$

Let us look first at the factor under the square root sign.

$$\frac{\alpha_e - \beta_h}{\alpha_h - \beta_e} = \frac{C_e + C_s}{C_e} \sim 1$$

if $C_s \ll C_e$.

We are thus left with the square root part of the term being

$$\sqrt{M^2/4 + (\kappa/2a + N^2)}. \tag{A.1}$$

Now, $M^2/4$ will be much bigger than $\kappa/2a + N^2$, because M will be the same size as the number of excess majority carriers. Thus we can

use the binomial expansion to expand this square root term as follows,

$$\sqrt{M^2/4 + (\kappa/2a + N^2)} \equiv \frac{M}{2} + \frac{1}{M}(\kappa/2a + N^2).$$

Substituting into the expression for m^0 leads to

$$m^0 = -\frac{d}{2a} - \frac{dN^2}{\kappa} + \frac{I_{\rm dc}}{e\kappa} - \frac{1}{\kappa M}\left(\frac{\kappa}{2a + N^2}\right)\frac{(\alpha_e\alpha_h - \beta_e\beta_h)}{\alpha_e - \beta_h}. \quad \text{(A.2)}$$

Finally we look at the $(\alpha_e\alpha_h - \beta_e\beta_h)/(\alpha_e - \beta_h)$ factor appearing. Substituting leads to

$$\begin{aligned}\frac{\alpha_e\alpha_h - \beta_e\beta_h}{\alpha_e - \beta_h} &= \frac{1}{R_l}\left[\frac{C_s + C_e + C_h}{C_h(C_e + C_s)}\right] \\ &= \frac{1}{R_l}\left[\frac{C_e + C_h}{C_hC_e}\right] = \frac{1}{R_l}\left[\frac{1}{C_e} + \frac{1}{C_h}\right]\end{aligned}$$

if C_s is small. This is just the time constant of the combined electron-hole capacitance. Thus

$$m^0 = \frac{P - P_{\rm th}}{\kappa}.$$

where

$$\begin{aligned}P &= \frac{I_{\rm dc}}{e} \\ P_{\rm th} &= \left(d + \frac{1}{\kappa M R_l}\left[\frac{1}{C_e} + \frac{1}{C_h}\right]\right)\left(\frac{\kappa}{2a + N^2}\right)\end{aligned}$$

One can apply the same simplifications of the α and β terms to the expressions for n_e^0 and n_h^0 to obtain simplified expressions for them.

Appendix B

Calculation of Spectrum in Terms of Photon Number Correlation Function

This appendix details the manipulation of the photon number correlation function required to obtain the spectrum of the output light for the single-mode semiconductor laser.

For the single variable case, the internal spectrum can be expressed in terms of the photon number correlation function as follows:

$$\langle b^\dagger(0)b^\dagger(t)b(t)b(0)\rangle = \mathrm{Tr}\{b\{e^{\mathcal{L}t}(b^\dagger\rho(0)b)\}b^\dagger\}, \tag{B.1}$$

where $\rho(0) = \sum p(m,0)|m\rangle\langle m|$ is the density operator at time zero, and $p(m,0)$ is the probability that the system is in a state containing m photons at time $t = 0$. Now,

$$e^{\mathcal{L}t}\rho(0) = \sum p(m,t|m',0)p(m',0)|m\rangle\langle m|, \tag{B.2}$$

where $p(m,t|m',0)$ is the probability of being in a state containing m photons at time t, conditioned on being in a state containing m' photons at $t = 0$, and

$$\begin{aligned} b^\dagger\rho(0)b &= \sum p(m,0)m|m-1\rangle\langle m-1| \\ &= \sum p(m+1,0)(m+1)|m\rangle\langle m|. \end{aligned} \tag{B.3}$$

Therefore

$$e^{\mathcal{L}t}(b^\dagger\rho(0)b) = \sum p(m,t|m',0)p(m'+1,0)(m'+1)|m\rangle\langle m|, \qquad \text{(B.4)}$$

and

$$\begin{aligned} be^{\mathcal{L}t}(b^\dagger\rho(0)b)b^\dagger &= \sum(m+1)(m'+1) \\ &\quad \times p(m+1,t|m',0)p(m'+1,0)|m\rangle\langle m|. \end{aligned} \qquad \text{(B.5)}$$

Thus we can evaluate the trace to get

$$\begin{aligned} \mathrm{Tr}\{b\{e^{\mathcal{L}t}(b^\dagger\rho(0)b)\}b^\dagger\} &= \sum_{mm'}(m+1)(m'+1) \\ &\quad \times p(m+1,t|m',0)p(m'+1,0) \\ &= \sum_{mm'} mm'p(m,t|m'-1,0)p(m',0) \\ &= \sum_{m'} m'p(m',0)\langle m,t|m'-1,0\rangle, \end{aligned} \qquad \text{(B.6)}$$

where $\langle m,t|m'-1,0\rangle$ means the average number of photons in state m, given that the photons were initially in the state $m'-1$.

One can use the quantum regression theorem to calculate this average because we know that $\langle m,t|M,0\rangle = e^{-\lambda t}(M-\mu)+\mu$, where μ is the steady-state value of m, and λ is the relaxation constant. Thus we can write

$$\begin{aligned} \langle b^\dagger(0)b^\dagger(t)b(t)b(0)\rangle &= \sum m'p(m',0)\{e^{-\lambda t}(m'-1-\mu)+\mu\} \\ &= e^{-\lambda t}\langle m'^2\rangle + e^{-\lambda t}\langle m'(-1-\mu)\rangle \\ &\quad + \langle m'\rangle\mu. \end{aligned} \qquad \text{(B.7)}$$

For the multiple variable case a similar procedure applies. We are interested in our case in the calculation of the photon intensity spectrum, hence we isolate this element from the vector of variables to which we apply the quantum regression theorem.

A repeat of the above process for the many variable case leads to an expression for the trace given by

$$\mathrm{Tr}\{be^{\mathcal{L}t}(b^\dagger\rho(0)b)b^\dagger\} = \left(\sum_{m'} m'p(\mathbf{m}',0)\langle m,t|\begin{pmatrix}\hat{\mathbf{m}}'\\ m'-1\end{pmatrix},0\rangle\right)_0, \quad \text{(B.8)}$$

where $p(\mathbf{m}',0)$ is the probability of being in the state $\mathbf{m}'$ initially (in other words, the number of electrons, holes and photons given by $\mathbf{m}'$), and where $\hat{\mathbf{m}}'$ is the vector describing the state of the electron and holes only. Here we are interested only in the element of the vector which gives the photon number, This is symbolized by the subscript 0 on the left hand side. Now, applying the quantum regression theorem to this expression we obtain

$$\begin{aligned}\langle b^\dagger(0)b^\dagger(t)b(t)b(0)\rangle &= \left(\sum_{m'} m'p(\mathbf{m}',0)\left\{e^{-At}\left[\begin{pmatrix}\hat{\mathbf{m}}'\\ m'-1\end{pmatrix}\right.\right.\right.\\ &\quad \left.\left.\left.-\mathbf{M}\right]+\mathbf{M}\right\}\right)_0, \quad \text{(B.9)}\end{aligned}$$

where $\mathbf{M}$ is the vector of steady-state values for the electrons, holes, and photon numbers, and A is the drift matrix of the system. This can be rewritten

$$\begin{aligned}\langle b^\dagger(0)b^\dagger(t)b(t)b(0)\rangle &= \left(\sum_{m'} m'p(\mathbf{m}',0)\mathbf{M}_0\right.\\ &\quad \left.+\sum_{m'} m'p(\mathbf{m}',0)e^{-At}\left[\begin{pmatrix}\hat{\mathbf{m}}'\\ m'-1\end{pmatrix}-\mathbf{M}\right]\right)_0\\ &= (M_0\mathbf{M})_0\\ &\quad +\left(e^{-At}\left[\begin{pmatrix}\langle m'\hat{\mathbf{m}}'\rangle\\ \langle m'^2\rangle - M_0\end{pmatrix}-M_0\mathbf{M}\right]\right)_0 \quad \text{(B.10)}\end{aligned}$$

where $M_0 = \langle m'\rangle$ or in other words $M_0 = \sum_{m'} m'p(\mathbf{m}',0)$. Thus

$$\begin{aligned}\langle b^\dagger(0)b^\dagger(t)b(t)b(0)\rangle &= (M_0\mathbf{M})_0\\ &\quad +\left(e^{-At}\begin{pmatrix}\langle m'\hat{\mathbf{m}}'\rangle - M_0\hat{\mathbf{M}}_0\\ \langle M'^2\rangle - M_0^2 - M_0\end{pmatrix}\right)_0 \quad \text{(B.11)}\end{aligned}$$

where

$$\mathbf{M} = \begin{pmatrix} \hat{\mathbf{M}}_0 \\ M_0 \end{pmatrix}.$$

This can now be written as

$$\begin{aligned} \langle b^\dagger(0)b^\dagger(t)b(t)b(0)\rangle &= (M_0\mathbf{M})_0 + \left[e^{-At}\begin{pmatrix} \langle m'\hat{\mathbf{m}}'\rangle - M_0\hat{\mathbf{M}}_0 \\ \langle M'^2\rangle - M_0^2 \end{pmatrix}\right]_0 \\ &\quad - \left[e^{-At}\begin{pmatrix} 0 \\ 0 \\ M_0 \end{pmatrix}\right]_0 \\ &= (M_0\mathbf{M})_0 \\ &\quad + [e^{-At}\sigma]_{00} - e^{-At}\begin{pmatrix} 0 \\ 0 \\ M_0 \end{pmatrix}, \end{aligned} \tag{B.12}$$

where σ is the stationary covariance matrix $\langle \mathbf{x}_s(t), \mathbf{x}_s^T(t)\rangle$. Then

$$\begin{aligned} \langle b^\dagger(0)b^\dagger(t)b(t)b(0)\rangle &= (M_0\mathbf{M})_0 + [e^{-At}\sigma]_{00} \\ &\quad - \left[e^{-At}\begin{pmatrix} 0 & 0 & 0 \\ 0 & 0 & 0 \\ 0 & 0 & 1 \end{pmatrix}\right]_{00} M_0 \\ &= (M_0\mathbf{M})_0 + \left[e^{-At}\{\sigma - \mathbf{U}\}M_0\right]_{00} \end{aligned} \tag{B.13}$$

where

$$U = \begin{pmatrix} 0 & 0 & 0 \\ 0 & 0 & 0 \\ 0 & 0 & 1 \end{pmatrix}.$$

Thus

$$\begin{aligned} (2.71) &= \frac{\kappa}{2\pi}\int_{-\infty}^{\infty} e^{-i\omega t}\left(M_0^2 + \left[e^{-At}\{\sigma - \mathbf{U}\}M_0\right]_{00}\right. \\ &\quad \left. -\langle b^\dagger(0)b(0)\rangle^2\right) dt \end{aligned}$$

$$= \frac{\kappa}{2\pi}\int_0^\infty dt e^{-i\omega t}e^{-At}\left[\sigma - \mathbf{U}M_0\right] + h.c.$$

$$= \frac{\kappa}{2\pi}(A+i\omega)^{-1}\left\{BB^T - M_0(\mathbf{U}A^T + A\mathbf{U})\right\}(A^T - i\omega)^{-1}, \tag{B.14}$$

where $A\sigma + \sigma A^T + BB^T$.

Appendix C

Pumping

The quantum mechanical contributions to the equations of motion for n_e, n_h, $\tilde{n}_e$, and $\tilde{n}_h$ due to the pumping are given here. These contributions are obtained by applying Kirchoff's laws to the pump circuit given in Section 3.5 and rearranging.

The central part of the circuit, shown in Fig 3.3, can be written as an equivalent circuit for which we have

$$J = \frac{V_P}{R_P} - \frac{\tilde{V}_L}{\tilde{R}_L} - \frac{V_L}{R_L} \tag{C.1}$$

$$R = \frac{R_P R_L \tilde{R}_L}{\tilde{R}_L R_L + R_P R_L + R_P \tilde{R}_L} \tag{C.2}$$

$$V = \frac{V_P \tilde{R}_L R_L - \tilde{V}_L R_P R_L - V_L R_P \tilde{R}_L}{\tilde{R}_L R_L + R_P R_L + R_P \tilde{R}_L}. \tag{C.3}$$

Applying Kirchoff's laws to the circuit, making the correspondences $Q_e = -en_e, Q_h = e(n_h - M)$, and rearranging leads to the following pumping contributions to the equations of motion for $n_e, n_h, \tilde{n}_e$ and $\tilde{n}_h$,

$$\begin{aligned}
\dot{n}_e|_p &= -\alpha_e n_e - \beta_e(n_h - M) + P_e \\
&\quad + f\frac{\sqrt{2k}}{e}\left\{\frac{R_s(R_u + R_h)}{(R_P + R_L)}[\sqrt{T_P R_P}R_L\xi_P(t) - \sqrt{T_L R_L}R_P\xi_L(t)]\right. \\
&\quad \left. + \sqrt{T_u R_u}R_h R_s \xi_u(t) - \sqrt{T_s R_s}(RR_u + RR_h + R_h R_u)\xi_s(t)\right.
\end{aligned}$$

$$
\begin{aligned}
&+\sqrt{T_e R_e}\xi_e(t)[R_h(R+R_u+R_s)+R_u(R+R_s)] \\
&+R_u R_s\sqrt{T_h R_h}\xi_h(t)\Big\} \qquad \text{(C.4)}
\end{aligned}
$$

$$
\begin{aligned}
\dot{n}_h\big|_p \;=\; & -\beta_h n_e - \alpha_h(n_h - M) + P_h \\
&+f\frac{\sqrt{2k}}{e}\left\{\frac{R_u(R_s+R_e)}{(R_P+R_L}[\sqrt{T_P R_P}R_L\xi_P(t) - \sqrt{T_L R_L}R_P\xi_L(t)]\right. \\
&+\sqrt{T_s R_s}R_e R_u\xi_s(t) - \sqrt{T_u R_u}(RR_s + RR_e + R_e R_s)\xi_u(t) \\
&+\sqrt{T_h R_h}\xi_h(t)[R_e(R+R_u+R_s)+R_s(R+R_u)] \\
&\left.+R_u R_s\sqrt{T_e R_e}\xi_e(t)\right\} \qquad \text{(C.5)}
\end{aligned}
$$

$$
\begin{aligned}
\dot{\tilde{n}}_e\big|_p \;=\; & -\tilde{\alpha}_e\tilde{n}_e - \tilde{\beta}_e(\tilde{n}_h - \tilde{M}) + \tilde{P}_e \\
&+f\frac{\sqrt{2k}}{e}\left\{\frac{\tilde{R}_s(\tilde{R}_u+\tilde{R}_h)}{(\tilde{R}_P+\tilde{R}_L)}[\sqrt{\tilde{T}_P\tilde{R}_P}\tilde{R}_L\tilde{\xi}_P(t) - \sqrt{\tilde{T}_L\tilde{R}_L}\tilde{R}_P\tilde{\xi}_L(t)]\right. \\
&+\sqrt{\tilde{T}_u\tilde{R}_u}\tilde{R}_h\tilde{R}_s\tilde{\xi}_u(t) - \sqrt{\tilde{T}_s\tilde{R}_s}(R\tilde{R}_u + R\tilde{R}_h + \tilde{R}_h\tilde{R}_u)\tilde{\xi}_s(t) \\
&+\sqrt{\tilde{T}_e\tilde{R}_e}\tilde{\xi}_e(t)[\tilde{R}_h(R+\tilde{R}_u+R_s)+\tilde{R}_u(R+\tilde{R}_s)] \\
&\left.+\tilde{R}_u\tilde{R}_s\sqrt{\tilde{T}_h\tilde{R}_h}\tilde{\xi}_h(t)\right\} \qquad \text{(C.6)}
\end{aligned}
$$

$$
\begin{aligned}
\dot{\tilde{n}}_h\big|_p \;=\; & -\tilde{\beta}_h\tilde{n}_e - \tilde{\alpha}_h(\tilde{n}_h - \tilde{M}) + \tilde{P}_h \\
&+f\frac{\sqrt{2k}}{e}\left\{\frac{\tilde{R}_u(\tilde{R}_s+\tilde{R}_e)}{(\tilde{R}_P+\tilde{R}_L)}[\sqrt{\tilde{T}_P\tilde{R}_P}\tilde{R}_L\tilde{\xi}_P(t) - \sqrt{\tilde{T}_L\tilde{R}_L}\tilde{R}_P\tilde{\xi}_L(t)]\right. \\
&+\sqrt{\tilde{T}_s\tilde{R}_s\tilde{R}_e\tilde{R}_u\tilde{\xi}_s(t)} - \sqrt{\tilde{T}_u\tilde{R}_u}(R\tilde{R}_s + R\tilde{R}_e + \tilde{R}_e\tilde{R}_s)\tilde{\xi}_u(t) \\
&+\sqrt{\tilde{T}_h\tilde{R}_h}\tilde{\xi}_h(t)[\tilde{R}_e(R+\tilde{R}_u+\tilde{R}_s)+\tilde{R}_s(R+\tilde{R}_u)] \\
&\left.+\tilde{R}_u\tilde{R}_s\sqrt{\tilde{T}_e\tilde{R}_e}\tilde{\xi}_e(t)\right\}, \qquad \text{(C.7)}
\end{aligned}
$$

where

$$
\begin{aligned}
\alpha_e \;=\; & f\left[((R_u+R_h)(R+R_s)+R_h R_u)\frac{(C_s+C_e)}{C_s C_e}\right. \\
&\left.-\frac{R_u R_s}{C_s}\right] \qquad \text{(C.8)}
\end{aligned}
$$

$$\alpha_h = f\left[((R_s+R_e)(R+R_u)+R_eR_s)\frac{(C_s+C_h)}{C_sC_h} - \frac{R_uR_s}{C_s}\right] \quad \text{(C.9)}$$

$$\beta_e = f\left[\frac{R_sR_u(C_h+C_s)}{C_sC_h} - \frac{(R_u+R_h)(R+R_s)}{C_s} - \frac{R_hR_u}{C_s}\right] \quad \text{(C.10)}$$

$$\beta_h = f\left[\frac{R_sR_u(C_e+C_s)}{C_sC_e} - \frac{(R_s+R_e)(R+R_u)}{C_s} - \frac{R_eR_s}{C_s}\right] \quad \text{(C.11)}$$

$$\tilde{\alpha}_e = \tilde{f}\left[((\tilde{R}_u+\tilde{R}_h)(R+\tilde{R}_s)+\tilde{R}_h\tilde{R}_u)\frac{(\tilde{C}_s+\tilde{C}_e)}{\tilde{C}_s\tilde{C}_e} - \frac{\tilde{R}_u\tilde{R}_s}{\tilde{C}_s}\right] \quad \text{(C.12)}$$

$$\tilde{\alpha}_h = \tilde{f}\left[((\tilde{R}_s+\tilde{R}_e)(R+\tilde{R}_u)+\tilde{R}_e\tilde{R}_s)\frac{(\tilde{C}_s+\tilde{C}_h)}{\tilde{C}_s\tilde{C}_h} - \frac{\tilde{R}_u\tilde{R}_s}{\tilde{C}_s}\right] \quad \text{(C.13)}$$

$$\tilde{\beta}_e = \tilde{f}\left[\frac{\tilde{R}_s\tilde{R}_u(\tilde{C}_h+\tilde{C}_s)}{\tilde{C}_s\tilde{C}_h} - \frac{\tilde{R}_u+\tilde{R}_h)(R+\tilde{R}_s)}{\tilde{C}_s} - \frac{\tilde{R}_h\tilde{R}_u}{\tilde{C}_s}\right] \quad \text{(C.14)}$$

$$\tilde{\beta}_h = \tilde{f}\left[\frac{\tilde{R}_s\tilde{R}_u(\tilde{C}_e+\tilde{C}_s)}{\tilde{C}_s\tilde{C}_e} - \frac{(\tilde{R}_s+\tilde{R}_e)(R+\tilde{R}_u)}{\tilde{C}_s} - \frac{\tilde{R}_e\tilde{R}_s}{\tilde{C}_s}\right], \quad \text{(C.15)}$$

and

$$P_e = f\frac{\bar{V}}{e}(R_u+R_h)R_s \quad \text{(C.16)}$$

$$P_h = f\frac{\bar{V}}{e}(R_s + R_e)R_u \tag{C.17}$$

$$\tilde{P}_e = \tilde{f}\frac{\bar{V}}{e}(\tilde{R}_u + \tilde{R}_h)\tilde{R}_s \tag{C.18}$$

$$\tilde{P}_h = \tilde{f}\frac{\bar{V}}{e}(\tilde{R}_s + \tilde{R}_e)\tilde{R}_u. \tag{C.19}$$

In the above equations

$$f = \frac{(R + R_{su})}{d^u_{se}d^s_{uh} - R^2_u R^2_s} \tag{C.20}$$

$$\tilde{f} = \frac{(R + \tilde{R}_{su})}{\tilde{d}^u_{se}\tilde{d}^s_{uh} - (\tilde{R}_u\tilde{R}_s)^2}, \tag{C.21}$$

where

$$d^i_{jk} = (R + R_i)(R_j + R_k) + R_j R_k \tag{C.22}$$

$$R_{su} = R_s + R_u \tag{C.23}$$

$$\tilde{d}^i_{jk} = (R + \tilde{R}_i)(\tilde{R}_j + \tilde{R}_k) + \tilde{R}_j\tilde{R}_k \tag{C.24}$$

$$\tilde{R}_{su} = \tilde{R}_s + \tilde{R}_u \tag{C.25}$$

$$\bar{V} = \frac{V_P R_L \tilde{R}_L}{R_L\tilde{R}_L + R_P R_L + R_P\tilde{R}_L} = \frac{V_P R}{R_P}, \tag{C.26}$$

is the dc component of V, k is Boltzmann's constant and e is the electronic charge. The term V_P appearing in Equation (C.26) can be related to the pump current by considering the capacative branches of Fig 3.2 to be open circuits, and calculating the current through R_P in terms of V_P to give

$$V_P = I_p R_P + \frac{I_P\tilde{R}_{su}R_{su}\tilde{R}_L R_L}{[R_L\tilde{R}_L(R_{su} + \tilde{R}_{su}) + (R_L + \tilde{R}_L)\tilde{R}_{su}R_{su}]}. \tag{C.27}$$

Appendix D

Transformation to a Fokker-Planck Equation

This appendix details the conversion of the multi-mode master equation in Section 3.6 to a Fokker-Planck equation. The details of the Kramers-Moyal expansion are given, and the drift and diffusion matrices are written in full.

Considering just the optical interaction part of the master equation for the many mode case, we have

$$\begin{aligned}\frac{\partial \rho_0(\underline{n})}{\partial t} &= -\sum_{i,j}\Big\{G_{ij}(\underline{n})b_i b_j^\dagger \rho_0(\underline{n}) - G_{ij}(\underline{n}+\underline{e})b_j^\dagger \rho_0(\underline{n}+\underline{e})b_i \\ &\quad + F_{ij}^*(\underline{n})b_i^\dagger b_j \rho_0(\underline{n}) - F_{ij}^*(\underline{n}-\underline{e})b_j \rho_0(\underline{n}-\underline{e})b_i^\dagger \\ &\quad - F_{ij}(\underline{n}-\underline{e})b_i \rho_0(\underline{n}-\underline{e})b_j^\dagger + F_{ij}(\underline{n})\rho_0(\underline{n})b_j^\dagger b_i \\ &\quad - G_{ij}^*(\underline{n}+\underline{e})b_i^\dagger \rho_0(\underline{n}+\underline{e})b_j + G_{ij}^*(\underline{n})\rho_0(\underline{n})b_j b_i^\dagger\Big\}. \quad \text{(D.1)}\end{aligned}$$

Before conversion to the positive-P representation takes place, the master equation is modified slightly in order to make the Kramers-Moyal expansion possible. There are four terms which correspond to coupling to neighbouring states. Analogous terms to these four terms, but which couple to the state $\underline{n}$ rather than states $\underline{n}+\underline{e}$ or $\underline{n}-\underline{e}$, are added to and subtracted from the master equation, and the terms are re-grouped to

give

$$\begin{aligned}\frac{\partial \rho_0(\underline{n})}{\partial t} &= -\sum_{ij}\Big\{G_{ij}(\underline{n})b_i b_j^\dagger \rho_0(\underline{n}) - G_{ij}(\underline{n})b_j^\dagger \rho_0(\underline{n})b_i \\ &+G_{ij}^*(\underline{n})\rho_0(\underline{n})b_j b_i^\dagger - G_{ij}^*(\underline{n})b_i^\dagger \rho_0(\underline{n})b_j \\ &+F_{ij}^*(\underline{n})b_i^\dagger b_j \rho_0(\underline{n}) - F_{ij}^*(\underline{n})b_j \rho_0(\underline{n})b_i^\dagger \\ &+F_{ij}(\underline{n})\rho_0(\underline{n})b_j^\dagger b_i - F_{ij}(\underline{n})b_i \rho_0(\underline{n})b_j^\dagger \\ &-G_{ij}(\underline{n}+\underline{e})b_j^\dagger \rho_0(\underline{n}+\underline{e})b_i - G_{ij}(\underline{n})b_j^\dagger \rho_0(\underline{n})b_i \\ &-G_{ij}^*(\underline{n}+\underline{e})b_i^\dagger \rho_0(\underline{n}+\underline{e})b_j - G_{ij}^*(\underline{n})b_i^\dagger \rho_0(\underline{n})b_j \\ &-F_{ij}^*(\underline{n}-\underline{e})b_j \rho_0(\underline{n}-\underline{e})b_i^\dagger - F_{ij}^*(\underline{n})b_j \rho_0(\underline{n})b_i^\dagger \\ &-F_{ij}(\underline{n}-\underline{e})b_i \rho_0(\underline{n}-\underline{e})b_j^\dagger - F_{ij}(\underline{n})b_i \rho_0(\underline{n})b_j^\dagger\Big\}. \quad \text{(D.2)}\end{aligned}$$

Only the terms in the second set of brackets will undergo a Kramers-Moyal expansion. Converting to the positive-P representation gives

$$\begin{aligned}\frac{\partial P(\mathbf{X})}{\partial t} &= -\sum_{ij}\Bigg\{G_{ij}(\underline{n})\left[\frac{\partial}{\partial \beta_i^*}\beta_j^* - \frac{\partial^2}{\partial \beta_j \partial \beta_i^*}\right] \\ &+G_{ij}^*(\underline{n})\left[\frac{\partial}{\partial \beta_i}\beta_j - \frac{\partial^2}{\partial \beta_i \partial \beta_j^*}\right] \\ &+F_{ij}(\underline{n})\left[-\frac{\partial}{\partial \beta_i^*}\beta_j^*\right] + F_{ij}^*(\underline{n})\left[-\frac{\partial}{\partial \beta_i}\beta_j\right]\Bigg\} P(\mathbf{X}) \\ &-\sum_{ij}\Bigg\{\left(-\beta_j^*\beta_i + \frac{\partial}{\partial \beta_j}\beta_i + \beta_j^*\frac{\partial}{\partial \beta_i^*} - \frac{\partial^2}{\partial \beta_j \partial \beta_i^*}\right) \\ &\times\left[G_{ij}(\underline{n}+\underline{e})P(\mathbf{X}+\underline{e}) - G_{ij}(\underline{n})P(\mathbf{X})\right] \\ &+\left(-\beta_i^*\beta_j + \frac{\partial}{\partial \beta_i}\beta_j + \beta_i^*\frac{\partial}{\partial \beta_j^*} - \frac{\partial^2}{\partial \beta_i \partial \beta_j^*}\right) \\ &\times\left[G_{ij}^*(\underline{n}+\underline{e})P(\mathbf{X}+\underline{e}) - G_{ij}^*(\underline{n})P(\mathbf{X})\right] \\ &-\beta_j\beta_i^*\left[F_{ij}^*(\underline{n}-\underline{e})P(\mathbf{X}-\underline{e}) - F_{ij}^*(\underline{n})P(\mathbf{X})\right] \\ &-\beta_i\beta_j^*\left[F_{ij}(\underline{n}-\underline{e})P(\mathbf{X}-\underline{e}) - F_{ij}(\underline{e})P(\mathbf{X})\right]\Bigg\}. \quad \text{(D.3)}\end{aligned}$$

Performing the Kramers-Moyal expansion and dropping terms greater

than second order gives

$$\begin{aligned}
\frac{\partial P(\mathbf{X})}{\partial t} &= -\sum_{ij}\Bigg\{\frac{\partial}{\partial\beta_i^*}\left[G_{ij}(\underline{n})\beta_j^* - F_{ij}(\underline{n})\beta_j^*\right] \\
&+\frac{\partial}{\partial\beta_i}\left[G_{ji}^*(\underline{n})\beta_j - F_{ji}^*(\underline{n})\beta_j\right] \\
&+\frac{\partial}{\partial n_e}\left[2\beta_j^*\beta_i F_{ij}^r(\underline{n}) - 2(\delta_{ij}+\beta_j^*\beta_i)G_{ij}^r(\underline{n})\right] \\
&+\frac{\partial}{\partial n_h}\left[2\beta_j^*\beta_i F_{ij}^r(\underline{n}) - 2(\delta_{ij}+\beta_j^*\beta_i)G_{ij}^r(\underline{n})\right] \\
&+\frac{\partial^2}{\partial\beta_j\beta_i^*}\left[-2G_{ij}^r(\underline{n})\right] \\
&+\frac{\partial^2}{\partial n_e\partial\beta_j}\left[2\beta_i G_{ij}^r(\underline{n})\right] + \frac{\partial^2}{\partial n_e\partial\beta_i^*}\left[2\beta_j^* G_{ij}^r(\underline{n})\right] \\
&+\frac{\partial^2}{\partial n_h\partial\beta_j}\left[2\beta_i G_{ij}^r(\underline{n})\right] + \frac{\partial^2}{\partial n_h\partial\beta_i^*}\left[2\beta_j^* G_{ij}^r(\underline{n})\right] \\
&+\frac{1}{2}\left[\frac{\partial^2}{\partial n_e^2} + \frac{\partial^2}{\partial n_h^2} + \frac{\partial^2}{\partial n_e\partial n_h} + \frac{\partial^2}{\partial n_e\partial n_h}\right] \\
&\times\left[2\beta_j^*\beta_i F_{ij}^r(\underline{n}) - 2(\delta_{ij}+\beta_j^*\beta_i)G_{ij}^r(\underline{n})\right]\Bigg\}P(\mathbf{X}), \quad \text{(D.4)}
\end{aligned}$$

where $\mathbf{X}$ is given by Equation (3.14).

Carrying out the same procedure for all terms which contribute to the master equation (the remaining part of Equations (3.4), (3.6), and the non-lasing terms appearing in Equation(2.52)), one obtains an FPE

which can be written in the form of Equation (3.13) where

$$\mathcal{A}(\mathbf{X}) = \begin{pmatrix} \sum_{lj}[2\beta_j^*\beta_l F_{lj}^r(\underline{n}) - 2(\delta_{lj} + \beta_j^*\beta_l)G_{lj}^r(\underline{n})] - A(\underline{n}) + B(\underline{n}) + P_e(\underline{n}) \\ \sum_{lj}[2\beta_j^*\beta_l F_{lj}^r(\underline{n}) - 2(\delta_{lj} + \beta_j^*\beta_l)G_{lj}^r(\underline{n})] - A(\underline{n}) + B(\underline{n}) + P_h(\underline{n}) \\ 2|\beta_1|^2\tilde{F}_{11}^r(\underline{n}) - 2(|\beta_1|^2+1)\tilde{G}_{11}^r(\underline{n}) - \tilde{A}(\underline{n}) + \tilde{B}(\underline{n}) + \tilde{P}_e(\underline{n}) \\ 2|\beta_1|^2\tilde{F}_{11}^r(\underline{n}) - 2(|\beta_1|^2+1)\tilde{G}_{11}^r(\underline{n}) - \tilde{A}(\underline{n}) + \tilde{B}(\underline{n}) + \tilde{P}_h(\underline{n}) \\ \sum_j[G_{j1}^*(\underline{n})\beta_j - F_{j1}^*(\underline{n})\beta_j] + \tilde{F}_{11}(\underline{n})\beta_1 - \tilde{G}_{11}^*(\underline{n})\beta_1 - \kappa_1\beta_1/2 \\ \sum_j[G_{j2}^*(\underline{n})\beta_j - F_{j2}^*(\underline{n})\beta_j] - \kappa_2\beta_2/2 - i\Delta_2\beta_2 \\ \sum_j[G_{j3}^*(\underline{n})\beta_j - F_{j3}^*(\underline{n})\beta_j] - \kappa_3\beta_3/2 - i\Delta_3\beta_3 \\ \sum_j[G_{1j}(\underline{n})\beta_j^* - F_{1j}(\underline{n})\beta_j^*] - \tilde{G}_{11}(\underline{n})\beta_1^* + \tilde{F}_{11}^*\beta_1^* - \kappa_1\beta_1^*/2 \\ \sum_j[G_{2j}(\underline{n})\beta_j^* - F_{2j}(\underline{n})\beta_j^*] - \kappa_2\beta_2^*/2 + i\Delta_2\beta_2^* \\ \sum_j[G_{3j}(\underline{n})\beta_j^* - F_{3j}(\underline{n})\beta_j^*] - \kappa_3\beta_3^*/2 + i\Delta_3\beta_3^* \end{pmatrix}, \tag{D.5}$$

and where

$$\mathcal{D}_{cc}(\mathbf{X}) = \begin{pmatrix} r_{lj} + D_e(\underline{n}) & r_{lj} + D_{eh}(\underline{n}) & 0 & 0 \\ r_{lj} + D_{he}(\underline{n}) & r_{lj} + D_h(\underline{n}) & 0 & 0 \\ 0 & 0 & \tilde{r}_{11} + \tilde{D}_e(\underline{n}) & \tilde{r}_{11} + \tilde{D}_{eh}(\underline{n}) \\ 0 & 0 & \tilde{r}_{11} + \tilde{D}_{he}(\underline{n}) & \tilde{r}_{11} + \tilde{D}_h(\underline{n}) \end{pmatrix}, \tag{D.6}$$

$$\mathcal{D}_{cf}(\mathbf{X}) = \begin{pmatrix} s_1 & s_2 & s_3 & s_1^* & s_2^* & s_3^* \\ s_1 & s_2 & s_3 & s_1^* & s_2^* & s_3^* \\ \tilde{s}_1 & 0 & 0 & \tilde{s}_1^* & 0 & 0 \\ \tilde{s}_1 & 0 & 0 & \tilde{s}_1^* & 0 & 0 \end{pmatrix}, \tag{D.7}$$

$$\mathcal{D}_{fc}(\mathbf{X}) = \begin{pmatrix} s_1 & s_1 & \tilde{s}_1 & \tilde{s}_1 \\ s_2 & s_2 & 0 & 0 \\ s_3 & s_3 & 0 & 0 \\ s_1^* & s_1^* & \tilde{s}_1^* & \tilde{s}_1^* \\ s_2^* & s_2^* & 0 & 0 \\ s_3^* & s_3^* & 0 & 0 \end{pmatrix}, \tag{D.8}$$

and

$$\mathcal{D}_{ff}(\mathbf{X}) = \begin{pmatrix} 0 & 0 & 0 & t_{11}+\tilde{t}_{11} & t_{21} & t_{31} \\ 0 & 0 & 0 & t_{12} & t_{22} & t_{32} \\ 0 & 0 & 0 & t_{13} & t_{23} & t_{33} \\ t_{11}+\tilde{t}_{11} & t_{12} & t_{13} & 0 & 0 & 0 \\ t_{21} & t_{22} & t_{23} & 0 & 0 & 0 \\ t_{31} & t_{32} & t_{33} & 0 & 0 & 0 \end{pmatrix}, \tag{D.9}$$

make up the matrix

$$\mathcal{D}(\mathbf{X}) = \begin{pmatrix} \mathcal{D}_{cc}(\mathbf{X}) & \mathcal{D}_{cf}(\mathbf{X}) \\ \mathcal{D}_{fc}(\mathbf{X}) & \mathcal{D}_{ff}(\mathbf{X}) \end{pmatrix}, \tag{D.10}$$

where

$$\begin{aligned} r_{lj} &= \sum_{lj}[2(\delta_{lj}+\beta_j^*\beta_l)G_{lj}^r(\underline{n}) + 2\beta_j^*\beta_l F_{lj}^r(\underline{n})] \\ &\quad + A(\underline{n}) + B(\underline{n}) \qquad \text{(D.11)} \\ s_l &= -\sum_j 2\beta_j G_{jl}^r(\underline{n}) \qquad \text{(D.12)} \\ s_l^* &= \sum_j 2\beta_j^* G_{lj}^r(\underline{n}) \qquad \text{(D.13)} \end{aligned}$$

$$t_{lj} = 2G^r_{lj}(\underline{n}) + \kappa_l \bar{N}_l \delta_{lj} \tag{D.14}$$

$$\tilde{r}_{11} = [2(1+\beta_1^*\beta_1)\tilde{G}^r_{11}(\underline{n}) + 2\beta_1^*\beta_1 \tilde{F}^r_{11}(\underline{n})] + \tilde{A}(\underline{n}) + \tilde{B}(\underline{n}) \tag{D.15}$$

$$\tilde{s}_1 = -2\beta_1 \tilde{G}^r_{11}(\underline{n}) \tag{D.16}$$

$$\tilde{s}_1^* = 2\beta_1^* \tilde{G}^r_{11}(\underline{n}) \tag{D.17}$$

$$\tilde{t}_{11} = 2\tilde{G}^r_{11}(\underline{n}), \tag{D.18}$$

and from Equations (C.4)-(C.7) we can make the correspondences

$$P_e(\underline{n}) = P_e - \alpha_e n_e - \beta_e(n_h - M) \tag{D.19}$$

$$P_h(\underline{n}) = P_h - \beta_h n_e - \alpha_h(n_h - M) \tag{D.20}$$

$$\tilde{P}_e(\underline{n}) = \tilde{P}_e - \tilde{\alpha}_e \tilde{n}_e - \tilde{\beta}_e(\tilde{n}_h - \tilde{M}) \tag{D.21}$$

$$\tilde{P}_h(\underline{n}) = \tilde{P}_h - \tilde{\beta}_h \tilde{n}_e - \tilde{\alpha}_h(\tilde{n}_h - \tilde{M}) \tag{D.22}$$

$$\begin{aligned} D_e(\underline{n}) = \frac{2k}{e^2} f^2 \Big[& R^2 R_s^2 (R_u + R_h)^2 \left(\frac{T_P}{R_P} + \frac{T_L}{R_L}\right) \\ & + T_u R_u R_s^2 R_h^2 + T_s R_s (R_u R + R_h R + R_h R_u)^2 \\ & + T_e R_e [R_u(R + R_s) + R_h(R + R_s + R_u)]^2 \\ & + T_h R_h R_s^2 R_u^2 \Big] \end{aligned} \tag{D.23}$$

$$\begin{aligned} D_{eh}(\underline{n}) = \frac{2k}{e^2} f^2 \Big[& R^2 R_s R_u (R_s + R_e)(R_u + R_h) \left(\frac{T_P}{R_P} + \frac{T_L}{R_L}\right) \\ & - T_u R_u R_h R_s (R_s R + R_e R + R_e R_s) \\ & - T_s R_s R_e R_u (R_u R + R_h R + R_h R_u) \\ & + T_e R_e R_s R_u [R_u(R + R_s) + R_h(R + R_s + R_u)] \\ & + T_h R_h R_s R_u [R_s(R + R_u) \\ & + R_e(R + R_s + R_u)]] \end{aligned} \tag{D.24}$$

$$\begin{aligned} D_{he}(\underline{n}) = \frac{2k}{e^2} f^2 \Big[& R^2 R_s R_u (R_s + R_e)(R_u + R_h) \left(\frac{T_P}{R_P} + \frac{T_L}{R_L}\right) \\ & - T_u R_u R_h R_s (R_s R + R_e R + R_e R_s) \\ & - T_s R_s R_e R_u (R_u R + R_h R + R_h R_u) \\ & + T_e R_e R_s R_u [R_u(R + R_s) + R_h(R + R_s + R_u)] \end{aligned}$$

$$
\begin{aligned}
&+T_h R_h R_s R_u [R_s(R+R_u) \\
&+R_e(R+R_s+R_u)]] \qquad \text{(D.25)}
\end{aligned}
$$

$$
\begin{aligned}
D_h(\underline{n}) &= \frac{2k}{e^2} f^2 \Big[R^2 R_u^2 (R_s+R_e)^2 (\frac{T_P}{R_P} + \frac{T_L}{R_L}) \\
&+T_s R_s R_u^2 R_e^2 + T_u R_u (R_s R + R_e R + R_e R_s)^2 \\
&+T_h R_h [R_s(R+R_u) + R_e(R+R_s+R_u)]^2 \\
&+T_e R_e R_s^2 R_u^2 \Big] \qquad \text{(D.26)}
\end{aligned}
$$

$$
\begin{aligned}
\tilde{D}_e(\underline{n}) &= \frac{2k}{e^2} \tilde{f}^2 \Big[R^2 \tilde{R}_s^2 (\tilde{R}_u + \tilde{R}_h)^2 (\frac{\tilde{T}_P}{\tilde{R}_P} + \frac{\tilde{T}_L}{\tilde{R}_L}) \\
&+\tilde{T}_u \tilde{R}_u \tilde{R}_s^2 \tilde{R}_h^2 + \tilde{T}_s \tilde{R}_s (\tilde{R}_u R + \tilde{R}_h R + \tilde{R}_h \tilde{R}_u)^2 \\
&+\tilde{T}_e \tilde{R}_e [\tilde{R}_u (R+\tilde{R}_s) + \tilde{R}_h (R+\tilde{R}_s+\tilde{R}_u)]^2 \\
&+\tilde{T}_h \tilde{R}_h \tilde{R}_s^2 \tilde{R}_u^2 \Big] \qquad \text{(D.27)}
\end{aligned}
$$

$$
\begin{aligned}
\tilde{D}_{eh}(\underline{n}) &= \frac{2k}{e^2} \tilde{f}^2 \Big[R^2 \tilde{R}_s \tilde{R}_u (\tilde{R}_s + \tilde{R}_e)(\tilde{R}_u + \tilde{R}_h)(\frac{\tilde{T}_P}{\tilde{R}_P} + \frac{\tilde{T}_L}{\tilde{R}_L}) \\
&-\tilde{T}_u \tilde{R}_u \tilde{R}_h \tilde{R}_s (\tilde{R}_s R + \tilde{R}_e R + \tilde{R}_e \tilde{R}_s) \\
&-\tilde{T}_s \tilde{R}_s \tilde{R}_e \tilde{R}_u (\tilde{R}_u R + \tilde{R}_h R + \tilde{R}_h \tilde{R}_u) \\
&+\tilde{T}_e \tilde{R}_e \tilde{R}_s \tilde{R}_u [\tilde{R}_u (R+\tilde{R}_s) + \tilde{R}_h (R+\tilde{R}_s+\tilde{R}_u)] \\
&+\tilde{T}_h \tilde{R}_h \tilde{R}_s \tilde{R}_u [\tilde{R}_s (R+\tilde{R}_u) \\
&+\tilde{R}_e (R+\tilde{R}_s+\tilde{R}_u)] \Big] \qquad \text{(D.28)}
\end{aligned}
$$

$$
\begin{aligned}
\tilde{D}_{he}(\underline{n}) &= \frac{2k}{e^2} \tilde{f}^2 \Big[R^2 \tilde{R}_s \tilde{R}_u (\tilde{R}_s + \tilde{R}_e)(\tilde{R}_u + \tilde{R}_h)(\frac{\tilde{T}_P}{\tilde{R}_P} + \frac{\tilde{T}_L}{\tilde{R}_L}) \\
&-\tilde{T}_u \tilde{R}_u \tilde{R}_h \tilde{R}_s (\tilde{R}_s R + \tilde{R}_e R + \tilde{R}_e \tilde{R}_s) \\
&-\tilde{T}_s \tilde{R}_s \tilde{R}_e \tilde{R}_u (\tilde{R}_u R + \tilde{R}_h R + \tilde{R}_h \tilde{R}_u) \\
&+\tilde{T}_e \tilde{R}_e \tilde{R}_s \tilde{R}_u [\tilde{R}_u (R+\tilde{R}_s) + \tilde{R}_h (R+\tilde{R}_s+\tilde{R}_u)] \\
&+\tilde{T}_h \tilde{R}_h \tilde{R}_s \tilde{R}_u [\tilde{R}_s (R+\tilde{R}_u) \\
&+\tilde{R}_e (R+\tilde{R}_s+\tilde{R}_u)] \Big] \qquad \text{(D.29)}
\end{aligned}
$$

$$
\begin{aligned}
\tilde{D}_h(\underline{n}) &= \frac{2k}{e^2} \tilde{f}^2 \Big[R^2 \tilde{R}_u^2 (\tilde{R}_s + \tilde{R}_e)^2 (\frac{\tilde{T}_P}{\tilde{R}_P} + \frac{\tilde{T}_L}{\tilde{R}_L})
\end{aligned}
$$

$$
\begin{aligned}
&+\tilde{T}_s\tilde{R}_s\tilde{R}_u^2\tilde{R}_e^2 + \tilde{T}_u\tilde{R}_u(\tilde{R}_sR + \tilde{R}_eR + \tilde{R}_e\tilde{R}_s)^2 \\
&+\tilde{T}_h\tilde{R}_h[\tilde{R}_s(R + \tilde{R}_u) + \tilde{R}_e(R + \tilde{R}_s + \tilde{R}_u)]^2 \\
&+\tilde{T}_e\tilde{R}_e\tilde{R}_s^2\tilde{R}_u^2\Big], \qquad \text{(D.30)}
\end{aligned}
$$

where f and $\tilde{f}$ are defined in Equations (C.20) and (C.21).

Appendix E

Stochastic Differential Equations

This appendix gives the stochastic differential equations in Section 3.7 in full, for both the field mode amplitudes, and the photon numbers.

From the Fokker-Planck equation one can write down the following Ito stochastic differential equations,

$$\begin{aligned} d(n_e) &= \Big\{ \sum_{lj} [2\beta_j^* \beta_l F_{lj}^r(\underline{n}) - 2(\delta_{lj} + \beta_j^* \beta_l) G_{lj}^r(\underline{n})] \\ &\quad - A(\underline{n}) + B(\underline{n}) + \dot{n}_e|_p \Big\} dt \\ &\quad + \sum_{lj} (v_{lj} d\eta_j \beta_l^* + v_{lj}^* \beta_l d\eta_j^* + \bar{v}_{lj} d\bar{\eta}_j \beta_l^* + \bar{v}_{lj}^* \beta_l d\bar{\eta}_j^*) \\ &\quad + \sum_l (w_l d\xi_l) + i \sum_{lj} (f_{lj} d\zeta_{lj} + \bar{f}_{lj} d\bar{\zeta}_{lj}) \end{aligned} \tag{E.1}$$

$$\begin{aligned} d(n_h) &= \Big\{ \sum_{lj} [2\beta_j^* \beta_l F_{lj}^r(\underline{n}) - 2(\delta_{lj} + \beta_j^* \beta_l) G_{lj}^r(\underline{n})] \\ &\quad - A(\underline{n}) + B(\underline{n}) + \dot{n}_h|_p \Big\} dt \\ &\quad + \sum_{lj} (v_{lj} d\eta_j \beta_l^* + v_{lj}^* \beta_l d\eta_j^* + \bar{v}_{lj} d\bar{\eta}_j \beta_l^* + \bar{v}_{lj}^* \beta_l d\bar{\eta}_j^*) \\ &\quad + \sum_l (w_l d\xi_l) + i \sum_{lj} (f_{lj} d\zeta_{lj} + \bar{f}_{lj} d\bar{\zeta}_{lj}) \end{aligned} \tag{E.2}$$

$$
\begin{aligned}
d(\tilde{n}_e) &= \Big\{2|\beta_1|^2\tilde{F}^r_{11}(\underline{n}) - 2(|\beta_1|^2+1)\tilde{G}^r_{11}(\underline{n}) \\
&\quad -\tilde{A}(\underline{n}) + \tilde{B}(\underline{n}) + \dot{\tilde{n}}_e\Big|_p\Big\}dt \\
&\quad +\tilde{v}_{11}\beta_1^* d\tilde{\eta} + \tilde{v}^*_{11}\beta_1\tilde{\eta}^* + \tilde{\tilde{v}}_{11}\beta_1^*\tilde{\tilde{\eta}} + \tilde{\tilde{v}}^*_{11}\beta_1^*\tilde{\tilde{\eta}}^* \\
&\quad +\tilde{w}_1 d\tilde{\xi} + i(\tilde{f}_{11}d\tilde{\zeta} + \tilde{\tilde{f}}_{11}d\tilde{\tilde{\zeta}}) + \sqrt{\tilde{A}(\underline{n}) + \tilde{B}(\underline{n})}d\tilde{W} \qquad \text{(E.3)} \\
d(\tilde{n}_h) &= \Big\{2|\beta_1|^2\tilde{F}^r_{11}(\underline{n}) - 2(|\beta_1|^2+1)\tilde{G}^r_{11}(\underline{n}) \\
&\quad -\tilde{A}(\underline{n}) + \tilde{B}(\underline{n}) + \dot{\tilde{n}}_h\Big|_p\Big\}dt \\
&\quad +\tilde{v}_{11}\beta_1^* d\tilde{\eta} + \tilde{v}^*_{11}\beta_1\tilde{\eta}^* + \tilde{\tilde{v}}_{11}\beta_1^*\tilde{\tilde{\eta}} + \tilde{\tilde{v}}^*_{11}\beta_1^*\tilde{\tilde{\eta}}^* \\
&\quad +\tilde{w}_1 d\tilde{\xi} + i(\tilde{f}_{11}d\tilde{\zeta} + \tilde{\tilde{f}}_{11}d\tilde{\tilde{\zeta}}) + \sqrt{\tilde{A}(\underline{n}) + \tilde{B}(\underline{n})}d\tilde{W} \qquad \text{(E.4)} \\
d(\beta_l) &= \Big\{\sum_j [G^*_{jl}(\underline{n})\beta_j - F^*_{jl}(\underline{n})\beta_j] \\
&\quad +[\tilde{G}^*_{11}(\underline{n})\beta_1 - \tilde{F}^*_{11}(\underline{n})\beta_1]\delta_{l1} - \kappa_l\beta_l - i\Delta_l\beta_l\Big\}dt \\
&\quad -\sum_j v_{lj}d\eta_j + \sqrt{\kappa_l\bar{N}_l}d\Xi_l - \tilde{v}_{11}d\tilde{\eta}\delta_{l1} \qquad \text{(E.5)} \\
d(\beta_l^*) &= \Big\{\sum_j [G_{lj}(\underline{n})\beta_j^* - F_{lj}(\underline{n})\beta_j^*] \\
&\quad +[\tilde{G}_{11}(\underline{n})\beta_1^* - \tilde{F}_{11}(\underline{n})\beta_1^*]\delta_{l1} - \kappa_l\beta_l^* + i\Delta_l\beta_l^*\Big\}dt \\
&\quad -\sum_j v^*_{lj}d\eta^*_j + \sqrt{\kappa_l\bar{N}_l}d\Xi^*_l - \tilde{v}_{11}d\tilde{\eta}^*\delta_{l1}, \qquad \text{(E.6)}
\end{aligned}
$$

where $F^r_{lj}(\underline{n})$ and $G^r_{lj}(\underline{n})$ are the real parts of $F_{lj}(\underline{n})$ and $G_{lj}(\underline{n})$, and where

$$
\begin{aligned}
\langle d\eta_j(t)d\eta^*_k(t')\rangle &= \langle d\Xi_j(t)d\Xi^*_k(t')\rangle = \langle d\xi_j(t)d\xi_k(t')\rangle \\
&= \langle d\bar{\eta}_j(t)d\bar{\eta}^*_k(t') = \delta(t-t')\delta_{jk} \qquad \text{(E.7)} \\
\langle d\zeta_{ij}(t)d\zeta_{kl}(t')\rangle &= \langle d\bar{\zeta}_{ij}(t)d\bar{\zeta}_{kl}(t')\rangle = \delta(t-t')\delta_{ik}\delta_{jl} \qquad \text{(E.8)} \\
\langle d\tilde{\eta}(t)d\tilde{\eta}^*(t')\rangle &= \langle d\tilde{\xi}(t)d\tilde{\xi}(t')\rangle = \langle d\tilde{\tilde{\eta}}(t)d\tilde{\tilde{\eta}}^*(t')\rangle \\
&= \delta(t-t') \qquad \text{(E.9)} \\
\langle d\tilde{\zeta}(t)d\tilde{\zeta}(t')\rangle &= \langle d\tilde{\tilde{\zeta}}(t)d\tilde{\tilde{\zeta}}(t')\rangle = \delta(t-t') \qquad \text{(E.10)}
\end{aligned}
$$

$$\langle d\tilde{W}_1(t) d\tilde{W}_1(t') \rangle = \delta(t-t'), \tag{E.11}$$

and

$$\sum_j v_{lj} v^*_{kj} = 2G^r_{kl}(\underline{n}) \tag{E.12}$$

$$\sum_j \bar{v}_{lj} \bar{v}^*_{kj} = 2F^r_{kl}(\underline{n}) \tag{E.13}$$

$$\tilde{v}_{11} \tilde{v_{11}}^* = 2\tilde{G}^r_{11}(\underline{n}) \tag{E.14}$$

$$\tilde{\bar{v}}_{11} \tilde{\bar{v}}^*_{11} = 2\tilde{F}^r_{11}(\underline{n}) \tag{E.15}$$

$$w_l = \sqrt{2G^r_{ll}(\underline{n})} \tag{E.16}$$

$$f_{lj} = \sqrt{2G^r_{lj}(\underline{n})\beta^*_j \beta_l} \tag{E.17}$$

$$\bar{f}_{lj} = \sqrt{2F^r_{lj}(\underline{n})\beta^*_j \beta_l} \tag{E.18}$$

$$\tilde{f}_{11} = \sqrt{2\tilde{G}^r_{11}(\underline{n})|\beta_1|^2} \tag{E.19}$$

$$\tilde{\bar{f}}_{11} = \sqrt{2\tilde{F}^r_{11}(\underline{n})|\beta_1|^2} \tag{E.20}$$

and any other noises have the definitions as given in Chapter 2.

From equations (E.5), (E.6) and (3.15) the Ito stochastic differential equations for the photon numbers are

$$\begin{aligned} d(m_l) = & \Big\{ \sum_j [G_{lj}(\underline{n})\beta_l \beta^*_j + G^*_{jl}(\underline{n})\beta_j \beta^*_l \\ & - F_{lj}(\underline{n})\beta_l \beta^*_j - F^*_{jl}(\underline{n})\beta_j \beta^*_l] \\ & - \kappa_l |\beta_l|^2 + 2G^r_{ll}(\underline{n}) + \kappa_l \bar{N}_l \\ & + (\tilde{G}^*_{11}(\underline{n}) m_1 + \tilde{G}_{11}(\underline{n}) m_1 \\ & - \tilde{F}^*_{11}(\underline{n}) m_1 - \tilde{F}_{11}(\underline{n}) m_1)\delta_{l1} \Big\} dt \\ & + \beta_l (- \sum_j v^*_{lj} d\eta^*_j + \sqrt{\kappa_l \bar{N}_l} d\Xi^*_l) \\ & + \beta^*_l (- \sum_j v_{lj} d\eta_j + \sqrt{\kappa_l \bar{N}_l} d\Xi_l) \\ & + (2\tilde{G}^r_{11}(\underline{n}) - \beta_1 \tilde{v}^*_{11} d\tilde{\eta}^* - \beta^*_1 \tilde{v}_{11} d\tilde{\eta}) \delta_{l1} dt \end{aligned} \tag{E.21}$$

where $m_l = |\beta_l|^2$.

Making the rotating wave approximation we can drop all terms containing $\beta_l \beta_j^*$ in which $l \neq j$. This leads to a significant simplification of the equations. In addition, we make the same approximations as in the single mode case (equations (2.87)-(2.90)). This allows us to make the substitutions

$$F_{lj}(\underline{n}) = a_{lj} N^2 \tag{E.22}$$
$$G_{lj}(\underline{n}) = a_{lj} n_e n_h \tag{E.23}$$
$$A(\underline{n}) = d n_e n_h \tag{E.24}$$
$$B(\underline{n}) = 0 \tag{E.25}$$
$$\tilde{F}_{11}(\underline{n}) = \tilde{a}_{11} \tilde{N}^2 \tag{E.26}$$
$$\tilde{G}_{11}(\underline{n}) = \tilde{a}_{11} \tilde{n}_e \tilde{n}_h \tag{E.27}$$
$$\tilde{A}(\underline{n}) = \tilde{d} \tilde{n}_e \tilde{n}_h \tag{E.28}$$
$$\tilde{B}(\underline{n}) = 0, \tag{E.29}$$

where a_{lj} is the multi-mode analogue of the parameter c of the single-mode case, and the subscripts come about for the multi-mode case due to the mode dependent coupling constant contained in the a_{lj}.

The simplified equations are thus

$$\begin{aligned} d(n_e) = & \Big\{ \sum_j [2 m_j a_{jj} N^2 - 2(1+m_j) a_{jj} n_e n_h] \\ & - d n_e n_h + \dot{n}_e|_p \Big\} dt \\ & + \sum_{lj} (v_{lj} d\eta_j \beta_l^* + v_{lj}^* \beta_l d\eta_j^* + \bar{v}_{lj} d\bar{\eta}_j \beta_l^* + \bar{v}_{lj}^* \beta_l d\bar{\eta}_{lj}) \\ & + \sum_l (w_l d\xi_l) + i \sum_{lj} (f_{lj} d\zeta_{lj} + \bar{f}_{lj} d\bar{\zeta}_{lj}) \\ & + \sqrt{d n_e n_h}\, dW_1 \\ d(n_h) = & \Big\{ \sum_j [2 m_j a_{jj} N^2 - 2(1+m_j) a_{jj} n_e n_h] \end{aligned} \tag{E.30}$$

$$
\begin{aligned}
& -dn_e n_h + \dot{n}_h\big|_p \Big\} dt \\
& + \sum_{lj} (v_{lj} d\eta_j \beta_l^* + v_{lj}^* \beta_l d\eta_j^* + \bar{v}_{lj} d\bar{\eta}_j \beta_l^* + \bar{v}_{lj}^* \beta_l d\bar{\eta}_j^*) \\
& + \sum_{l} (w_l d\xi_l) + i \sum_{lj} (f_{lj} d\zeta_{lj} + \bar{f}_{lj} d\bar{\zeta}_{lj}) \\
& + \sqrt{dn_e n_h}\, dW_1 \qquad \text{(E.31)}
\end{aligned}
$$

$$
\begin{aligned}
d(\tilde{n}_e) \;=\; & \Big\{ 2m_1 \tilde{a}_{11} \tilde{N}^2 - 2(m_1+1)\tilde{a}_{11} \tilde{n}_e \tilde{n}_h \\
& - \tilde{d}\tilde{n}_e \tilde{n}_h + \dot{\tilde{n}}_e\big|_p \Big\} dt \\
& + \tilde{v}_{11} \beta_1^* d\tilde{\eta} + \tilde{v}_{11}^* \beta_1 \tilde{\eta}^* + \tilde{\bar{v}}_{11} \beta_1^* \tilde{\bar{\eta}} + \tilde{\bar{v}}_{11}^* \beta_1 \tilde{\bar{\eta}}^* + \tilde{w}_1 d\tilde{\xi} \\
& + i(\tilde{f}_{11} d\tilde{\zeta} + \tilde{\bar{f}}_{11} d\tilde{\bar{\zeta}}) + \sqrt{\tilde{d}\tilde{n}_e \tilde{n}_h}\, d\tilde{W} \qquad \text{(E.32)}
\end{aligned}
$$

$$
\begin{aligned}
d(\tilde{n}_h) \;=\; & \Big\{ 2m_1 \tilde{a}_{11} \tilde{N}^2 - 2(m_1+1)\tilde{a}_{11} \tilde{n}_e \tilde{n}_h \\
& - \tilde{d}\tilde{n}_e \tilde{n}_h + \dot{\tilde{n}}_h\big|_p \Big\} dt \\
& + \tilde{v}_{11} \beta_1^* d\tilde{\eta} + \tilde{v}_{11}^* \beta_1 \tilde{\eta}^* + \tilde{\bar{v}}_{11} \beta_1^* \tilde{\bar{\eta}} + \tilde{\bar{v}}_{11}^* \beta_1 \tilde{\bar{\eta}}^* + \tilde{w}_1 d\tilde{\xi} \\
& + i(\tilde{f}_{11} d\tilde{\zeta} + \tilde{\bar{f}}_{11} d\tilde{\bar{\zeta}}) + \sqrt{\tilde{d}\tilde{n}_e \tilde{n}_h}\, d\tilde{W} \qquad \text{(E.33)}
\end{aligned}
$$

$$
\begin{aligned}
d(m_l) \;=\; & \Big\{ 2a_{ll} n_e n_h (m_l + 1) - 2a_{ll} N^2 m_l - \kappa_l m_l \Big\} dt \\
& - \beta_l \sum_j v_{lj}^* d\eta_j^* - \beta_l^* \sum_j v_{lj} d\eta_j \\
& + (2\tilde{a}_{11} \tilde{n}_e \tilde{n}_h (m_1 + 1) - 2\tilde{a}_{11} \tilde{N}^2 m_1) \delta_{l1} dt \\
& + (-\beta_1 \tilde{v}_{11}^* d\tilde{\eta}^* - \beta_1^* \tilde{v}_{11} d\tilde{\eta}) \delta_{l1}. \qquad \text{(E.34)}
\end{aligned}
$$

Appendix F

Steady-state solutions

The procedure used to find steady-state solutions (as referred to in Section 3.7) for the multi-mode semiconductor system is detailed in this appendix.

If the noise terms in equations (E.30)-(E.34) are dropped and the time derivatives set to zero, then for $P_e = P_h$, the equations can be rearranged to give

$$n_e = \frac{(\alpha_h - \beta_e)(n_h - M)}{(\alpha_e - \beta_h)} \tag{F.1}$$

$$n_h = \frac{c_2 M + c_3}{2c_2} + \frac{\sqrt{(c_2 M + c_3)^2 - 4c_2(c_3 M - P_h - c_1)}}{2c_2} \tag{F.2}$$

$$\tilde{n}_e = \frac{(\tilde{\alpha}_h - \tilde{\beta}_e)(\tilde{n}_h - \tilde{M})}{\tilde{\alpha}_e - \tilde{\beta}_h} \tag{F.3}$$

$$\tilde{n}_h = \frac{\tilde{c}_2 \tilde{M} + \tilde{c}_3}{2\tilde{c}_2} + \frac{\sqrt{(\tilde{c}_2 \tilde{M} + \tilde{c}_3)^2 - 4\tilde{c}_2(\tilde{c}_3 \tilde{M} - \tilde{P}_h - \tilde{c}_1)}}{2\tilde{c}_2} \tag{F.4}$$

$$m_1 = \frac{2a_{11} n_e n_h + 2\tilde{a}_{11} \tilde{n}_e \tilde{n}_h}{2a_{11} N^2 - 2a_{11} n_e n_h + 2\tilde{a}_{11} \tilde{N}^2 - 2\tilde{a}_{11} \tilde{n}_e \tilde{n}_h + \kappa_1} \tag{F.5}$$

$$m_2 = \frac{2a_{22} n_e n_h}{2a_{22} N^2 - 2a_{22} n_e n_h + \kappa_2} \tag{F.6}$$

$$m_3 = \frac{2a_{33} n_e n_h}{2a_{33} N^2 - 2a_{33} n_e n_h + \kappa_3}, \tag{F.7}$$

where

$$c_1 = 2(a_{11}m_1 + a_{22}m_2 + a_{33}m_3)N^2 \quad \text{(F.8)}$$

$$c_2 = [2(1 + a_{11})m_1 + 2(1 + a_{22})m_2 + 2(1 + a_{33})m_3 + d]\frac{(\alpha_h - \beta_e)}{(\alpha_e - \beta_h)} \quad \text{(F.9)}$$

$$c_3 = \frac{(\beta_h\beta_e - \alpha_h\alpha_e)}{\alpha_e - \beta_h} \quad \text{(F.10)}$$

$$\tilde{c_1} = 2(\tilde{a}_{11}m_1 + \tilde{a}_{22}m_2 + \tilde{a}_{33}m_3)\tilde{N}^2 \quad \text{(F.11)}$$

$$\tilde{c_2} = [2(1 + \tilde{a}_{11})m_1 + 2(1 + \tilde{a}_{22})m_2 + 2(1 + \tilde{a}_{33})m_3 + \tilde{d}]\frac{(\tilde{\alpha_h} - \tilde{\beta}_e)}{(\tilde{\alpha}_e - \tilde{\beta}_h)} \quad \text{(F.12)}$$

$$\tilde{c_3} = \frac{(\tilde{\beta}_h\tilde{\beta}_e - \tilde{\alpha}_h\tilde{\alpha}_e)}{\tilde{\alpha}_e - \tilde{\beta}_h}. \quad \text{(F.13)}$$

The bisection algorithm is used in conjunction with these equations to obtain steady-state solutions. In other algorithms we have tried, we have discovered that the dominant mode lies very close to the point at which the stability changes, and hence changes rapidly with a change in the parameters of the system. Algorithms which search for a solution for m_1^0 thus can easily evolve to a solution which is unstable. The algorithm is hence written in such a way as to decrease the probability of going to the wrong solution by looking at the solution for m_1^{-1}, which varies much more smoothly than the solution for m_1. The bisection algorithm is in two parts. First, solutions for (F.1)-(F.5) are found with $m_2 = m_3 = 0$. Then, using these solutions, (F.6)-(F.7) are evaluated and used to find a new solution for (F.1)-(F.5). Since m_2 and m_3 are much smaller than m_1, we expect that including them will not have a great influence on the value of m_1, and thus we remain on the stable branch of the solution. These two parts are repeated until the solutions no longer change.

The solutions are found as follows;

1. We choose a range of numbers which contains the steady-state solution.

2. We take the midpoint of this range to be the initial value of m_1 which we call m_1^0.

3. We evaluate (F.1)-(F.4) using this value of m_1^0, and with $m_2 = m_3 = 0$.

4. We re-evaluate m_1 from (F.5) using the values found for $n_e, n_h, \tilde{n}_e$, and $\tilde{n}_h$ in the previous step.

5. We compare m_1^0 with m_1 by evaluating $m_1^{-1} - m_1^{0-1}$. If $m_1^{-1} - m_1^{0-1}$ is greater than zero, then $m_1 < m_1^0$, and so we can choose a new range which has the same lower boundary as previously, but a new upper boundary of m_1^0, and repeat the procedure from Step 2. If $m_1^{-1} - m_1^{0-1}$ is less than zero, then $m_1 > m_1^0$, and so we can choose a new range which has the same upper boundary as previously, but a new lower boundary of m_1^0, and repeat the procedure from Step 2.

6. When $|m_1^{-1} - m_1^{0-1}|$ becomes less than some user-set tolerance (we used 10^{-10}), one can evaluate m_2^0 and m_3^0 using the solutions for $m_1, n_e, n_h, \tilde{n}_e$, and repeat the procedure from Step 1.

7. When the value of m_1 does not change from the value found with the previous values of $m_2, m_3, n_e, n_h, \tilde{n}_e$, and $\tilde{n}_h$, the steady-state solutions have been found.

This algorithm was found to give good results provided parameters are chosen for which the central mode is the dominant mode. If this is not the case, then m_2^0 or m_3^0 are close to a change in stability and the bisection algoritm fails. In such a situation the bisection algorithm should be modified so that solutions for m_2^0 and m_3^0 can be found first.

Appendix G

Linearised SDEs

The linearised drift and diffusion matrices used in the calculation of the spectrum for the multi-mode system in Section 3.8 are given here.

The matrices in Equation (3.16) are made up of the matrices

$$\mathcal{E}_{cc}(\mathbf{Y}_0) = \begin{pmatrix} \sum_j (r_j + d) n_h^0 + \alpha_e & \sum_j (r_j + d) n_e^0 + \beta_e & 0 & 0 \\ \sum_j (r_j + d) n_h^0 + \beta_h & \sum_j (r_j + d) n_e^0 + \alpha_h & 0 & 0 \\ 0 & 0 & (\tilde{r}_1 + \tilde{d}) \tilde{n}_h^0 + \tilde{\alpha}_e & (\tilde{r}_1 + \tilde{d}) \tilde{n}_e^0 + \tilde{\beta}_e \\ 0 & 0 & (\tilde{r}_1 + \tilde{d}) \tilde{n}_h^0 + \tilde{\beta}_h & (\tilde{r}_1 + \tilde{d}) \tilde{n}_e^0 + \tilde{\alpha}_h \end{pmatrix} \quad \text{(G.1)}$$

$$\mathcal{E}_{cf}(\mathbf{Y}_0) = \begin{pmatrix} -s_{11} & -s_{22} & -s_{33} \\ -s_{11} & -s_{22} & -s_{33} \\ -\tilde{s}_{11} & 0 & 0 \\ -\tilde{s}_{11} & 0 & 0 \end{pmatrix} \tag{G.2}$$

$$\mathcal{E}_{fc}(\mathbf{Y}_0) = \begin{pmatrix} -r_1 n_h^0 & -r_1 n_e^0 & -\tilde{r}_1 \tilde{n}_h^0 & -\tilde{r}_1 \tilde{n}_e^0 \\ -r_2 n_h^0 & -r_2 n_e^0 & 0 & 0 \\ -r_3 n_h^0 & -r_3 n_e^0 & 0 & 0 \end{pmatrix}, \tag{G.3}$$

and

$$\mathcal{E}_{ff}(\mathbf{Y}_0) = \begin{pmatrix} s_{11} + \kappa_1 + \tilde{s}_{11} & 0 & 0 \\ 0 & s_{22} + \kappa_2 & 0 \\ 0 & 0 & s_{33} + \kappa_3 \end{pmatrix}, \tag{G.4}$$

so

$$\mathcal{E}(\mathbf{Y}_0) = \begin{pmatrix} \mathcal{E}_{cc}(\mathbf{Y}_0) & \mathcal{E}_{cf}(\mathbf{Y}_0) \\ \mathcal{E}_{fc}(\mathbf{Y}_0) & \mathcal{E}_{ff}(\mathbf{Y}_0) \end{pmatrix}, \tag{G.5}$$

where

$$r_j = 2a_{jj}(m_j^0 + 1) \tag{G.6}$$

$$s_{jj} = 2a_{jj}(N^2 - n_e n_h) \tag{G.7}$$

$$\tilde{r}_1 = 2\tilde{a}_{11}(m_1^0 + 1) \tag{G.8}$$

$$\tilde{s}_{11} = 2\tilde{a}_{11}(\tilde{N}^2 - \tilde{n}_e \tilde{n}_h). \tag{G.9}$$

The matrix $\mathcal{G}(\mathbf{Y}_0) = \mathcal{F}(\mathbf{Y}_0)\mathcal{F}^{\mathrm{T}}(\mathbf{Y}_0)$ is given here for brevity, rather

than the $\mathcal{F}(\mathbf{Y}_0)$, which are 5×31 matrices! Thus we have

$$\mathcal{G}_{cc}(\mathbf{Y}_0) = \begin{pmatrix} \sum_j u(m_j^0) & \sum_j u(m_j^0) & 0 & 0 \\ +D_e(\underline{n}) & +D_{eh}(\underline{n}) & & \\ \sum_j u(m_j^0) & \sum_j u(m_j^0) & 0 & 0 \\ +D_{he}(\underline{n}) & +D_h(\underline{n}) & & \\ 0 & 0 & \tilde{u}(m_1^0) & \tilde{u}(m_1^0) \\ & & +\tilde{D}_e(\underline{n}) & +\tilde{D}_{eh}(\underline{n}) \\ 0 & 0 & \tilde{u}(m_1^0) & \tilde{u}(m_1^0) \\ & & +\tilde{D}_{he}(\underline{n}) & +\tilde{D}_h(\underline{n}) \end{pmatrix} \tag{G.10}$$

$$\mathcal{G}_{cf}(\mathbf{Y}_0) = \begin{pmatrix} -2t(m_1^0) & -2t(m_2^0) & -2t(m_3^0) \\ -2t(m_1^0) & -2t(m_2^0) & -2t(m_3^0) \\ -2\tilde{t}(m_1^0) & 0 & 0 \\ -2\tilde{t}(m_1^0) & 0 & 0 \end{pmatrix} \tag{G.11}$$

$$\mathcal{G}_{fc}(\mathbf{Y}_0) = \begin{pmatrix} -2t(m_1^0) & -2t(m_1^0) & -2\tilde{t}(m_1^0) & -2\tilde{t}(m_1^0) \\ -2t(m_2^0) & -2t(m_2^0) & 0 & 0 \\ -2t(m_3^0) & -2t(m_3^0) & 0 & 0 \end{pmatrix} \tag{G.12}$$

$$\mathcal{G}_{ff}(\mathbf{Y}_0) = \begin{pmatrix} 2t(m_1^0) & 0 & 0 \\ +2\tilde{t}(m_1^0) & & \\ 0 & 2t(m_2^0) & 0 \\ 0 & 0 & 2t(m_3^0) \end{pmatrix}, \tag{G.13}$$

where

$$\mathcal{G}(\mathbf{Y}_0) = \begin{pmatrix} \mathcal{G}_{cc}(\mathbf{Y}_0) & \mathcal{G}_{cf}(\mathbf{Y}_0) \\ \mathcal{G}_{fc}(\mathbf{Y}_0) & \mathcal{G}_{ff}(\mathbf{Y}_0) \end{pmatrix}, \tag{G.14}$$

and

$$t(m_j^0) = 2m_j^0 a_{jj} n_e^0 n_h^0 \tag{G.15}$$

$$u(m_j^0) = t(m_j^0 + 1) + 2m_j^0 a_{jj} N^2 + d n_e^0 n_h^0 \tag{G.16}$$

$$\tilde{t}(m_1^0) = 2m_1^0 \tilde{a}_{11} \tilde{n}_e^0 \tilde{n}_h^0 \tag{G.17}$$

$$\tilde{u}(m_1^0) = \tilde{t}(m_1^0 + 1) + 2m_1^0 \tilde{a}_{11} \tilde{N}^2 + \tilde{d} \tilde{n}_e^0 \tilde{n}_h^0. \tag{G.18}$$

Bibliography

[Adler 1946] R. Adler, Proc. IRE **34**, 351 (1946).

[Agarwal 1991] G.S. Agarwal *et al.*, Phys. Rev. A **43**, 6451 (1991).

[Agrawal 1986] G.P. Agrawal and N.K. Dutta, *Long-Wavelength Semiconductor Lasers* (Van Nostrand Reinhold, New York, 1986).

[Averin 1986] D.V. Averin and K.K. Likharev, J. Low Temp. Phys. **62**, 345 (1986).

[Ballagh 1992] R.J. Ballagh and A.W. McCord, Int. J. Nonlinear Opt. Phys., **1**, 393 (1992).

[Basov 1961] N.G. Basov, O.N. Krokhin, and Y.M. Popov, Sov. Phys. JETP **13**, 1320 (1961).

[Benkert 1990] C. Benkert *et al.*, Phys. Rev. A **41**, 2756 (1990).

[Bergou 1989a] J. Bergou *et al.*, Opt. Commun. **72**, 82 (1989).

[Bergou 1989b] J. Bergou *et al.*, Phys. Rev. A **40**, 5073 (1989).

[Bernard 1961] M.G.A. Bernard and G. Duraffourg, Phys. Status Solidi **1**, 699 (1961).

[Buczek 1972] C.J. Buczek, and R.J. Freiberg, IEEE J. Quantum Electron. QE-**8**, 641 (1972).

[Carmichael 1993] H.J. Carmichael, Phys. Rev. Lett. **70**, 2273 (1993).

[Chow 1975] W.W. Chow, M.O. Scully, and E.W. van Stryland, Opt. Commun. **15**, 6 (1975).

[Chow 1993] W.W. Chow, S. Koch, and M. Sargent III, *Semiconductor Laser Physics* (Springer Verlag, New York, 1993).

[Dum 1992] R. Dum, A.S. Parkins, P. Zoller, C.W. Gardiner, Phys. Rev. A **46**, 4382 (1992).

[Dumke 1962] W. Dumke, Phys. Rev. **127**, 1559 (1962).

[Farinas 1995] A.D. Farinas, E.K. Gustafson, and R.L. Byer, J. Opt. Soc. Am. B**12**, 328 (1995).

[Filipowicz 1986] P. Filipowicz, J. Javanainen, and P. Meystre, Opt. Commun. **58**, 327 (1986); Phys. Rev. A **34**, 3077 (1986).

[Fontanelle 1995] M.T. Fontanelle and L. Davidovich, Phys. Rev. A **51**, 2560 (1995).

[Freeman 1993a] M.J. Freeman *et al.*, Opt. Lett. **18**, 379 (1993).

[Freeman 1993b] M.J Freeman *et al.*, Opt. Lett. **18**, 2141 (1993).

[Gardiner 1983] C.W. Gardiner, *Handbook of Stochastic Methods* (Springer Verlag, Berlin, 1983).

[Gardiner 1991] C.W. Gardiner, *Quantum Noise* (Springer Verlag. Heidelberg, 1991).

[Gardiner 1992] C.W. Gardiner, A.S. Parkins, and P. Zoller, Phys. Rev. A **46**, 4363 (1992).

[Gardiner 1993] C.W. Gardiner, Phys. Rev. Lett. **70**, 2269 (1993).

[Gillner 1990] L. Gillner, G. Björk, and Y. Yamamoto, Phys. Rev. A **41**, 5053 (1990).

[Golubev 1984] Y.M. Golubev and I.V. Sokolov, Sov. Phys. JETP **60**, 234 (1984).

[Haake 1989] F. Haake, S.M. Tan, and D.F. Walls, Phys. Rev. A **40**. 7121 (1989).

[Haken 1967] H. Haken *et al.*, Z. Phys. **206**, 369 (1967).

[Hall 1962] R.N. Hall *et al.*, Phys. Rev. Lett. **9**, 366 (1962).

[Harris 1992] M. Harris *et al.*, Phys. Rev. Lett. **69**, 2360 (1992).

[Haug 1967a] H. Haug, Z. Phys. **200**, 57 (1967).

[Haug 1967b] H. Haug and H. Haken, Z. Phys. **204**, 262 (1967).

[Haug 1969] H. Haug, Phys. Rev. **184**, 338 (1969).

[Haug 1985] H. Haug, J. Lumin. **30**, 171 (1985).

[Haug 1993] H. Haug and S. Koch, *Quantum theory of the Electronic and Optical Properties of Semiconductors* (World Scientific, Hong Kong, 1993).

[Haus 1984] H.A. Haus, and Y. Yamamoto, Phys. Rev. A **29**, 1261 (1984).

[Herzel 1993] F. Herzel, K. Henneberger, and W. Vogel, IEEE J. Quantum Electron. QE-**29**, 2891 (1993).

[Holonyak 1962] N. Holonyak Jr. and S.F. Bevacqua, Appl. Phys. Lett. **1**, 82 (1962).

[Imamoğlu 1992a] A. Imamoğlu, Y. Yamamoto, and P. Solomon, Phys. Rev. B **46**, 9555 (1992).

[Imamoğlu 1992b] A. Imamoğlu, and Y. Yamamoto, Phys. Rev. B **46**, 15 982 (1992).

[Imamoğlu 1993] A. Imamoğlu, and Y. Yamamoto, Phys. Rev. Lett. **70**, 3327 (1993).

[Imamoğlu 1994] A. Imamoglu and Y. Yamamoto, Phys. Rev. Lett. **72**, 210 (1994).

[Inoue 1992] S. Inoue *et al*, Phys. Rev. A **46**, 2757 (1992).

[Kennedy 1989] T.A.B. Kannedy and D.F. Walls, Phys. Rev. A **40**, 6366 (1989).

[Kitching 1995] J. Kitching, A. Yariv, and Y. Shevy, Phys. Rev. Lett. **74**, 3372 (1995).

[Lai 1991] Y. Lai, H. Haus, and Y. Yamamoto, Opt. Lett. **16**, 1517 (1991).

[Lang 1980] R. Lang and K. Kobayashi, IEEE J. Quantum Electron. QE-**16**, 347 (1980).

[Lax 1966] M. Lax, Phys. Rev. **145**, 110 (1966).

[Lindberg 1988] M. Lindberg and S.W. Koch, Phys. Rev. B **38**, 3342 (1988).

[Loudon 1994] R. Loudon *et al.*, Phys. Rev. A **50**, 658 (1994).

[Louisell 1974] W. Louisell, *Quantum Statistical Properties of Radiation* (Wiley, New York, 1974).

[Machida 1986] S. Machida and Y. Yamamoto, Opt. Commun. **57**, 290 (1986).

[Machida 1987] S. Machida, Y. Yamamoto, and Y. Itaya, Phys. Rev. Lett. **58**, 1000 (1987).

[Machida 1988] S. Machida and Y. Yamamoto, Phys. Rev. Lett. **60**, 792 (1988).

[Marin 1995] F. Marin *et al.*, Phys. Rev. Lett. **75**, 4606 (1995).

[Marte 1988a] M.A.M. Marte and D.F. Walls, Phys. Rev. A **37**, 1235 (1988).

[Marte 1988b] M.A.M. Marte, H. Ritsch, and D.F. Walls, Phys. Rev. Lett. **61**, 1093 (1988).

[Marte 1988c] M.A.M. Marte, H. Ritsch, and D.F. Walls, Phys. Rev. A **38**, 3577 (1988).

[Marte 1989] M.A.M. Marte and P. Zoller, Phys. Rev. A **40**, 5774 (1989).

[Marte 1990] M.A.M. Marte and P. Zoller, Quantum Opt. **2**, 229 (1990).

[McCall 1992] S.L. McCall *et al.*, App. Phys. Lett. **60**, 289 (1992).

[McClelland 1991] D.E. McClelland, H.A. Bachor, and J.C. Wang, Opt. Commun. **84**, 184 (1991).

[McCord 1990] A.W. McCord and R.J. Ballagh, J. Opt. Soc. Am. B **7**, 73 (1990).

[Meystre 1991] P.Meystre and M.J. Sargent, *Elements of Quantum Theory* (Springer Verlag, Heidelberg, 1991).

[Mølmer 1993] K. Mølmer, Y. Castin, J. Dalibard, J. Opt. Soc. Am. B **10**, 524 (1993).

[Müller 1987] J.F. Müller, R. Mewis, and H. Haug, Z. Phys. B **69**, 231 (1987).

[Nathan 1962] M.I. Nathan *et al.*, Appl. Phys. Lett. **1**, 62 (1962).

[Poizat 1996] J.-P. Poizat, *private communication.*

[Quist 1962] T.M. Quist *at al.*, Appl. Phys. Lett. **1**, 91 (1962).

[Ralph 1996] T.C. Ralph, C.C. Harb, and H.A. Bachor, *preprint.*

[Richardson 1990] W.H. Richardson and R.M. Shelby, Phys. Rev. Lett. **64**, 400 (1990).

[Richardson 1991] W.H. Richardson, S. Machida, and Y. Yamamoto, Phys. Rev. Lett. **66**, 2867 (1991).

[Ritsch 1991] H. Ritsch, P. Zoller, C.W. Gardiner, and D.F. Walls, Phys. Rev. A **44**, 3361 (1991).

[Saleh 1991] B.E.A. Saleh and M.C. Teich, *Fundamentals of Photonics* (Wiley Interscience, New York, 1991).

[Schawlow 1958] A.L. Schawlow and C.H. Townes, Phys. Rev. **112**, 1940 (1958).

[Schmitt-Rink 1988] S. Schmitt-Rink, D.S. Chemla, and H. Haug, Phys. Rev. B **37**, 941 (1988).

[Scully 1967] M.O. Scully and W.E. Lamb Jr., Phys. Rev. **159**, 208 (1967).

[Siegman 1986] A.E. Siegman, *Lasers* (University Science, Mill Valley, California, 1986).

[Spano 1986] P. Spano, S. Piazzolla, and M. Tamburrini, IEEE J. Quantum Electron. QE-**22**, 427 (1986).

[Stover 1966] H.L. Stover and W.H. Steier, Appl. Phys. Lett. **8**, 91 (1966).

[Stratonovich 1967] R.L. Stratonovich, *Topics in the Theory of Random Noise*,(Gordon and Breach, New York, 1967 v. II).

[Teich 1985] M.C. Teich and B.E.A. Saleh, J. Opt. Soc. Am. B**2**, 275 (1985).

[Vahala 1983a] K. Vahala and A. Yariv, IEEE J. Quantum Electron. QE-**19**, 1096 (1983).

[Vahala 1983b] K. Vahala and A. Yariv, IEEE J. Quantum Electron. QE-**19**, 1102 (1983).

[Wang 1993] H. Wang, M.J. Freeman, and D.G. Steel, Phys. Rev. Lett. **71**, 3951 (1993).

[Wilson 1992] A.C. Wilson *et al.*, Opt. Commun. **110**, 365 (1994).

[Yamamoto 1983] Y. Yamamoto, IEEE J. Quantum Electron. QE-**19**, 34 (1983).

[Yamamoto 1986] Y. Yamamoto, S. Machida, and O. Nilsson, Phys. Rev. A **34**, 4025 (1986).

[Yamamoto 1987] Y. Yamamoto and S. Machida, Phys. Rev. A **35**, 5114 (1987).

[Yamamoto 1991] *Coherence, Amplification, and Quantum Effects in Semiconductor Lasers* ed. Y. Yamamoto (John Wiley and Sons, New York, 1991).

[Yamanishi 1996] M. Yamanishi *et al.*, Phys. Rev. Lett. *to appear* (1996).

Errata

Pg 40 $\rho_T(\underline{n})$ defined by Eqn (2.16) has an implicit time dependence, which is not made evident until Eqn (2.40).

Pg 43 Eqn (2.39) should read $\int_0^\infty dt e^{\mathcal{L}_1 t} = \mathcal{L}_1^{-1}\mathcal{Q}$.

Pg 47 Eqn (2.55) should read $\left.\frac{\partial \rho_o(\underline{n})}{\partial t}\right|_{P_1} = P[\rho_o(n_e-1, n_h-1) - \rho_o(n_e, n_h)]$.

Pg 56 The first line of the second paragraph has a bracket missing, and should read 'The substitutions (2.87)-(2.90) are used throughout...'

Pg 66 The summation on the third line of Eqn (3.4) should only be over l.

Pg 74 p is the ratio of the central to the side mode decay constants and so its definition is $\frac{\kappa_1}{\kappa_2}$, not $\frac{\kappa_2}{\kappa_1}$.

Pg 79 The figure caption for Fig 3.4 should mention that we calculate these noises at a value of ω of 7 MHz.

Pg 82 The figure caption for Fig 3.6 should mention that we have used a pump threshold of 18mA and that we vary the pump rate from below this value to above this value.

Pg 120 There is a spelling mistake in the second to last line of text – capacative should be spelt capacitive.

Pg 121 Eqn (D.1) should contain the additional term $-i\Delta_j[b_j^\dagger b_j, \rho_o(\underline{n})]$.

Pg 122 Eqn (D.2) should have an additional set of brackets around the terms in the last four lines.